Cloning, expression, purification, biochemical, structure characterization and application of α-L-arabinofuranosidase (*Ps*GH43_12) of family 43 glycoside hydrolase from *Pseudopedobactor saltans*

PhD Thesis

By

Abhijeet Thakur

October 2020

DEPARTMENT OF BIOSCIENCES AND BIOENGINEERING
INDIAN INSTITUTE OF TECHNOLOGY GUWAHATI
GUWAHATI – 781039, ASSAM, INDIA

Cloning, expression, purification, biochemical, structure characterization and application of α-L-arabinofuranosidase (*Ps*GH43_12) of family 43 glycoside hydrolase from *Pseudopedobactor saltans*

A Thesis

Submitted in partial fulfillment of the requirements for the Degree of

Doctor of Philosophy

by

Abhijeet Thakur

Under supervision of

Professor Arun Goyal

October 2020

DEPARTMENT OF BIOSCIENCES AND BIOENGINEERING
INDIAN INSTITUTE OF TECHNOLOGY GUWAHATI
GUWAHATI – 781039, ASSAM, INDIA

INDIAN INSTITUTE OF TECHNOLOGY GUWAHATI

DEPARTMENT OF BIOSCIENCES & BIOENGINEERING

STATEMENT

I do hereby declare that the content embodied in this thesis entitled as **"Cloning, expression, purification, biochemical, structure characterization and application of α-L-arabinofuranosidase (*Ps*GH43_12) of family 43 glycoside hydrolase from *Pseudopedobacter saltans*"** is the result of investigations carried out by me in the Department of Biosciences and Bioengineering, Indian Institute of Technology Guwahati, Guwahati, India under the guidance of Professor Arun Goyal.

In keeping with the general practice of reporting scientific observations, due acknowledgements have been made wherever the work described is based on the findings of other investigators.

October, 2020

Abhijeet Thakur

(156106027)

INDIAN INSTITUTE OF TECHNOLOGY GUWAHATI

DEPARTMENT OF BIOSCIENCES & BIOENGINEERING

CERTIFICATE

It is certified that the work described in this thesis entitled **"Cloning, expression, purification, biochemical, structure characterization and application of α-L-arabinofuranosidase (*Ps*GH43_12) of family 43 glycoside hydrolase from *Pseudopedobacter saltans*"** by **Abhijeet Thakur (Roll No. 156106027)** for the award of degree of Doctor of Philosophy is an authentic record of the results obtained from the research work carried out under my supervision at the Department of Biosciences & Bioengineering, Indian Institute of Technology Guwahati, Guwahati, India and this work has not been submitted elsewhere for a degree.

Dr. Arun Goyal *(MTech, PhD)*
(FAMI, FBRS, FABAP, FNABS, FNAAS, FIFIB)
Professor and former Head
(Thesis Supervisor)
Department of Biosciences & Bioengineering
Indian Institute of Technology Guwahati
Guwahati, 781 039, India

ACKNOWLEDGEMENTS

The journey towards successful completion of a Ph.D. degree requires persistence, hard work and above all support of many people. I was very fortunate in meeting people who helped and supported me in achieving my goals.

Here I acknowledge their contributions and express my gratitude to those who supported, encouraged, inspired and assisted me in this journey.

First and foremost, I express my gratitude to my enthusiastic Ph.D. supervisor Prof. Arun Goyal, Department of Biosciences & Bioengineering, IIT Guwahati, for his excellent guidance and for all the contribution of ideas and time to make my Ph.D. experience both stimulating and productive. He inspired me to do good research. The enthusiasm and the joy he has for research was extremely motivational, especially during the negative result days. Despite his busy schedule and tons of academic work he made himself available for discussions and helped me meeting the deadlines. His support, constructive criticism and valuable suggestions provided me with an opportunity to always learn something new and carry out the research work with more diligence and zest. I shall forever remain grateful to him for all that he has done.

I would also like to express my sincere gratitude to all my doctoral committee members Dr. Senthilkumar Sivaprakasam, Dr. Ajaikumar B. Kunnumakkara, Prof. Vimal Katiyar and Prof. Arun Goyal for their valuable suggestions and constructive criticism that has helped me to refine my work and thus led to the successful completion of my thesis.

I am thankful to Department of Biosciences & Bioengineering and Central Instrumentation Facility (CIF), IITG for providing infrastructural support and instruments for my research work. I am also thankful to IIT Guwahati for Param-Ishan Supercomputing facility. I would further like to express my thanks to Mr. Prasad Gosavi and Ms. Navjot Kaur Saini from the Anton Paar, India, for providing SAXS data collection facility.

I would also like to thank the present and former Heads of the Department of Biosciences & Bioengineering, IIT Guwahati, Prof. Latha Rangan, Prof. K. Pakshirajan, and Prof. Venkata. V. Dasu for providing the necessary facilities.

I am extremely thankful for the support received from all the other teaching and non-teaching staff members of the Department of Biosciences and Bioengineering, IIT Guwahati.

I wish to acknowledge MHRD, Govt. of India for providing financial assistance in the form of research scholarship. I would also like to extend my thanks to DBT-Twining project grant number, BT/PR24786/NER/95/853/2017 to Prof. Arun Goyal from Department of Biotechnology, Ministry of Science and Technology, New Delhi, India for funding and supporting the research.

I extended my heartfelt gratitude to all the people with whom I shared the most memorable experience at IITG, the members of my lab, CEBL. First of all, I would like to thank all my seniors for their help and support. I am grateful to all my colleagues for their cooperation and immensely thankful to all the juniors for their help and lively environment in the lab.

I am thankful to all my batch mates and friends for their help and steadfast support. Especially I would like to thank Dr. Singhi, Dr. Sharma, Aman and Anurag for always being there for me. Finally, I extend my heartfelt regards to the most wonderful and supportive family. It is their prayers and wishes which have helped me come so far in my journey. I can't thank my parents enough for all their sacrifices. It is their blessings which made everything simpler and I dedicate this thesis to them.

At last, I thank God, the Almighty for everything. Without his blessings and grace, this thesis would not have been possible.

Abhijeet Thakur

October, 2020

SYNOPSIS

Introduction

Indian economy is based on agriculture. More than 50% of Indian population directly depends on agriculture for their livelihood. Owing to the diversity in the climate, different crops are grown in a year in India. Majorly wheat, rice, maize, sugarcane, barley, sorghum, etc. are the crops grown in India (Birthal et al., 2014). The edible portion of the plant is used to derive energy for metabolic functioning of living being whereas; non-edible part is coined as agro waste. Annually, the worldwide production of lignocellulosic biomass is approximately, 200 billion tons from agriculture sector (Guo et al., 2010) whereas, every year 200 million tons of lignocellulosic agricultural debris is generated in India (Singh and Gu 2010a). The enormous amount of agro-waste produced every year is neither adding any economic benefits to the farmer nor is good for the environment. Several waste management strategies are practiced such as landfills, incineration, pyrolysis, etc. Some of these methods of waste management cause environmental pollution. To fulfil the great energy demands, the best possible way is to utilize lignocellulosic wastes to produce energy. The energy demand is rapidly increasing. In 2010 the demand was of 13 billion tons of oil equivalent and it is expected to increase to 45 billion tons of oil equivalent by 2050 (Zhang and Konan 2010). The use of non-renewable energy sources such as coal, oil and natural gas to fulfil energy demand will cause depletion in their reservoirs. This also leads to an increase in fuel price with increasing demand. To accomplish the energy requirement, renewable sources such as nuclear energy, wind

energy, hydro energy, solar energy and bioenergy are focused. Bioenergy contributes the highest share, 14% out of 18% of total renewable energy supply (Berndes et al., 2003). Bioenergy is harvested either from forest biomass or from agricultural residues. The lignocellulosic residues collected from the agricultural field can be transformed into the source for energy such as methane, bioethanol, butanol, biodiesel and biohydrogen, etc. The essential part for plant biomass conversion to biofuel is, the breakdown of its complex structure.

The plant cell wall exhibits semi-rigidity and possesses complex architecture. The plant cell wall helps in the exchange of materials essential for cell metabolism and provides the protection. It is composed of complex polysaccharides like cellulose, hemicellulose and pectin. Cellulose is homogeneous, while hemicellulose is heterogeneous and branched in nature. The backbone of hemicelluloses such as xylan arabinan are made up of pentoses (xylose, arabinose) and glucan and mannan of hexoses (glucose, galactose and mannose) linked by glycosidic bond (Thakur et al., 2019). Xylan is the most abundant and complex hemicellulose having xylose backbone and numerous substitutions of arabinose, glucuronic acid, acetic acid, *p*-coumaric acid and ferulic acid (Ahmed et al., 2013). The occurrence of side-chain substitution depends on the source of xylan. Arabinose side chains are found in arabinan, arabinoxylan, arabinogalactan, oat spelt xylan and pectin polysaccharides. These side chains interact with other polysaccharides and forms a complex network resulting in the recalcitrant nature of the plant polysaccharide and difficulty in their hydrolysis.

α-L-Arabinofuranosidases (EC 3.2.1.55) are present in family 2, 3, 43, 51, 54 and 62 of glycoside hydrolases (Lombard et al., 2013). The family 43 glycoside hydrolase (GH43) contains enzymes such as β-1,4-xylosidase (EC 3.2.1.37), β-1,3-xylosidase (EC 3.2.1.-), β-1,4-endoxylanase (EC 3.2.1.8), galactan 1,3- β-galactosidase (EC 3.2.1.145), α-L-arabinofuranosidase (EC 3.2.1.55) and arabinanase (EC 3.2.1.99) which exhibit different activities. The mode of action of hydrolysis by α-L-arabinofuranosidase is via overall inversion of the anomeric configuration (Saha 2000). α-L-Arabinofuranohydrolase is involved in hydrolysis of L-arabinose side chain linkages, specifically catalyzing the hydrolysis of terminal nonreducing α-L-1,2-, α-L-1,3-, and α-L-1,5-arabinofuranosyl residues from different oligosaccharides and polysaccharides (Saha 2000; Saha and Bothast 1997; Sozzi et al., 2002). The family 43 glycoside hydrolase on the basis of their sequence identity, biochemical properties and structural characteristics has been subdivided into 37 subfamilies (Mewis et al., 2016). The subfamily GH43_12, contains enzymes having β-xylosidase and α-L-arabinofuranosidase activities. Till date, 1115 enzymes from different microbial forms of life *viz.* Archea, bacteria and fungi are identified but only 13 enzymes of subfamily GH43_12 have been characterized (http://www.cazy.org/GH43_12_all.html). The characterized arabinofuranosidases from *Butyrivibrio fibrisolvens* (Hespell and O'Bryan, 1992), from compost starter culture (Wagschal et al., 2007), from *Bifidobacterium animalis* (Viborg et al., 2013) and from *Bacteroides ovatus* (Zhou et al., 2020) displayed very low enzyme activity and thermal stability. Therefore, an efficient arabinofuranosidase having significantly higher activity and thermal stability is needed to be explored.

Some strains of the genus *Pseudopedobacter* are heparinase producing, obligately aerobic, mesophilic, Gram-negative rod shaped bacteria (Liolios et al., 2011). Few therapeutic enzymes such as chondroitin AC lyase of family 8 polysaccharide lyase (Rani and Goyal 2016) and heparinase II/III of family 12 polysaccharide lyase from *P. saltans* are reported (Balasubramaniam et al., 2018). However, one hemicellulosic enzyme xylanase (*Ps*GH10A) was reported from this microorganism (Sharma et al., 2018). In the present study, the gene encoding α-L-arabinofuranosidase (*Ps*GH43_12) with a locus tag of Pedsa_2580 and GenBank accession no. ADY53124.1 was identified and retrieved from NCBI after the analysis of available whole-genome sequencing data. The gene encoding α-L-arabinofuranosidase, *Ps*GH43_12 of family 43 glycoside hydrolase from *Pseudopedobacter saltans* was cloned in pET28a(+) vector and expressed in BL-21 (DE3) cells. The His-tag containing enzyme was purified to its homogeneity by immobilized metal ion chromatography (IMAC).

Present work

The present work entitled as "Cloning, expression, purification, biochemical, structure characterization and application of α-L-arabinofuranosidase of family 43 Glycoside Hydrolase (*Ps*GH43_12) from *Pseudopedobactor saltans*" has been divided into 5 chapters.

Chapter 1 is a general introduction, which mainly focuses on the brief review of literature dedicated to the bioeconomy, the lignocellulosic waste and the structural component of the plant cell wall with elaborated description of heteroxylan.

This chapter describes classification and mode of action of α-L-arabinofuranosidases and their potential applications followed by significance of the work.

Chapter 2 describes the cloning, expression and purification of first α-L-arabinofuranosidase of family 43 glycoside hydrolase, (*Ps*GH43_12) from *Pseudopedobacter saltans* DSM12145**.** The gene encoding a putative α-L-arabinofuranosidase, *Ps*GH43_12 belonging to Glycoside hydrolase family 43 (GH43) from *Pseudopedobacter saltans* DSM12145 (GenBank Accession No: ADY53124.1) was cloned, expressed and purified. The molecular architecture revealed a signal peptide (29 amino acid residues) at N-terminal followed by a catalytic module *Ps*GH43_12 of 557 amino acid residues. The PCR amplified gene fragment encoding *Ps*GH43_12 showed a band of ~1.7 kb. The restriction enzyme digested fragments of gene encoding *Ps*GH43_12 was ligated with linearized pET-28a(+) expression vector. The ligated mixture was transformed into *E. coli* DH5α competent cells. The positive clones containing recombinant plasmid DNA were screened by restriction enzyme digestion using enzymes, *Nhe*I and *Xho*I. The restriction enzyme digested products were electrophoresed and the band of ~ 5.3 kb was produced for pET-28a(+) vector and corresponding band of ~1.7 kb was produced from the insert fragment for gene encoding *Ps*GH43_12. The recombinant plasmid DNA containing gene encoding *Ps*GH43_12 was transformed into *E. coli* BL-21 (DE3) cells. The recombinant, *Ps*GH43_12 was expressed as soluble homogenous protein. The purified recombinant *Ps*GH43_12 displayed a single band of molecular mass approximately, 65 kDa by SDS-PAGE analysis. The amount of purified recombinant *Ps*GH43_12 obtained from 100 ml *E. coli* BL-21 (DE3) cells was 3.5 mg.

Chapter 3 mainly focuses on the biochemical characterization of α-L-arabinofuranosidase (*Ps*GH43_12) and its potential to hydrolyze plant biomass. *Ps*GH43_12 displayed the maximum activity at 50°C and pH 6.5. The enzyme *Ps*GH43_12 was more stable than several previously reported arabinofuranosidases as it exhibited activity in a broad pH range (pH 5 - 9) and broad temperature range (35 - 55°C). The substrate specificity analysis of *Ps*GH43_12 revealed higher activity against soluble arabinoxylan substrates. The enzyme displayed specific activities, 88.7 U/mg and 78.9 U/mg, against rye arabinoxylan and wheat arabinoxylan, respectively under optimized conditions. The analysis of the kinetics parameters of *Ps*GH43_12 against rye arabinoxylan gave K_m, 3.02 mg/ml and $V_{max,}$ 103 µmole/min/mg. *Ps*GH43_12 also displayed the activity against 4-*p*NP-α-L-arabinofuranoside with V_{max} 100.7 U/mg, K_m 2.17 mM, and k_{cat}/k_m 50.27 s^{-1} mM^{-1}. The metal ions, Mg^{2+}, Ca^{2+}, Li^{+} or Na^{+} at 10 mM concentration markedly enhanced the activity of *Ps*GH43_12 by 54%, 33%, 15% or 11%, respectively. The TLC analysis displayed the release of only L-arabinosyl moiety from rye arabinoxylan after *Ps*GH43_12 hydrolysis confirming its specificity towards α-L-arabinofuranoside.

The TLC, HPLC and Mass spectrometric analysis of *Ps*GH43_12 hydrolysed products of rye arabinoxylan showed the release of arabinose residue present as side chain substitution in arabinoxylan. The regioselectivity analysis of *Ps*GH43_12 action towards arabinoxylan by NMR revealed the release of α- L-Araf substitution at O3 and O2, O3 position and therefore, it was classified as type III α- L-arabinofuranosidase. The enzymatic saccharification of mild alkali pretreated finger miller stalk (FMS) by *Ps*GH43_12 in combination with xylanase (*Ct*Xyn11A) from

Clostridium thermocellum and xylosidase (*Bo*GH43) from *Bacteroides ovatus* resulted in a 2-fold increase in the TRS yield (148 mg/g) in 24 h as compared with TRS yield (70 mg/g) produced by xylanase (*Ct*Xyn11A) and xylosidase (*Bo*GH43) in 56h. *Ps*GH43_12 in combination with both xylanase and xylosidase released the maximum concentration of total reducing sugar from pretreated finger millet stalk displaying the synergistic effect of three enzymes. The TLC analysis of the pretreated FMS hydrolysed by mixture of *Bo*GH43 and *Ct*Xyn11A showed xylooligosaccharides and xylose. However, the addition of *Ps*GH43_12 to above combination gave mostly xylose and arabinose sugars. All these results confirmed the synergistic behaviour of the three enzymes. Thus the utilization of these three enzymes for enzymatic saccharification of lignocellulosic biomass in a synergistic manner can be exploited for higher scale bioethanol production.

Chapter 4 describes the structure and molecular dynamics of α-L-arabinofuranosidase (*Ps*GH43_12) of family 43 glycoside hydrolase, subfamily 12 from *Pseudopedobacter saltans*. *Ps*GH32_12 is the first α-L-arabinofuranosidase from *Pseudopedobacter saltans*. The 3D structure of α-L-arabinofuranosidase (*Ps*GH43_12) of a family 43, glycoside hydrolase from *Pseudopedobacter saltans* modeled by comparative modeling was compact and stable. Ramachandran plot showed 95.7% residues in favored and 3.3% in the generously allowed region and only 1% residues in the disallowed region. The modeled *Ps*GH43_12 structure displayed 5-bladed β-propeller fold at N-terminal and β–sandwich fold at C terminal. The secondary structure analysis of *Ps*GH43_12 by circular dichroism revealed 2.7% α-helices 30.33% β-strands and 66.97% random

coils. The *Ps*GH43_12 modeled structure displayed 5-bladed β–propeller fold at N-terminal and β–sandwich fold at C terminal. The docking studies revealed that the active site of *Ps*GH43_12 can accommodate xylotetraose, followed by, xylotriose, arabinoxylotriose, arabinoxylobiose, arabinoxylotetraose, xylobiose and arabinose. Molecular docking analysis confirmed the involvement of active site residues Asp71, Asp180 and Glu247 in the catalysis, which was also confirmed by the site-directed mutagenesis of these residues. The protein melting study of *Ps*GH43_12 showed complete unfolding at 65°C and did not require any metal ion for its stability. SAXS analysis displayed that *Ps*GH43_12 is monomeric and a fully folded state in solution form. Guinier analysis gave the radius of gyration between (Rg) 2.8 ± 0.09 nm at 5 mg/ml protein concentration. The maximum dimension and Rg of *Ps*GH43_12 estimated from P(R) plot were 9.0 nm and 2.81 nm, respectively. Kratky plot analysis of *Ps*GH43_12 displayed a fully folded state in solution form. The *ab initio* derived dummy model of *Ps*GH43_12 displayed a bell-like shape. The *ab initio* derived dummy model superposed well with its comparative modeled structure except the N-terminal His_6-tag region.

Chapter 5 gave insights about the efficient hydrolysis of sugarcane bagasse (SB) by endo-β-xylanase (*Ct*Xyn11A), α-L-arabinofuranosidase (*Ps*GH43_12) and xylosidase (*Bo*GH43). The SAA pretreatment gave the least hemicellulose loss than other pretreatments including alkali pretreatment. Moreover, SAA gave the maximum TRS yield of 8.3 mg/g of unoptimized SAA ptd SB after saccharification by endo-β-1,4-xylanase, *Ct*Xyn11A. The optimized conditions for SAA pretreatment process by Box-Behnken design were aqueous ammonia concentration, 18.5% wt%, temperature,

70°C solid to liquid (S/L) ratio of 1:9 and the incubation time period, 14 h. The TRS yield after *Ct*Xyn11A saccharification of optimised pretreated SAA was 15.3 mg/g of optimized SAA pretreated SB. Out of 100 g of pretreated biomass, the remaining 78 g of solid residue of SB contained 17.5 g (22.4%) hemicellulose. The FTIR and FESEM analyses of the SAA pretreated SB confirmed the structure disruption and delignification. The first step of saccharification of SB by *Ct*Xyn11A and *Ps*GH43_12 gave $TRS_{(XOS)}$ yield of 93.2 ± 3.2 mg/g ptd SB. The second step saccharification by xylosidase (*Bo*GH43) gave final TRS yield of 164.7 mg/g of ptd SB. The HPLC analysis of released products after second step saccharification displayed 69.6% conversion of xylan to xylose. This study demonstrated the optimization of pretreatment method and enzymatic saccharification by recombinant hemicellulases, resulting in efficient saccharification of 73.5% from SB. The future prospective of the study can be the use of this hydrolysed product for xylitol and bioethanol fermentation. These pretreatment and saccharification conditions can be used for large scale hydrolysis of the biomass.

CONTENTS

Statement……..……..……..... i
Certificate……... iii
Acknowledgements……..... v
Synopsis…….. vii
Contents……...……... xvii

Chapter 1. General Introduction **1**
1.1. Bioeconomy…….…….... 1
1.2. Plant cell wall……..……... 3
1.3. Hemicellulose…...……..…….. 3
1.4. Arabinoxylan…… 6
1.5. Hemicellulases…….. 9
1.6. α-L-arabinofuranosidase ……...……. 9
1.7. Microorganism…….. 12
1.8. Industrial applications of α-L-arabinofuranosidase…… 13
1.8.1. Quality enhancement of the bread…… 14
1.8.2. Flavor enhancement in juices and wine…… 15
1.8.3. Arabinoxylan and arabinoxylan oligosaccharide (AXOS) as prebiotic 16
1.8.4. Production of sugar alcohols from agricultural wastes 17
1.9. Significance of the investigation……..…… 19
1.10. Objectives of the present study 20
1.10.1. Specific objectives of the present study 21
1.11. References 22

Chapter 2. Cloning, expression and purification of first α-L-arabinofuranosidase of family 43 glycoside hydrolase, (*Ps*GH43_12) from *Pseudopedobacter saltans* DSM12145 **33**
2.1. Introduction……..... 33
2.2. Material and methods…… 36
2.2.1. Chemicals, reagents, kits and bacterial strains..... 36
2.2.2. Sequence analysis of *Ps*GH43_12……..... 37
2.2.3. PCR amplification of gene encoding *Ps*GH43_12…….. 37
2.2.4. Agarose gel electrophoresis of PCR amplified products…… 38
2.2.5. DNA loading dye buffer……... 39
2.2.6. Extraction of DNA from agarose gel…… 40
2.2.7. Preparation of culture medium……. 41
2.2.8. Preparation of *E. coli* DH5α competent cells…… 42
2.2.9. Cloning of gene encoding *Ps*GH43_12 into pET28a(+) vector…… 43
2.2.10.Restriction digestion of PCR amplified gene encoding for *Ps*GH43_12 and pET28a(+) vector DNA…….. 44

2.2.11.Ligation of restriction digested gene encoding *Ps*GH43_12 insert into pET-28a(+) vector……..... 45
2.2.12. Transformation of ligated recombinant DNA into *E. coli* DH5α cells……... 46
2.2.13. Isolation of plasmid DNA from transformed colonies by miniprep... 47
2.2.14. Screening of recombinant plasmid DNA for positive clone by restriction digestion..... 48
2.2.15. Transformation and expression of protein *Ps*GH43_12 in *E. coli* BL-21(DE3)..... 49
2.2.16. Recombinant *Ps*GH43_12 protein expression analysis by SDS-PAGE……..... 49
2.2.17 Purification of recombinant *Ps*GH43_12 protein 50
2.2.18 Protein concentration determination of purified *Ps*GH43_12 protein by UV method..... 52
2.2.19 Protein concentration determination of purified protein *Ps*GH43_12 by Bradford method..... 52
2.3. Results and Discussion……..... 54
2.3.1. Sequence analysis of *Ps*GH43_12 ……..... 54
2.3.2 PCR amplification of gene encoding *Ps*GH43_12……. 55
2.3.3 Digestion of PCR insert DNA and vector DNA by restriction enzyme. 55
2.3.4 Cloning of gene encoding *Ps*GH43_12 into pET-28a (+) vector..... 56
2.3.5 Expression and purification of recombinant protein……... 60
2.3.6 Protein Estimation of purified *Ps*GH43_12 recombinant ……. 61
2.4. Conclusion…….. 62
2.5. References…… 63

Chapter 3. Biochemical characterization, regioselective and synergistic action of α-L-arabinofuranosidase of family 43 glycoside hydrolase (*Ps*GH43_12) from *Pseudopedobacter saltans* **67**
3.1. Introduction……..... 67
3.2. Material and methods…….. 70
3.2.1. Microbes, plasmids and chemicals ……..... 70
3.2.2. Enzyme assay ……..... 70
3.2.2.1. Against natural substrates…… 70
3.2.2.2. Against synthetic substrates 70
3.2.3. Biochemical characterization of α-L arabinofuranosidase **(***Ps*GH43_12**)**……..... 71
3.2.3.1. pH and Temperature optimization…… 71
3.2.3.2. pH and Temperature stability……... 72
3.2.3.3. Substrate specificity and kinetic parameters of *Ps*GH43_12….. 72
3.2.3.4. Effect of metal ion on *Ps*GH43_12 activity..... 73
3.2.3.5. Mode of action analysis of *Ps*GH43_12 by TLC, mass spectrometry and HPLC..... 73
3.2.4. Regioselectivity analysis of *Ps*GH43_12 towards rye arabinoxylan….. 74
3.2.5. Synergistic behaviour of *Ps*GH43_12……..... 75

3.3. Results and discussion……..... 77

3.3.1. pH and temperature optimization of *Ps*GH43_12…… 77
3.3.2. pH and temperature stability of *Ps*GH43_12…… 77
3.3.3. Substrate specificity and kinetic parameters of *Ps*GH43_12……... 79
3.3.4. Effect of metal ions on *Ps*GH43_12 activity ……... 81
3.3.5. Mode of action analysis of *Ps*GH43_12 by Thin layer chromatography. 82
3.3.6 Regioselectivity analysis of *Ps*GH43_12 towards rye arabinoxylan..... 83
3.3.7 Synergistic behaviour of *Ps*GH43_12 85
3.4. Conclusion…… 89
3.5. References……..... 90

Chapter 4. Structure and dynamics analysis of α-L-arabinofuranosidase (*Ps*GH43_12) from *Pseudopedobacter saltans* by Computational modeling and Small angle X-ray scattering **95**

4.1. Introduction…….…….. 95
4.2. Material and methods..……...…….. 98
4.2.1. 4.2.1 Chemical, reagents and substrates ……. 98
4.2.2. Amino acid sequence retrieval and analysis…… 98
4.2.3. Comparative modeling, refinement and structure assessment of *Ps*GH43_12……..... 98
4.2.4. Molecular dynamic simulation of the *Ps*GH13_12 structure…….. 99
4.2.5. Molecular docking analysis of *Ps*GH43_12……. 100
4.2.6. Secondary structure and protein melting analysis of *Ps*GH43_12…….. 101
4.2.7. Small Angle X-ray Scattering Analysis (SAXS) of *Ps*GH43_12…… 102
4.2.8. Mutation of active site residues by site-directed mutagenesis…… 103
4.2.9. Purification of *Ps*GH43_12 mutants…… 104
4.2.10. Enzyme assay…….. 105
4.3. Results and discussion…….. 107
4.3.1. Sequence analysis of *Ps*GH43_12……..... 107
4.3.2. Structure modeling of *Ps*GH43_12 and validation ……. 109
4.3.3. Molecular dynamics simulation analysis of *Ps*GH43_12…… 110
4.3.4. Molecular docking analysis of *Ps*GH43_12……. 112
4.3.5. Secondary structure and protein melting analysis of *Ps*GH43_12……..…….. 116
4.3.6. Low-resolution structure analysis of *Ps*GH43_12 by Small Angle X-ray Scattering……... 118
4.3.7. Active site mutation by site directed mutagenesis 122
4.4. Conclusion…… 123
4.5. References…… 125

Chapter 5. Hemicellulose saccharification from Sugarcane bagasse by recombinant hemicellulases **129**
5.1. Introduction…….. 129
5.2. Material and methods…… 132
5.2.1. Chemical, reagents and substrates …….. 132
5.2.2. Biomass processing ……..... 132
5.2.3. Pretreatment of SB …….. 132
5.2.3.1. Alkaline pretreatment……... 132
5.2.3.2. Microwave assisted inorganic salt (MAIS) pretreatment using NaCl and $FeCl_3$..... 133
5.2.3.3. Soaking in aqueous ammonia (SAA) pretreatment …..... 133
5.2.4. Purification and activity assay of recombinant hemicellulases..... 133
5.2.5. Selection of best pretreatment method…….. 134
5.2.6. Optimization of SAA pretreatment …….. 135
5.2.7. FTIR analysis of untreated and pretreated SB…….. 135
5.2.8. Field emission scanning electron microscopic (FESEM) imaging of untreated and pretreated SB……. 135
5.2.9. Optimization of enzymatic saccharification……. 135
5.2.10. The TLC analysis…… 136
5.2.11. Determination of released products after second step saccharification by HPLC……. 137
5.3. Results and discussion…….. 139
5.3.1. Hemicellulose content determination ……..... 139
5.3.2. Purification and activity assay of recombinant hemicellulases ……. 140
5.3.3. Selection of best pretreatment based on saccharification by *Ct*Xyn11A…… 140
5.3.4. Optimization of soaking in aqueous ammonia (SAA) pretreatment…… 141
5.3.5. FTIR spectroscopic analysis of untreated and pretreated SB…..... 141
5.3.6. FESEM analysis of untreated and pretreated SB…….. 142
5.3.7. Optimization of hemicellulose hydrolysis of pretreated SB in the first step by *Ct*Xyn11A and *Ps*GH43_12 ……... 143
5.3.8. Optimization of hydrolysis of XOS produced in first step of saccharification from pretreated SB by *Bo*GH43 in the second step…... 147
5.3.9. Thin layer chromatography (TLC) analysis of hydrolysed products….. 149
5.3.10. Monosugars analysis after second step of saccharification by HPLC 150
5.3.11. Overall mass balance…….. 151
5.4. Conclusion…… 153
5.5. References……..... 154

List of publications …… xxi
List of conferences…….. xxiii
Vitae …… xxvii

Chapter 1

General Introduction

1.1 Bioeconomy

Indian economy is based on agriculture. More than 50% of Indian population directly depends on agriculture for their livelihood. Owing to the diversity in the climate, different crops are grown in a year in India. Majorly wheat, rice, maize, sugarcane, barley, sorghum, etc. are the crops grown in India (Birthal et al., 2014). The edible portion of the plant is used to derive energy for metabolic functioning of living being whereas; non-edible part is coined as agro waste. Annually, the worldwide production of lignocellulosic biomass is approximately, 200 billion tons from agriculture sector (Guo et al., 2010) whereas, every year 200 million tons of lignocellulosic agricultural biomass is generated in India (Singh and Gu 2010). The enormous amount of agro-waste produced every year is neither adding any economic benefits to the farmer nor is good for the environment. Several waste management strategies are practiced such as landfills, incineration, pyrolysis, etc. Some of these methods of waste management cause environmental pollution. To fulfil the great

energy demands, the best possible way is to utilize lignocellulosic wastes to produce energy. The energy demand is rapidly increasing. In 2010 the demand was of 13 billion tons of oil equivalent and it is expected to increase to 45 billion tons of oil equivalent by 2050 (Zhang and Konan 2010). As Per energy information administration, 2018 the demand of energy in India is approx 0.916 billion tons of oil equivalent as compared to world demand of approx 15 billion tons of oil equivalent. The use of non-renewable energy sources such as coal, oil and natural gas to fulfil energy demand will cause depletion in their reservoirs. This also leads to an increase in fuel price with increasing demand.

To accomplish the energy requirement, focus is on renewable sources such as nuclear energy, wind energy, hydro energy, solar energy and bioenergy. Bioenergy contributes the highest share, i.e. 14% out of 18% of total renewable energy supply (Berndes et al., 2003). Bioenergy is harvested either from forest biomass or from agricultural residues. The lignocellulosic residues collected from the agricultural field can be transformed into the source for energy such as methane, bioethanol, butanol, biodiesel and biohydrogen, etc. The essential step for plant biomass conversion to biofuel is the breakdown of its complex structure. Plant cell wall consists primarily of carbohydrates, protein and lignin. The carbohydrate part contains cellulose, which occurs in highest amount, composed of glucose. This is followed by hemicellulose, which is heterogeneous, and the backbone is generally consisted of chains of xylose, glucose or mannose containing the side chains. In plants, besides cellulose and hemicellulose, pectins are also available in their cell wall. All these polysaccharides differ from each other, based on composition of sugar residues and the kind of linkages among them. The hydrolysis of glycosidic bond present in a polysaccharide

by specific enzymes releases fermentable reducing sugars. These monosaccharides are fermented by fermenting microbes for biofuels production. Bioethanol is a substitute of fossil fuels that shares the sale of around 58 billion dollars per year in the world market. For fulfilling energy, demand global production of bioethanol is $8.6x10^7$ ton/year (Burk 2010). In most of the countries, the use of biofuels as a sustainable alternative is promoted for decreasing the depletion of fossil fuels and thus emission of hazardous gases.

1.2 Plant cell wall

The cell wall of the plant is a semi-rigid and complex structure. It is the outer most layer of the cell that plays key role in exchange of the substances necessary for cell metabolism and also in excretion of other waste substances from the cell. The cell wall is crucial for maintaining the cell structure and cell protection (Carpita and Gibeaut 1993). Cell wall acts as a buffer and between protoplasm and environment and is essential for cell signaling and cell-cell adhesion. It is a source of nutrition, fiber and energy. Plant cell wall is mainly composed of carbohydrates and also contains protein, lignin and water. Carbohydrate component of the cell wall is cellulose, hemicellulose and pectin. Cellulose is a linear homopolymer of glucose, whereas, the hemicelluloses are an important group of polysaccharides, which are interconnected and also connected to cellulose and pectins. The most significant hemicelluloses are xylans, arabinoxylans, mannans, galactomannans, arabinogalactan II. The major constituent of the primary walls of non-woody plant cells is pectin and is rich in most vegetables and fruit giving strength and flexibleness to the cell wall. The principal components of pectin are homogalacturonan and the substituted rhamnogalacturonan I and rhamnogalacturonan II (Dhillon et al., 2016).

1.3 Hemicellulose

Hemicellulose belongs to a group of diverse polysaccharides, which are assembled through a biosynthetic pathway distinct from that of cellulose. The vital biological role of hemicelluloses is to provide strength to the cell wall by interacting with cellulose and lignin (Scheller and Ulvskov 2010). The amount of hemicellulose of the dry weight of wood is frequently between 20 and 40%. Noticeable changes have been reported in the composition and content of hemicellulose within stem, branches, roots and bark.

Xylan belongs to the second most abundant structural component of the secondary walls of dicot plants. Xylan has a backbone of β-(1→4)-linked xylose residues. In general, xylans are found with numerous degree of substitution (Fig.1.1) based on the plant tissue types and species. The common side chain substitutions on the backbone are arabinose, acetic acid, glucuronic acid, ferulic acid, *p*-coumaric acid or 4-O-methyl glucuronic acid (Ordaz and Saulnier 2005). Depending on the relative richness of their substitutions within the xylan, it is further categorized into glucuronoxylan, arabinoxylans and xyloglucans etc. Arabinose and uronic acid chains stabilize the xylan structure against alkali-catalyzed deterioration. Hemicellulose contains various more prominent substitutions in the chains as an alternative for hydroxyl groups present at positions C2, C3 and C6 (Sjöström and Alén 2013).

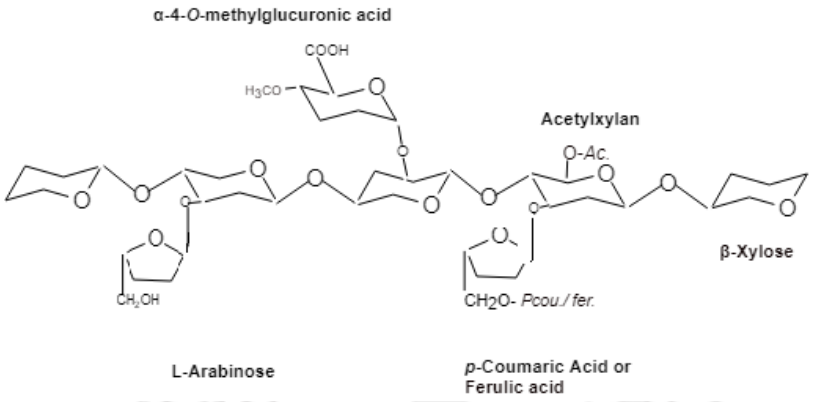

Fig. 1.1 Structure of heteroxylan showing different substitutions.

Glucuronoxylan is polymer of linear D-xylopyranosyl residues connected by β (1→4) glycosidic bonds. The glucuronate residue (generally methylated at C4 position) are attached by α2-3 linkage to many of the xylose residues of the backbone. At position C2, most of the xylans have substitution of single 4-O-methyl-α-D-glucuronic acid residues. This structure is usually referred to as 4-O-methyl-D-glucurono-D-xylan (Sjöström and Alén 2013).

Xyloglucan has a backbone of β-(1→4)-glucose residues, linked with β-(1→6)-D-xylose side chains. The primary cell wall of dicotyledonous plants consists of xyloglucan. Xyloglucan has a property to bind with cellulose microfibrils and therefore, xyloglucan-cellulose interactions are important determinants of the mechanical strength as well as the growth of cell wall (Cosgrove 2005).

Arabinoxylan (AX) is a non-starch polysaccharide, mainly found in cereal plants, considered as dietary fiber. Arabinoxylans have the β-(1→4)-linked xylose backbone with the substitution of one or more L-arabinofuranosyl units (Fig. 1.2), at position 2 or 3. AX is located in primary cell walls of grasses and monocot plants cereals like wheat, rye, barley, oat, rice, corn and sorghum (Brett and Waldron 1990). L-arabinosyl residues are extensively found in these polymers as side chains. The presence

of L-arabinosyl side chain hinders the enzymes, in the hydrolysis of hemicelluloses and pectins causing a technological bottleneck for the advancement of various industrial processes (Saha 2000).

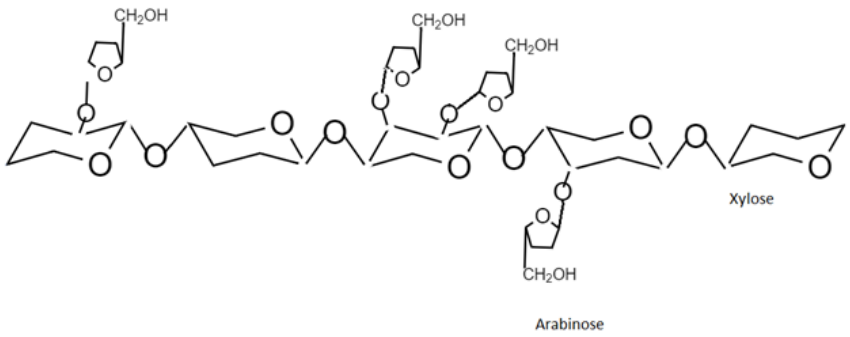

Fig. 1.2 Structure of arabinoxylans

Degradation of plant cell wall makes a nutrient pool available for recycling. Nature has gifted a diverse group of microorganisms with enzymes to disrupt the plant cell wall polysaccharides (Ochiai et al., 2007). Principally fungi and bacteria are responsible for the cell wall polysaccharides deterioration. Few insects and molluscs also release enzymes that act on the plant cell wall (Lynd et al., 2002). Due to the heterogeneous nature of hemicellulose, a single enzyme is not sufficient for the complete hydrolysis. Therefore, several enzymes are required for complete degradation of plant biomass. Some enzymes act on hemicellulose main chain and some act on the side chain. Side chain removing enzymes are essential as they act synergistically and enhance the rate of hydrolysis by other glycoside hydrolases.

1.4 Arabinoxylan

Arabinoxylan (AX) is an elemental part of plant cell wall, which is the non-starch polysaccharide and is non-digestible. All main cereal grains, including rye, wheat, rice, barley, oats, sorghum, maize are rich in AX (Izydorczyk and Biliaderis

1995). Moreover, it is present in other plants, such as psyllium (Fischer et al., 2004), rye grass and bamboo shoots (Dotsenko et al., 201; Zelaya et al., 2017). In the common cereal grains, the maximum amount of AX is present in rye followed by wheat, barley, oats, rice and sorghum (Table 1.1). In cereals, starchy endosperm, aleurone, bran tissues and some cereal's husk contain arabinoxylans in bulk. The content of arabinoxylan also depends on genetic and environmental factors (Holtekj∅ len et al., 2008). It has been reported that arabinoxylan content in wheat, rye and barley contains genotypic and environmental variations (Lempereur et al., 1997). However, the deciding factor is genus and species they belong, the amount of arabinoxylans and its molecular structure in a precise tissue may alter.

Table 1.1 Arabinose and xylose composition in different cereals.

Cereals	Arabinose quantity (%)	Arabinose/Xylose ratio	References
Rye	6.9-7.6	0.74 – 1.1	(Deryilly et al., 2001)
Wheat	5.5- 7.1	0.6	(Stone et al., 2009)
Barley	4 -5.4	0.7	(Izydorczyk and Dexter 2008)
Rice	2-3	0.8- 0.9	(Rao and Muralikrishna 2007)
Maize	1-2	0.8	(Freitas et al., 2003)
Oats	2- 2.7	--	(Hashimoto et al., 1987)
Sorghum	1.8	0.9	(Holtekj∅ len et al., 2008)

α-L-Arabinofuranosyl residues are linked to a few of the xylopyranosyl unit of backbone at 2, 3, or at both 2,3 positions (Fig. 1.2). Due to these conformations of arabinofuranosyl residues, four different molecular structures of AX exist: mono substituted xylopyranosyl at 2 or 3, disubstituted xylopyranosyl at 2,3 and without any substitution xylopyranosyl. The most of AX contains higher number of arabinofuranosyl substitution as mono substitution, while, a few AX contains two or more arabinofuranosyl residues attached by 1-2, 1-3, and 1-5 linkages. The secondary walls in the pericarp and testa tissues of bran contains other substitution of 4-O-methyl

glucuronic acid at C-2 position along with arabinose substitution at C-3 position and make a structure called (arabino)glucuronoxylans (AGX). In comparison to common cereals, AX from rice, sorghum, finger millets and maize bran are more complicated (Rao and Muralikrishna 2004; Ebringerova and Heinze 2000). They may contain ample amounts of glucuronic acid residues linked at O-2 and are specified as (glucurono)arabinoxylans (GAX). Sorghum GAX contains two additional arabinofuranosyl residues substituted at position C3 to the xylan backbone along with the arabinose substitution at position C2. The side chain substitution in Corncob AGX contains traces of xylopyranose, galactopyranose and α-D-glucuronic acid or 4-O-methyl-α-D-glucuronic sugar units in addition to arabinose units. The terminal xylose residue of corncob AGX substituted with one xylose and arabinose residue (Faulds et al., 1995).

AX exhibits various important characteristics like viscosity improvement, formation of a gel, stabilization of foam, absorption of water, restoration of fat, and prebiotic properties (Izydorczyk and Biliaderis 1995). As an ingredient of dietary fiber in cereals, AX enhances the nutritional value of foods by offering both soluble and insoluble fiber. Moreover, presence of the phenolic content in AX molecular structures, imparts antioxidant properties (Katapodis et al., 2003). The dietary fibers are essential for human health as they can lower down the blood cholesterol, regulate the level of blood glucose, show anti-cancer activity (Kendall et al., 2010) and are also effective against the proliferation of colorectal cancer (Samuelsen et al., 2011). On enzymatic treatment of AX arabino-xylooligosaccharides (AXOS) are produced which are described as potential prebiotics (Grootaert et al., 2007; Hughes et al., 2007). Due to the presence of AX in majority of cereals, it constitutes a compelling part of

ingested human dietary fiber. Agricultural by-products with less economic value, such as stalks, distiller's grain, seed cake, straw, hulls and husk of various grains, or banana peels, are potential sources of AX and other xylans.

1.5 Hemicellulases

Hemicellulases are a divergent group of enzymes which hydrolyse hemicelluloses, Hemicellulases include endo-β-1,4-xylanase, β-1,4-xylosidase, α-L-arabinofuranosidase, α-1,5-arabinanase, α-glucuronidase, β-1,4-mannanase, β-1,4-mannosidase, α-galactosidase, β-glucosidase, Endo-galactanase, acetyl mannan esterase, acetyl xylan esterase, ferulic acid esterase and *p*-coumaric acid esterase (Beg et al., 2001). Arabinose side chain is widely distributed in hemicellulose and pectins linked with cellulose and, thus to breakdown the integrity of plant cell wall it is necessary to remove this side chain. α-L-Arabinofuranosidase is one of the important hemicellulases, which cleaves α-L-arabinofuranosidic bond (1→2, 1→3 and 1→5) and plays a vital role towards complete degradation of hemicellulose and pectins by acting synergistically with other hemicellulases and pectic enzymes (Margolles-Clark et al., 1996).

1.6 α-L-arabinofuranosidase

α-L-Arabinofuranosidase is of two types endo α-L-arabinofuranosidase (EC 3.2.1.99) and exo α-L-arabinofuranosidase (EC 3.2.1.55). Endo α-L-arabinofuranosidase (EC 3.2.1.99) cleaves α (1→5) arabinofuranosidic linkage in arabinans, whereas, exo α-L-arabinofuranosidase (EC 3.2.1.55) cleaves the arabinose side chain from arabinose substituted polysaccharides (Wilkens et al., 2017). Exo α-L-Arabinofuranosidase (EC 3.2.1.55) are found in glycoside hydrolase (GH) families 2, 3, 43, 51, 54 and 62 (http://www.cazy.org/).

α-L-Arabinofuranosidase hydrolyses arabinofuranosyl residue present at the non-reducing end of AX (Fig. 1.3). As a result, arabinose is released in an exolytic mode from the substrates containing (1→2) and (1→3) α-L-arabinofuranosidic linkages (Saha 2000). The arabinose substitution in hemicellulose interact with cellulose, pectin and lignin make the structure complicated and provide strength to the biomass. The substitution of arabinose residue in hemicellulose and pectin hinders the activity of hemicellulolytic and pectinolytic enzymes. Therefore, α-L-arabinofuranosidase can be used in synergistic manner for the enhancement of plant biomass hydrolysis (Rye and Withers 2000; Shallom et al., 2002). Enzymatic hydrolysis releases soluble sugars, which are utilized by prokaryotic and eukaryotic microorganisms for the production of many value-added products like xylitol, bioethanol etc. (Margolles-Clark et al., 1996). The α-L-arabinofuranosidase does not differentiate on the basis of backbone to which arabinofuranosyl residues is attached and thus shows a wide range of substrate specificity (Rahman et al., 2003).

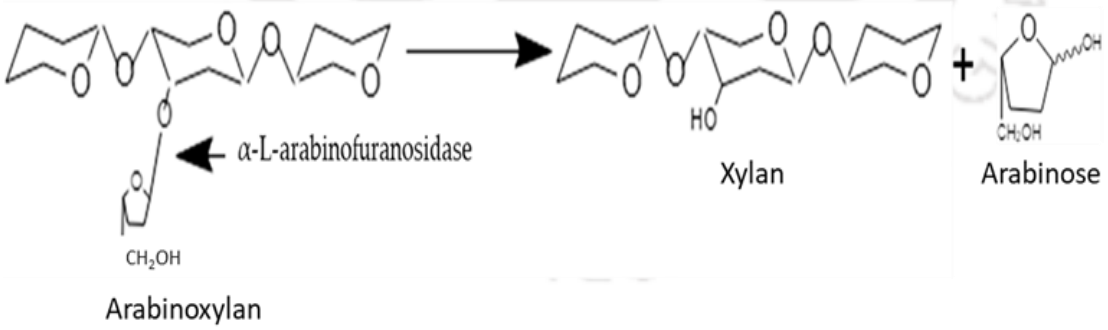

Fig. 1.3 Mode of action of α-L-arabinofuranosidase

α-L-Arabinofuranosidase hydrolyzes glycosidic bond by acid-base catalysis by employing two modes of action, firstly by either overall retention or by an inversion of the anomeric configuration (de Groot et al., 2003). It hydrolyzes the glycosidic linkage

by a double-displacement mechanism in two steps. Glycosylation is the first step in which, glycosidic oxygen is protonated and leaving group is stabilized by acid-base residue, which works as a general acid. Nucleophilic residue (Glutamic Acid) attacks the anomeric carbon of the scissile bond, and a covalent substrate-enzyme intermediate is formed with the opposite anomeric configuration of the glycosyl residue of the substrate. In the subsequent step of deglycosylation, a water molecule activated by acid-base residue behaves like a general base. The anomeric center of the substrate-enzyme intermediate is attacked by activated water molecule along the same direction of the original bond, releasing the L-arabinose, and maintain anomeric configuration with overall retention (Ferchichi et al., 2003; Hövel et al., 2003). The arabinose residue in the side chain of hemicelluloses and pectins form cross-linking within the plant cell wall structure. The occurrence of arabinose side chains also hinders the structure and function of hemicelluloses and pectins (De Vries et al., 2000). Due to their intrinsically more flexible water-hungry furanose conformations, they reduce the interaction between polymer chains. For the efficient hydrolysis of arabinose containing polysaccharide and industrial point of view there is a need to find more thermostable α-L-arabinofuranosidase. The biochemical properties of recombinant α-L-arabinofuranosidase from various fungi and bacteria are listed in (Table 1.2).

Table 1.2 Biochemical properties of α-L-arabinofuranosidase derived from different microorganisms

Organism	Mol mass (kDa)	Optimum Temp (°C)	Optimum pH	GH Family	References
Fungus					
Humicola insolens	50.6	50	5.0	43	Yang et al., 2015
Penicillium purpurogenum ABF 4	68.0	50	4.6	54	Ravanal and Eyzaguirre 2015
Aspergillus vadensis	53.0	60	3.5	54	Culleton et al., 2014
Penicillium chrysogenum 31B	31.0	35	5.0	43	Shinozaki et al., 2014
Chaetomium sp.	52.9	70	5.0	43	Yan et al., 2012
Aspergillus niveus	69.8	70	4.0-5.0	51	de Lima Damásio et al., 2012
Penicillium chrysogenum	35.0	40-50	5.0	62	Sakamoto et al., 2011
Bacterium					
Clostridium thermocellum B8	50	50	5-6	43	de Camargo et al., 2018
Clostridium thermocellum	34	50	5.4	43	Ahmed et al., 2013
Cellvibrio japonicus	-	25	7.0	43	Cartmell et al., 2011
Thermomicrobia bacterium	350	70	6.0	51	Birgisson et al., 2004
Bifidobacterium breve K-110	60	45	4.5	-	Shin et al., 2003
Bifidobacterium longum	260	45	6	51	Margolles and Clara 2003
Thermobacillus xylanilyticus	56	75	5.6-6.2	51	Debeche et al., 2000

1.7 Microorganism

Strains of the genus *Pseudopedobacter* are heparinase-producing, obligately aerobic, mesophillic, Gram-negative rods (Fig.1.4). *Pseudopedobacter saltans* can be phenotypically differentiated from most *Pedobacter* strains for its inability to assimilate D-cellobiose and the ability to utilize glycerol (Gallego et al., 2006 and Liolios et al., 2011). It has been isolated from the soil and belongs to phylum bacteroidetes, class sphingobacteria, order spingobacteriales and family sphingobacteriaceae.

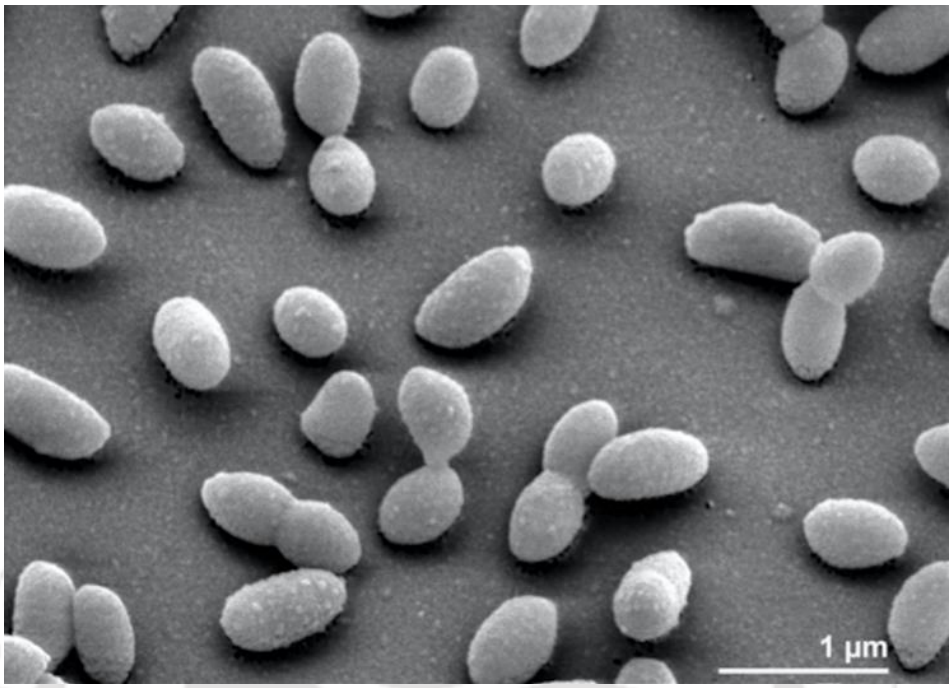

Fig. 1.4 Scanning electron micrograph of *P. saltans* strain 113T (Liolios et al., 2011).

1.8 Industrial applications of α-L-arabinofuranosidase

α-L-Arabinofuranosidase has several industrial applications (Fig 1.5). It is used in food and feed industry for extraction of coffee, starch and plant oils. It is also used in paper and pulp industry, bioethanol production, for enriching flavor of wine in brewing industry, for clarification of fruit juices in juice industry. Production of therapeutic compound for example, released arabinose inhibits intestinal sucrase and act as antiglycemic agent and arabinoxylan oligosaccharide is a potential prebiotic (Numan and Bhosle 2006) are also reported.

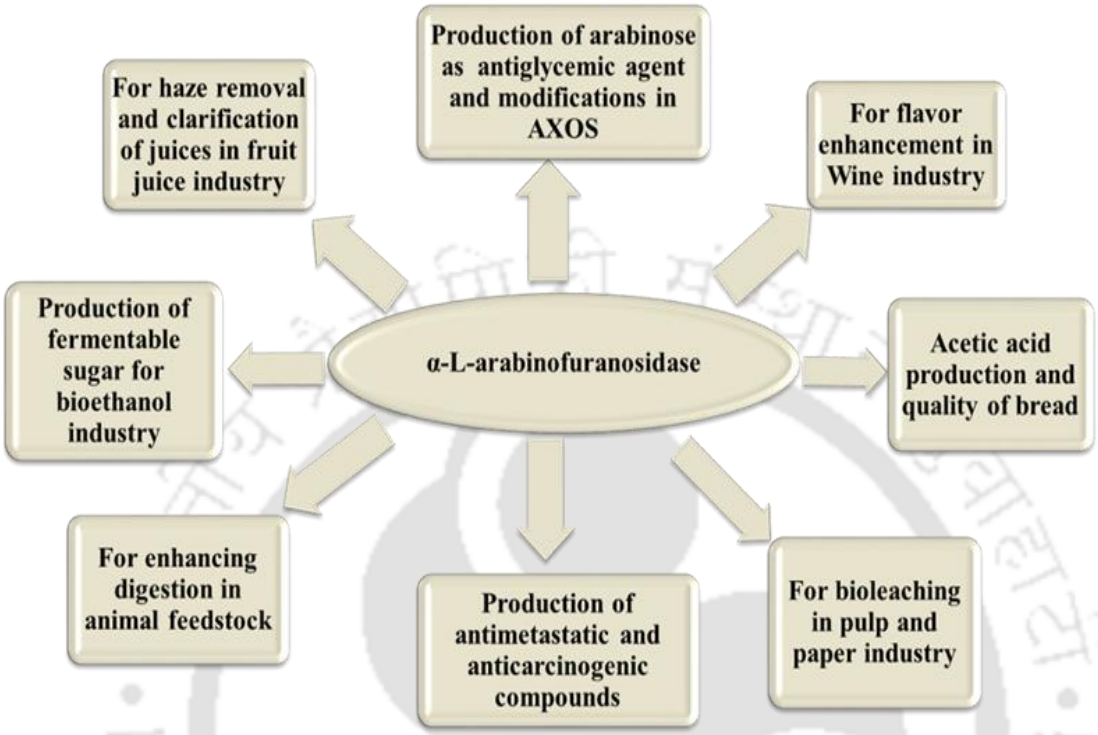

Fig. 1.5 Applications of α-L-arabinofuranosidase.

1.8.1 Quality enhancement of the bread

Wheat and rye flour are majorly used in bread making processes. AX content in wheat is 1.5-3% and 7-8% in rye, out of which water-soluble AX is present in very little quantity (Shewry et al., 2010; Gebruers et al., 2010). The arabinose residue present in arabinoxylan increases the water uptake and absorbs around 30% of water in dough, which reduces volume of dough and changes texture. In sourdough fermentation the solubilization of AX while fermentation contributes to the constructive effects on the bread quality (Yang et al., 2017). Pentosans are one of the necessary additives in bread that improve the texture of bread (Yegin et al., 2018). Wheat flour enzymes slightly hydrolyze the pentosans, which were added in the dough. Pentosans hydrolysis is further done by exogenic xylanolytic enzymes

including α-L-arabinofuranosidase added to the dough (Fessas and Schiraldi 1998), resulting in the release of free pentosans, which is further used by a sourdough lactic acid bacterium. During the sourdough fermentation, the arabinofuranosidases release arabinose and also synergistically enhance the activity of other enzymes. The soluble carbohydrates availability increases, thus acidification and acetic acid production also increases. The quality of bread is improved by α -L-arabinofuranosidase, pentosanase and other enzymes, which have been investigated as natural supplements (Gobbetti et al., 2000). The treatment with arabinofuranosidase releases the trapped water in AX, which improves dough handling, crumb structure and increases the dough volume and thus delays the staling of bread and enhance the bread shelf-life. The improved bread quality and shelf life gives economic benefits to the bread industries (Bosetto et al., 2016; Jiménez and Martinez-Anaya 1999).

1.8.2 Flavor enhancement in juices and wine

Aromatic compounds are one of the important constituents of wine. Fermenting microbes like yeast and bacteria produce aromatic compounds during fruits fermentation. The fruits used in wine industry including grapes produce volatile compounds along with some non-volatile compounds. These volatile compounds are responsible for aroma in wine. The non-volatile compounds lose their aromatic properties because they are attached to carbohydrates as glycoconjugates and are thus flavorless (Zhu et al., 2017). The glycoconjugates are precursor of glycosidic aroma in wine. Glycoconjugates exist in the form of di-glycosides that are attached to monosaccharide moieties such as α-L-arabinofuranose, α-L-arabinopyranose, α-L-rhamnopyranose, β-D-apiofuranose, β-D-glucopyranose or β-D-xylopyranose (Guo et al., 1993; Williams et al., 1982). Terpene is one of the important aromatic molecules,

which is generally attached to α-L-arabinofuranose. α-L-Arabinofuranosidase hydrolyse monoterpene and give rise to volatile terpenes and L-arabinose (Mateo and Di Stefano 1997; Belda et al., 2017).

Fruits are rich in carbohydrate polysaccharides such as pectin and arabinan. The polysaccharides, proteins and polyphenols form precipitates during storage. α-L-Arabinofuranosidase is used for clarification of juices in fruit juice industry. For clarification of fruit juices, the pectinolytic enzymes are used in combination with α-L-arabinofuranosidase. The addition of α-L-arabinofuranosidase removes arabinose side chain from hemicelluloses that helps in the degradation of pectin and arabinan by pectinolytic enzymes and α-1,5 arabinanase respectively (Churms et al., 1983; De Vries et al., 1982). The enzymatic treatment enhances the solubility of juices by reducing the haze formation. The treatment of apple, grape, orange and peach juices with α-L-arabinofuranosidase and xylanase together cause improved clarity, reducing sugar content and juice yield (İlgü et al., 2018).

1.8.3 Arabinoxylan and arabinoxylan oligosaccharide (AXOS) as prebiotic

The arabinofuranosidase cleaves the arabinosyl residue present in the side chains of arabinoxylan backbone. Arabinoxylan oligosaccharide (AXOS) of varying backbone lengths and substitution of arabinose side chains can be produced by the action of xylanolytic enzymes. The breakdown of xylan produces short chain AXOS which are not completely hydrolyzed, and these oligosaccharides are beneficial for growth of probiotic bacteria. The degree of substitution and polymerization varies in AXOS depending on the source of arabinoxylan, which may be further modified by arabinofuranosidase and xylosidase treatment (Falck et al., 2018). The elucidation of relationship between structure and functions of AXOS with changing polymerization

and substitution is interesting area for investigation. Several species of bacteria found in human alimentary canal have been reported for producing the efficient enzymes to hydrolyze AX (Van Laere et al., 2000). Species, like lactobacilli, bacteroides and non-pathogenic clostridia, found in the intestine are efficient in hydrolysing complex carbohydrates. It was reported that species *Bacteroides ovatus* and *Bacteroides thetaiotaomicron* belonging to the *Bacteroides fragilis* group play a crucial role in the metabolism of carbohydrates, as they secrete several carbohydrate-active enzymes (Berg et al., 1978; Cummings and Macfarlane 1991). AXOS produced from rye and rye bran are reported to affect positively on the growth of various *Lactobacillus* strains (Koistinen et al., 2018). Besides prebiotic effect, AX and AXOS play a vital role in human health by lowering cholesterol level and the risk of type II diabetes and obesity by reducing postprandial glucose level (Amrein et al., 2003; Lu et al., 2000; Möhlig et al., 2005).

1.8.4 Production of sugar alcohols from agricultural wastes

Agricultural waste majorly contains cellulose, hemicellulose and lignin. The enzymatic production of alcohol from sugar upon release from lignocellulosic biomass is a promising alternative to the chemical process. The Saccharification of plant polysaccharides to monomeric sugars by enzymatic hydrolysis is reported earlier (Sartori et al., 2015). Cocktail of enzymes are required for complete hydrolysis of plant polysaccharides like cellulases, hemicellulases. Cellulases (endoglucanase, cellobiohydrolase and glucosidase) converts cellulose to glucose whereas, hemicellulases like xylanase, xylosidase and arabinofuranosidase releases xylose and arabinose from hemicellulose present in agricultural waste. L-arabinose released by arabinofuranosidase is converted to xylitol (Sakakibara et al., 2009). Released sugar,

undergo through hydrogenation reaction in presence of metal catalyst for production of sugar alcohols such as xylitol, arabitol, galatitol, sorbitol, mannitol etc. (Tathod and Dhepe 2015). Sugar alcohols are used as low calorie sweeteners, which have several properties such as very low glycaemic index, non-carcinogenicity, and they improve dental health, favour absorption of calcium ions and B vitamins etc. (Grembecka 2015).

1.9 Significance of the investigation

The increasing human population and pollution are the present day major challenges, extensive research in the food and fuel industry is one way of facing these challanges. Modern civilization is highly dependent on fossil fuel to fulfil its energy demand. However, owing to the limited stock of fossil fuel there is a need to find some alternative renewable source of energy. The concept of converting waste into energy can accomplish the energy needs and also help in reducing solid waste pool size. Several microorganisms have been reported for producing enzymes which can hydrolyse plant biomass (Table 1.2). The genome of *Pseudopedobacter saltans* was sequenced in 2011 (Liolios et al., 2011) and not explored much till date. Only a few enzymes, such as chondroitin AC lyase of family 8 polysaccharide lyase (Rani and Goyal 2016) and heparinase II/III of family 12 polysaccharide lyase (Balasubramaniam et al., 2018) from *Pseudopedobacter saltans* have been reported. However, one hemicellulosic enzyme, xylanase *Ps*GH10A of family 10 glycoside hydrolase was reported from this microorganism (Sharma et al., 2018). α-L-Arabinofuranosidases from various micoorganisms are reported to have applications in food, paper and fuel industries (Numan and Bhosle 2006). No α-L-arabinofuranosidase has been reported from *Pseudopedobacter saltans*. There is need to explore efficient enzymes from the new microorganisms by keeping industrial demands in mind. Arabinofuranosidases often display modular behaviour and their conformational dynamics, molecular arrangement and protein stability is still unknown. The gene encoding a putative α-L-arabinofuranosidase of family 43 glycoside hydrolase (GH43) was identified in *Pseudopedobacter saltans* genome. Therefore, in the proposed work, the gene encoding a family 43 glycoside hydrolase (GenBank Accession number

ADY53124.1) from *Pseudopedobacter saltans* will be cloned, expressed and purified. The biochemical and functional characterization of α-L-arabinofuranosidase of family 43 glycoside hydrolase from *Pseudopedobacter saltans* will be carried out. The structural characterization by computational and solution scattering method will be performed to determine the molecular organization and conformational dynamics. Further, α-L-arabinofuranosidase alone or in combination with other xylanolytic enzymes will be used in enzymatic saccharification of lignocellulosic biomass for bioethanol production.

1.10 Objectives of the present study

α-L-Arabinofuranosidase (*Ps*GH43_12) belonging to glycoside hydrolase family 43 (*Ps*GH43_12) (GenBank: Acc No. ADY53124) from *Pseudopedobacter saltans* is chosen for the study. The gene encoding putative α-L arabinofuranosidase (*Ps*GH43_12) will be cloned, expressed, purified and biochemically characterized. The amino acid sequence of *Ps*GH43_12 was analyzed and found to be new. The structure, molecular arrangement and conformational dynamics of modular arabinofuranosidase (*Ps*GH43_12) in solution are not known yet. Therefore, the *in silico* structure characterization and biophysical characterization of *Ps*GH43_12 for understanding its flexibility, conformational arrangement and the overall molecular organization in solution will be undertaken. The synergistic behaviour of *Ps*GH43_12 with other enzymes, xylanase and xylosidase for enhanced saccharification of hemicellulosic plant biomass will be investigated. The specific objectives of the proposed study are listed below.

1.10.1 Specific objectives of the present study

1. Cloning, expression and purification of first α-L-arabinofuranosidase of family 43 glycoside hydrolase, (*Ps*GH43_12) from *Pseudopedobacter saltans* DSM12145
2. Biochemical characterization, regioselective and synergistic action of α-L-arabinofuranosidase of family 43 glycoside hydrolase (*Ps*GH43_12) from *Pseudopedobacter saltans*
3. Structure and dynamics analysis of α-L-arabinofuranosidase (*Ps*GH43_12) from *Pseudopedobacter saltans* by Computational modeling and Small angle X-ray scattering
4. Efficient saccharification of sugarcane bagasse hemicellulose by recombinant hemicellulases

1.11 References

Ahmed, S., Luis, A. S., Bras, J. L., Ghosh, A., Gautam, S., Gupta, M. N., & Goyal, A. (2013). A novel α-L-arabinofuranosidase of family 43 glycoside hydrolase (*Ct*43Araf) from *Clostridium thermocellum*. *PLoS One*, *8*(9), e73575.

Amrein, T. M., Gränicher, P., Arrigoni, E., & Amadò, R. (2003). In vitro digestibility and colonic fermentability of aleurone isolated from wheat bran. *LWT-Food Science and Technology*, 36(4), 451-460.

Balasubramaniam, K., Sharma, K., Rani, A., Rajulapati, V., & Goyal, A. (2018). Deciphering the mode of action, structural and biochemical analysis of heparinase II/III (*Ps*PL12a) a new member of family 12 polysaccharide lyase from *Pseudopedobacter saltans*. *Annals of Microbiology*, *68*(6), 409-418.

Beg, Q., Kapoor, M., Mahajan, L., & Hoondal, G. S. (2001). Microbial xylanases and their industrial applications: a review. *Applied Microbiology and Biotechnology*, *56*(3-4), 326-338.

Belda, I., Ruiz, J., Esteban-Fernández, A., Navascués, E., Marquina, D., Santos, A., & Moreno-Arribas, M. (2017). Microbial contribution to wine aroma and its intended use for wine quality improvement. *Molecules*, *22*(2), 189.

Berg, J. O., Nord, C. E., & Wadström, T. (1978). Formation of glycosidases in batch and continuous culture of Bacteroides fragilis. *Applied and Environmental Microbiology.*, *35*(2), 269-273.

Berndes, G., Hoogwijk, M., & Van den Broek, R. (2003). The contribution of biomass in the future global energy supply: a review of 17 studies. *Biomass and Bioenergy*, *25*(1), 1-28.

Birgisson, H., Fridjonsson, O., Bahrani-Mougeot, F. K., Hreggvidsson, G. O., Kristjansson, J. K., & Mattiasson, B. (2004). A new thermostable α-L-arabinofuranosidase from a novel thermophilic bacterium. *Biotechnology Letters*, *26*(17), 1347-1351.

Birthal, P. S., Khan, T. M., Negi, D. S., & Agarwal, S. (2014). Impact of climate change on yields of major food crops in India: Implications for food security. *Agricultural Economics Research Review*, *27*(347-2016-17126), 145-155.

Bosetto, A., Justo, P. I., Zanardi, B., Venzon, S. S., Graciano, L., Dos Santos, E. L., & Simão, R. D. C. G. (2016). Research progress concerning fungal and bacterial β-xylosidases. *Applied Biochemistry and Biotechnology*, *178*(4), 766-795.

Brett, C., & Waldron, K. (1990). Cell wall structure and the skeletal functions of the wall. In *Physiology and Biochemistry of Plant Cell Walls*, Springer, Dordrecht, 4-57.

Burk, M. J. (2010). Sustainable production of industrial chemicals from sugars. *International Sugar Journal*, *112*(1333), 30.

Carpita, N. C., & Gibeaut, D. M. (1993). Structural models of primary cell walls in flowering plants: consistency of molecular structure with the physical properties of the walls during growth. *The Plant Journal*, *3*(1), 1-30.

Cartmell, A., McKee, L. S., Peña, M. J., Larsbrink, J., Brumer, H., Kaneko, S., & Marles-Wright, J. (2011). The structure and function of an arabinan-specific α-1, 2-arabinofuranosidase identified from screening the activities of bacterial GH43 glycoside hydrolases. *Journal of Biological Chemistry*, *286*(17), 15483-15495.

Churms, S. C., Merrifield, E. H., Stephen, A. M., Walwyn, D. R., Polson, A., van der Merwe, K. J., & Costa, N. (1983). An L-arabinan from apple-juice concentrates. *Carbohydrate Research*, *113*(2), 339-344.

Cosgrove, D. J. (2005). Growth of the plant cell wall. *Nature Reviews Molecular Cell Biology*, *6*(11), 850.

Culleton, H., McKie, V. A., & de Vries, R. P. (2014). Overexpression, purification and characterisation of homologous α-L-arabinofuranosidase and endo-1, 4-β-D-glucanase in Aspergillus vadensis. *Journal of Industrial Microbiology & Biotechnology*, *41*(11), 1697-1708.

Cummings, J. H., & Macfarlane, G. T. (1991). The control and consequences of bacterial fermentation in the human colon. *Journal of Applied Bacteriology*, *70*(6), 443-459.

de Camargo, B. R., Claassens, N. J., Quirino, B. F., Noronha, E. F., & Kengen, S. W. (2018). Heterologous expression and characterization of a putative glycoside hydrolase family 43 arabinofuranosidase from *Clostridium thermocellum* B8. *Enzyme and Microbial Technology*, *109*, 74-83.

de Groot, M. J., van de Vondervoort, P. J., de Vries, R. P., Ruijter, G. J., & Visser, J. (2003). Isolation and characterization of two specific regulatory *Aspergillus niger* mutants shows antagonistic regulation of arabinan and xylan metabolism. *Microbiology*, *149*(5), 1183-1191.

de Lima Damásio, A. R., Pessela, B. C., Segato, F., Prade, R. A., Guisan, J. M., & Maria de Lourdes, T. M. (2012). Improvement of fungal arabinofuranosidase thermal stability by reversible immobilization. *Process Biochemistry*, *47*(12), 2411-2417.

De Vries, J. A., Rombouts, F. M., Voragen, A. G. J., & Pilnik, W. (1982). Enzymic degradation of apple pectins. *Carbohydrate Polymers*, *2*(1), 25-33.

De Vries, R. P., Kester, H. C., Poulsen, C. H., Benen, J. A., & Visser, J. (2000). Synergy between enzymes from Aspergillus involved in the degradation of plant cell wall polysaccharides. *Carbohydrate Research*, *327*(4), 401-410.

Debeche, T., Cummings, N., Connerton, I., Debeire, P., & O'Donohue, M. J. (2000). Genetic and Biochemical Characterization of a Highly Thermostable α-l-arabinofuranosidase from *Thermobacillus xylanilyticus*. *Applied and Environmental Microbiology*, *66*(4), 1734-1736.

Dervilly-Pinel, G., Rimsten, L., Saulnier, L., Andersson, R., & Åman, P. (2001). Water-extractable arabinoxylan from pearled flours of wheat, barley, rye and triticale. Evidence for the presence of ferulic acid dimers and their involvement in gel formation. *Journal of Cereal Science*, *34*(2), 207-214.

Dhillon, A., Fernandes, V. O., Dias, F. M., Prates, J. A., Ferreira, L. M., Fontes, C. M., & Goyal, A. (2016). A new member of family 11 polysaccharide lyase, rhamnogalacturonan lyase (*Ct*RGLf) from *Clostridium thermocellum*. *Molecular Biotechnology*, *58*(4), 232-240.

Dotsenko, G., Meyer, A. S., Canibe, N., Thygesen, A., Nielsen, M. K., & Lange, L. (2018). Enzymatic production of wheat and ryegrass derived xylooligosaccharides and evaluation of their in vitro effect on pig gut microbiota. *Biomass Conversion and Biorefinery*, *8*(3), 497-507.

Ebringerova, A., & Heinze, T. (2000). Xylan and xylan derivatives–biopolymers with valuable properties, 1. Naturally occurring xylans structures, isolation procedures and properties. *Macromolecular Rapid Communications*, *21*(9), 542-556.

Falck, P., Linares-Pastén, J. A., Karlsson, E. N., & Adlercreutz, P. (2018). Arabinoxylanase from glycoside hydrolase family 5 is a selective enzyme for production of specific arabinoxylooligosaccharides. *Food Chemistry*, *242*, 579-584.

Faulds, C. B., Kroon, P. A., Saulnier, L., Thibault, J. F., & Williamson, G. (1995). Release of ferulic acid from maize bran and derived oligosaccharides by *Aspergillus niger* esterases. *Carbohydrate Polymers*, *27*(3), 187-190.

Ferchichi, M., Rémond, C., Simo, R., & O'Donohue, M. J. (2003). Investigation of the functional relevance of the catalytically important Glu28 in family 51 arabinosidases. *FEBS Letters*, *553*(3), 381-386.

Fessas, D., & Schiraldi, A. (1998). Texture and staling of wheat bread crumb: effects of water extractable proteins and pentosans'. *Thermochimica Acta*, *323*(1-2), 17-26.

Fischer, M. H., Yu, N., Gray, G. R., Ralph, J., Anderson, L., & Marlett, J. A. (2004). The gel-forming polysaccharide of *psyllium* husk (Plantago ovata Forsk). *Carbohydrate Research*, *339*(11), 2009-2017.

Freitas, R. A., Gorin, P. A. J., Neves, J., & Sierakowski, M. R. (2003). A rheological description of mixtures of a galactoxyloglucan with high amylose and waxy corn starches. *Carbohydrate Polymers*, *51*(1), 25-32.

Gallego, V., García, M. T., & Ventosa, A. (2006). *Pedobacter aquatilis* sp. nov., isolated from drinking water, and emended description of the genus *Pedobacter*. *International Journal of Systematic and Evolutionary Microbiology*, *56*(8), 1853-1858.

Gebruers, K., Dornez, E., Bedo, Z., Rakszegi, M., Courtin, C. M., & Delcour, J. A. (2010). Variability in xylanase and xylanase inhibition activities in different cereals in the healthgrain diversity screen and contribution of environment and genotype to this variability in common wheat. *Journal of Agricultural and Food Chemistry*, *58*(17), 9362-9371.

Gobbetti, M., Lavermicocca, P., Minervini, F., De Angelis, M., & Corsetti, A. (2000). Arabinose fermentation by *Lactobacillus plantarum* in sourdough with added pentosans and α-L-arabinofuranosidase: a tool to increase the production of acetic acid. *Journal of Applied Microbiology*, *88*(2), 317-324.

Grembecka, M. (2015). Sugar alcohols-their role in the modern world of sweeteners: a review. *European Food Research and Technology*, *241*(1), 1-14.

Grootaert, C., Delcour, J. A., Courtin, C. M., Broekaert, W. F., Verstraete, W., & Van de Wiele, T. (2007). Microbial metabolism and prebiotic potency of arabinoxylan oligosaccharides in the human intestine. *Trends in Food Science & Technology*, *18*(2), 64-71.

Guo, W., Sakata, K., Watanabe, N., Nakajima, R., Yagi, A., Ina, K., & Luo, S. (1993). Geranyl 6-O-β-D-xylopyranosyl-β-D-glucopyranoside isolated as an aroma precursor from tea leaves for oolong tea. *Phytochemistry*, *33*(6), 1373-1375.

Guo, X. M., Trably, E., Latrille, E., Carrere, H., & Steyer, J. P. (2010). Hydrogen production from agricultural waste by dark fermentation: a review. *International Journal of Hydrogen Energy*, *35*(19), 10660-10673.

Hashimoto, S., Shogren, M. D., & Pomeranz, Y. (1987). Cereal pentosans: their estimation and significance. I. Pentosans in wheat and milled wheat products. *Cereal chemistry*, *64*(1), 30-34.

Holtekj⊘ len, A. K., Uhlen, A. K., & Knutsen, S. H. (2008). Barley carbohydrate composition varies with genetic and abiotic factors. *Acta Agriculturae Scandinavica Section B-Soil and Plant Science*, *58*(1), 27-34.

Hövel, K., Shallom, D., Niefind, K., Belakhov, V., Shoham, G., Baasov, T., & Schomburg, D. (2003). Crystal structure and snapshots along the reaction pathway of a family 51 α-L-arabinofuranosidase. *The EMBO Journal*, *22*(19), 4922-4932.

Hughes, S. A., Shewry, P. R., Li, L., Gibson, G. R., Sanz, M. L., & Rastall, R. A. (2007). In vitro fermentation by human fecal microflora of wheat arabinoxylans. *Journal of Agricultural and Food Chemistry*, *55*(11), 4589-4595.

İlgü, H., Sürmeli, Y., & Şanlı-Mohamed, G. (2018). A thermophilic α-l-arabinofuranosidase from *Geobacillus vulcani* GS90: heterologous expression, biochemical characterization, and its synergistic action in fruit juice enrichment. *European Food Research and Technology*, *244*(9), 1627-1636.

Izydorczyk, M. S., & Biliaderis, C. G. (1995). Cereal arabinoxylans: advances in structure and physicochemical properties. *Carbohydrate Polymers*, *28*(1), 33-48.

Izydorczyk, M. S., & Dexter, J. E. (2008). Barley β-glucans and arabinoxylans: Molecular structure, physicochemical properties, and uses in food products–a Review. *Food Research International*, *41*(9), 850-868.

Jiménez, T., & Martinez-Anaya, M. A. (1999, June). Enzymes, a key to improve bread and dough quality: degradation by products and relationship with quality. In *17th ICC Conference of the Cereal Across the Continents* (pp. 6-9).

Katapodis, P., Vardakou, M., Kalogeris, E., Kekos, D., Macris, B. J., & Christakopoulos, P. (2003). Enzymic production of a feruloylated oligosaccharide with antioxidant activity from wheat flour arabinoxylan. *European Journal of Nutrition*, *42*(1), 55-60.

Kendall, C. W., Esfahani, A., & Jenkins, D. J. (2010). The link between dietary fibre and human health. *Food Hydrocolloids*, *24*(1), 42-48.

Koistinen, V. M., Mattila, O., Katina, K., Poutanen, K., Aura, A. M., & Hanhineva, K. (2018). Metabolic profiling of sourdough fermented wheat and rye bread. *Scientific Reports*, *8*(1), 5684.

Lempereur, I., Rouau, X., & Abecassis, J. (1997). Genetic and agronomic variation in arabinoxylan and ferulic acid contents of durum wheat (*Triticum durumL.*) grain and its milling fractions. *Journal of Cereal Science*, *25*(2), 103-110.

Liolios, K., Sikorski, J., Lu, M., Nolan, M., Lapidus, A., Lucas, S., & Han, C. (2011). Complete genome sequence of the gliding, heparinolytic *Pedobacter saltans* type strain (113 T). *Standards in Genomic Sciences*, *5*(1), 30.

Lu, Z. X., Walker, K. Z., Muir, J. G., Mascara, T., & O'Dea, K. (2000). Arabinoxylan fiber, a byproduct of wheat flour processing, reduces the postprandial glucose response in normoglycemic subjects. *The American Journal of Clinical Nutrition*, *71*(5), 1123-1128.

Lynd, L. R., Weimer, P. J., Van Zyl, W. H., & Pretorius, I. S. (2002). Microbial cellulose utilization: fundamentals and biotechnology. *Microbiology and Molecular Biology Reviews*, *66*(3), 506-577.

Margolles, A., & Clara, G. (2003). Purification and functional characterization of a novel α-l-arabinofuranosidase from *Bifidobacterium longum* B667. *Applied and Environmental Microbiology*, *69*(9), 5096-5103.

Margolles-Clark, E., Tenkanen, M., Nakari-Setälä, T., & Penttilä, M. (1996). Cloning of genes encoding alpha-L-arabinofuranosidase and beta-xylosidase from *Trichoderma reesei* by expression in Saccharomyces cerevisiae. *Applied and Environmental Microbiology*, *62*(10), 3840-3846.

Mateo, J. J., & Di Stefano, R. (1997). Description of the β-glucosidase activity of wine yeasts. *Food Microbiology*, *14*(6), 583-591.

Möhlig, M., Koebnick, C., Weickert, M. O., Lueder, W., Otto, B., Steiniger, J., & Zunft, H. J. (2005). Arabinoxylan-enriched meal increases serum ghrelin levels in healthy humans. *Hormone and Metabolic Research*, *37*(05), 303-308.

Numan, M. T., & Bhosle, N. B. (2006). α-L-Arabinofuranosidases: the potential applications in biotechnology. *Journal of Industrial Microbiology and Biotechnology*, *33*(4), 247-260.

Ochiai, A., Itoh, T., Kawamata, A., Hashimoto, W., & Murata, K. (2007). Plant cell wall degradation by saprophytic Bacillus subtilis strains: gene clusters responsible for rhamnogalacturonan depolymerization. *Applied and Environmental Microbiology*, *73*(12), 3803-3813.

Ordaz-Ortiz, J. J., & Saulnier, L. (2005). Structural variability of arabinoxylans from wheat flour. Comparison of water-extractable and xylanase-extractable arabinoxylans. *Journal of Cereal Science*, *42*(1), 119-125.

Rahman, A. S., Kato, K., Kawai, S., & Takamizawa, K. (2003). Substrate specificity of the α-L-arabinofuranosidase from *Rhizomucor pusillus* HHT-1. *Carbohydrate Research*, *338*(14), 1469-1476.

Rani, A., & Goyal, A. (2016). A new member of family 8 polysaccharide lyase chondroitin AC lyase (*Ps*PL8A) from *Pedobacter saltans* displays endo-and exo-lytic catalysis. *Journal of Molecular Catalysis B: Enzymatic*, *134*, 215-224.

Rao, M. S., & Muralikrishna, G. (2004). Structural analysis of arabinoxylans isolated from native and malted finger millet (*Eleusine coracana*, ragi). *Carbohydrate Research*, *339*(14), 2457-2463.

Rao, R. S. P., & Muralikrishna, G. (2007). Structural characteristics of water-soluble feruloyl arabinoxylans from rice (*Oryza sativa*) and ragi (finger millet, *Eleusine coracana*): Variations upon malting. *Food Chemistry*, *104*(3), 1160-1170.

Ravanal, M. C., & Eyzaguirre, J. (2015). Heterologous expression and characterization of α-l-arabinofuranosidase 4 from *Penicillium purpurogenum* and comparison with the other isoenzymes produced by the fungus. *Fungal Biology*, *119*(7), 641-647.

Vasella, A., Davies, G. J., & Böhm, M. (2002). Glycosidase mechanisms. *Current Opinion in Chemical Biology*, *6*(5), 619-629.

Saha, B. C. (2000). α-L-Arabinofuranosidases: biochemistry, molecular biology and application in biotechnology. *Biotechnology Advances*, *18*(5), 403-423.

Sakakibara, Y., Saha, B. C., & Taylor, P. (2009). Microbial production of xylitol from L-arabinose by metabolically engineered Escherichia coli. *Journal of Bioscience and Bioengineering*, *107*(5), 506-511.

Sakamoto, T., Ogura, A., Inui, M., Tokuda, S., Hosokawa, S., Ihara, H., & Kasai, N. (2011). Identification of a GH62 α-L-arabinofuranosidase specific for arabinoxylan produced by Penicillium chrysogenum. *Applied Microbiology and Biotechnology*, *90*(1), 137-146.

Samuelsen, A. B., Rieder, A., Grimmer, S., Michaelsen, T. E., & Knutsen, S. H. (2011). Immunomodulatory activity of dietary fiber: arabinoxylan and mixed-linked beta-glucan isolated from barley show modest activities in vitro. *International Journal of Molecular Sciences*, *12*(1), 570-587.

Sartori, T., Tibolla, H., Prigol, E., Colla, L. M., Costa, J. A. V., & Bertolin, T. E. (2015). Enzymatic saccharification of lignocellulosic residues by cellulases obtained from solid state fermentation using *Trichoderma viride*. *BioMed Research International*, *2015*.

Scheller, H. V., & Ulvskov, P. (2010). Hemicelluloses. *Annual Review of Plant Biology*, *61*.

Shallom, D., Belakhov, V., Solomon, D., Gilead-Gropper, S., Baasov, T., Shoham, G., & Shoham, Y. (2002). The identification of the acid–base catalyst of α-arabinofuranosidase from *Geobacillus stearothermophilus* T-6, a family 51 glycoside hydrolase. *FEBS Letters*, *514*(2-3), 163-167.

Sharma, K., Antunes, I. L., Rajulapati, V., & Goyal, A. (2018). Molecular characterization of a first endo-acting β-1, 4-xylanase of family 10 glycoside

hydrolase (PsGH10A) from *Pseudopedobacter saltans* comb. nov. *Process Biochemistry*, *70*, 79-89.

Shewry, P. R., Piironen, V., Lampi, A. M., Edelmann, M., Kariluoto, S., Nurmi, T., & Boros, D. (2010). Effects of genotype and environment on the content and composition of phytochemicals and dietary fiber components in rye in the HEALTHGRAIN diversity screen. *Journal of Agricultural and Food Chemistry*, *58*(17), 9372-9383.

Shin, H. Y., Park, S. Y., Sung, J. H., & Kim, D. H. (2003). Purification and Characterization of α-l-arabinopyranosidase and α-l-arabinofuranosidase from Bifidobacterium breve K-110, a Human Intestinal Anaerobic Bacterium Metabolizing Ginsenoside Rb2 and Rc. *Applied and Environmental Microbiology*, *69*(12), 7116-7123.

Shinozaki, A., Kawakami, T., Hosokawa, S., & Sakamoto, T. (2014). A novel GH43 α-l-arabinofuranosidase of *Penicillium chrysogenum* that preferentially degrades single-substituted arabinosyl side chains in arabinan. *Enzyme and Microbial Technology*, *58*, 80-86.

Singh, J., & Gu, S. (2010). Biomass conversion to energy in India-a critique. *Renewable and Sustainable Energy Reviews*, *14*(5), 1367-1378.

Sjöström, E., & Alén, R. (Eds.). (2013). *Analytical Methods in Wood Chemistry, Pulping, and Paper making*. Springer Science & Business Media.

Stone, B., Morell, M.K., Khan, K. & Shewry, P.R., (2009). *Wheat: Chemistry and Technology*, Ed 4.

Tathod, A. P., & Dhepe, P. L. (2015). Efficient method for the conversion of agricultural waste into sugar alcohols over supported bimetallic catalysts. *Bioresource Technology*, *178*, 36-44.

Van Laere, K. M., Hartemink, R., Bosveld, M., Schols, H. A., & Voragen, A. G. (2000). Fermentation of plant cell wall derived polysaccharides and their corresponding oligosaccharides by intestinal bacteria. *Journal of Agricultural and Food Chemistry*, *48*(5), 1644-1652.

Wilkens, C., Andersen, S., Dumon, C., Berrin, J. G., & Svensson, B. (2017). GH62 arabinofuranosidases: structure, function and applications. *Biotechnology Advances*, *35*(6), 792-804.

Williams, P. J., Strauss, C. R., Wilson, B., & Massy-Westropp, R. A. (1982). Novel monoterpene disaccharide glycosides of *Vitis vinifera* grapes and wines. *Phytochemistry*, *21*(8), 2013-2020.

Yan, Q., Tang, L., Yang, S., Zhou, P., Zhang, S., & Jiang, Z. (2012). Purification and characterization of a novel thermostable α-l-arabinofuranosidase (α-l-AFase) from *Chaetomium sp*. *Process Biochemistry*, *47*(3), 472-478.

Yang, W., Jiang, Z., Liu, L., Lin, Y., Wang, L., & Zhou, S. (2017). The effect of pentosanase on the solubilisation and degradation of arabinoxylan extracted from whole and refined wheat flour. *Journal of the Science of Food and Agriculture*, *97*(3), 1034-1041.

Yang, X., Shi, P., Ma, R., Luo, H., Huang, H., Yang, P., & Yao, B. (2015). A new GH43 α-arabinofuranosidase from *Humicola insolens* Y1: biochemical characterization and synergistic action with a xylanase on xylan degradation. *Applied Biochemistry and Biotechnology*, *175*(4), 1960-1970.

Yegin, S., Altinel, B., & Tuluk, K. (2018). A novel extremophilic xylanase produced on wheat bran from *Aureobasidium pullulans* NRRL Y-2311-1: Effects on dough rheology and bread quality. *Food Hydrocolloids*, *81*, 389-397.

Zelaya, V. M., Fernández, P. V., Vega, A. S., Mantese, A. I., Federico, A. A., & Ciancia, M. (2017). Glucuronoarabinoxylans as major cell walls polymers from young shoots of the woody bamboo *Phyllostachys aurea*. *Carbohydrate Polymers*, *167*, 240-249.

Zhang, J., & Konan, D. E. (2010). The sleeping giant awakes: projecting global implications of China's energy consumption. *Review of Development Economics*, *14*(4), 750-767.

Zhu, F., Du, B., Ma, Y., & Li, J. (2017). The glycosidic aroma precursors in wine: occurrence, characterization and potential biological applications. *Phytochemistry Reviews*, *16*(3), 565-571.

Chapter 2

Cloning, expression and purification of first α-L-arabinofuranosidase of family 43 glycoside hydrolase, (*Ps*GH43_12) from *Pseudopedobacter saltans* DSM12145

2.1 Introduction

The plant cell wall exhibits semi-rigidity and possesses complex architecture. The plant cell wall helps in the exchange of materials essential for cell metabolism and provides the protection. It is composed of complex polysaccharides like cellulose, hemicellulose and pectin. Cellulose is homogeneous, while hemicellulose is heterogeneous and branched in nature. The backbone of hemicelluloses such as xylan arabinan are made up of pentoses (xylose, arabinose) and glucan and mannan of hexoses (glucose, galactose and mannose) linked by glycosidic bond (Thakur et al., 2019). Xylan is the most abundant and complex hemicellulose having xylose backbone and numerous substitutions of arabinose, glucuronic acid, acetic acid, *p*-coumaric acid and ferulic acid (Ahmed et al., 2013). The occurrence of side-chain substitution depends on the source of xylan. Arabinose side chains are found in arabinan, arabinoxylan, arabinogalactan, oat spelt xylan and pectin polysaccharides.

These side chains interact with other polysaccharides and forms a complex network resulting in the recalcitrant nature of the plant polysaccharide hydrolysis.

α-L-Arabinofuranosidases (EC 3.2.1.55) are present in family 2, 3, 43, 51, 54 and 62 of glycoside hydrolases (Lombard et al., 2013). The family 43 glycoside hydrolase (GH43) contains enzymes having different activities such as β-1,4-xylosidase (EC 3.2.1.37), β-1,3-xylosidase (EC 3.2.1.-), β-1,4-endoxylanase (EC 3.2.1.8), galactan 1,3- β-galactosidase (EC 3.2.1.145), α-L-arabinofuranosidase (EC 3.2.1.55) and arabinanase (EC 3.2.1.99). The mode of action of hydrolysis by α-L-arabinofuranosidase via overall inversion of the anomeric configuration (Saha 2000). α-L-Arabinofuranohydrolase is involved in hydrolysis of L-arabinose side chain linkages, specifically catalyzing the hydrolysis of terminal nonreducing α-L-1,2-, α-L-1,3-, and α-L-1,5-arabinofuranosyl residues from different oligosaccharides and polysaccharides (Saha 2000; Saha and Bothast 1997; Sozzi et al., 2002). The family 43 glycoside hydrolase based on the sequence identity, biochemical properties and structural characteristics has been subdivided into 37 subfamilies (Mewis et al., 2016). The subfamily GH43_12, contains enzymes having β-xylosidase and α-L-arabinofuranosidase activities. Till date, 1115 enzymes from different forms of life *viz.* Archea, bacteria and fungi are identified but only 13 enzymes have been characterized of subfamily GH43_12 (http://www.cazy.org/GH43_12_all.html). The characterized arabinofuranosidases from *Butyrivibrio fibrisolvens* (Hespell and O'Bryan, 1992), from compost starter culture (Wagschal et al., 2007), from *Bifidobacterium animalis* (Viborg et al., 2013) and from *Bacteroides ovatus* (Zhou et al., 2020) displayed very low enzyme activity and thermal stability. Therefore, an

efficient arabinofuranosidase having significantly higher activity and stability is needed to be explored.

Some strains of the genus *Pseudopedobacter* are heparinase producing, obligately aerobic, mesophilic, Gram-negative rod shaped bacteria (Liolios et al., 2011). Few therapeutic enzymes such as chondroitin AC lyase of family 8 polysaccharide lyase (Rani and Goyal 2016) and heparinase II/III of family 12 polysaccharide lyase from *P. saltans* are reported (Balasubramaniam et al., 2018). However, one hemicellulosic enzyme xylanase (*Ps*GH10A) was reported from this microorganism (Sharma et al., 2018). In the present study, the gene encoding α-L-arabinofuranosidase (*Ps*GH43_12) with a locus tag of Pedsa_2580 and GenBank accession no. ADY53124.1 was identified and retrieved from NCBI after the analysis of available whole-genome sequencing data. The gene encoding α-L-arabinofuranosidase, *Ps*GH43_12 of family 43 glycoside hydrolase from *Pseudopedobacter saltans* was cloned in pET28a(+) vector and expressed in BL-21 (DE3) cells. The His-tag containing enzyme was purified to its homogeneity by immobilized metal ion chromatography (IMAC).

2.2 Materials and Methods

2.2.1 Chemicals, reagents, kits and bacterial strains

The primers for PCR amplification of the gene encoding for *Ps*GH43_12 were procured from Eurofins, India. Molecular cloning enzymes such as restriction enzymes *Nhe*I, and *Xho*I, Taq DNA polymerase, T4 DNA ligase and their respective buffers were obtained from New England Biolabs (NEB), USA. dNTPs, $MgCl_2$, RNAse solution (20 mg/ml), glacial acetic acid (99.9% pure) Trizma base (Tris free base), ethidium bromide, bradford reagent, nuclease free water (pH 8.0) and components of polyacrylamide gel electrophoresis were obtained from Sigma-Aldrich Co. LLC., USA. Luria Bertani (LB) medium, Kanamycin, disodium ethylenediamine tetra acetate salt (EDTA), glucose, sodium hydroxide, sodium dodecyl sulphate (SDS) and isopropyl-β-D-thiogalactopyranoside (IPTG) were obtained from HiMedia Laboratories, India. PCR tubes (0.2 ml), MCTs (1.5 ml) were from Axygen, Germany. The GenElute miniprep plasmid isolation kit and GenElute gel-extraction kit was from Sigma-Aldrich Co. LLC., USA. Agarose gel for horizontal gel electrophoresis was prepared using low EEO agarose purchased from Sigma-Aldrich Co. LLC., USA. DNA marker, 1 kb NEB DNA ladder. SDS-PAGE was performed using Mini-PROTEAN Tetra Cell apparatus purchased from Bio-Rad Laboratories (India) Private Limited. The protein marker was procured from BioBharati LifeScience Private Limited, India, staining dye Coomassie Brilliant Blue R250 from Himedia Pvt. Ltd., India and methanol from Merck, India. All other reagents, buffer components and salts were purchased from Sisco Research Laboratories Pvt. Ltd., India. The expression vector, pET28a(+) was purchased from Novagen, Germany. The genomic DNA of *Pseudopedobacter saltans* (Strain No.

DSM-12145) was purchased from Leibniz Institute DSMZ-German Collection of Microorganisms and cell cultures. *E. coli* DH5α and *E. coli* BL-21 (DE3) cells were obtained from Novagen, Germany.

2.2.2 Sequence analysis of *Ps*GH43_12

The gene encoding α-L-arabinofuranosidase (*Ps*GH43_12) with a locus tag of Pedsa_2580 and GenBank accession no. ADY53124.1 was identified and retrieved from NCBI after the analysis of available whole-genome sequencing data. BLASTp analysis of *Ps*GH43_12against PDB was performed to identify the α-L-arabinofuranosidases coding region based on the homologous enzymes. The conserved structural domain of *Ps*GH43_12 was determined by referring to the NCBI-Conserved Domains Database. *Ps*GH43_12 subcellular localization was predicted by using the SignalP 4.1 server (http://www.cbs.dtu.dk/services/SignalP/). The physiochemical properties such as molecular mass, theoretical pI, amino acid composition, molar extinction coefficient of *Ps*GH43_12 were calculated by using ProtParam server (http://web.expasy.org/protparam/).

2.2.3 PCR amplification of gene encoding *Ps*GH43_12

The gene (GenBank Accession number ADY53124.1) encoding the catalytic module, *Ps*GH43_12 without the signal sequence was amplified by using the designed primers containing *NheI* and *XhoI* restriction sites. The forward primer was 5'-CGGCTAGCGTTGAACCGCAAGACACTAAAGAG-3' and the reverse primer was 5'-CCCTCGAGTTATTTTATGACTGATAGATCCATATTG-3'. The gene was amplified from the genomic DNA of *Pseudopedobacter saltans* and used as the template. The reaction composition and the PCR cycle conditions for gene amplification are mentioned in the Tables 2.1 and 2.2, respectively. PCR

amplification was performed on a thermal cycler (Applied Biosystems, GeneAmp PCR System 9700). The PCR amplicons obtained were electrophoresed on a 0.8% (w/v) agarose gel along with a DNA marker (1 kb NEB DNA ladder) as mentioned in Section 2.2.4.

Table 2.1 PCR reaction composition for amplification of gene encoding *Ps*GH43_12 from *Pseudopedobacter saltans*

PCR components	Volume (µl)	Final concentration
10x reaction buffer	6.0	
dNTP mix (100 mM)	0.2	0.3 mM
Forward primer (15 µM)	1.5	0.37 µM
Reverse primer (15 µM)	1.5	0.37 µM
Genomic DNA (2.2 ng/µl)	1.5	0.055 ng/µl
Taq DNA polymerase (2.5 U/µl)	0.5	0.04 U/µl
Sigma water, pH 8.0	48.8	
Total	60.0	--

Table 2.2 Thermal cycles for PCR amplification of gene encoding *Ps*GH43_12 from *Pseudopedobacter saltans.*

Step	Temperature (°C)	Time (min)	No. of Cycles
Initial Denaturation	94	4	1
Denaturation	94	0.5	
Annealing	62	0.66	30
Extension	72	2	
Final Extension	72	10	1
Hold	4	∞	

2.2.4 Agarose gel electrophoresis of PCR amplified products

The PCR amplified product was electrophoresed on 0.8% (w/v) agarose gel prepared in 1x TAE buffer. A stock solution of TAE buffer was prepared with the concentrations of components to make 10x buffer (400 mM Tris-acetate, 10 mM EDTA, pH 8.0) (Sambrook and Russell 2001). 0.8% (w/v) agarose gel was made by taking, 0.4 g of agarose in 50 ml of 1x TAE buffer. The mixture was boiled in microwave oven for about 90 s or till the agarose dissolved completely. After cooling

it to the room temperature, 5.0 µl of ethidium bromide (5.0 mg/ml) was added and the solution was poured in to the casting tray of horizontal gel electrophoresis apparatus (Genaxy Scientific Pvt. Ltd, India) with the combs appropriately placed. The solution was allowed to solidify. After 15-20 min, the gel was placed in electrophoresis unit filled with 1x TAE electrophoresis running buffer and after removing the combs, 4 µl of the PCR DNA sample was mixed with 1 µl of the 5x DNA loading buffer (PCR DNA sample and 5x DNA loading buffer in 4:1 ratio) and was loaded into the wells. The gel was run at a constant voltage, 70 V till the dye migrated about two-third distance of the gel. The DNA bands were then visualized under UV light at 302/312 nm in a gel documentation system (Bio-RAD XR, USA). After the analysis of PCR amplicon on agarose gel, the DNA band was extracted from the gel and purified for further use.

2.2.5 DNA loading dye buffer

The DNA loading dye buffer was prepared by mixing the components mentioned below in Table 2.3. A 5x stock solution of DNA loading buffer was prepared and 1 volume of it mixed with 4 volumes of DNA to make it to 1x before loading on to the agarose gels. The final pH of the DNA loading dye was adjusted to pH 8.0.

Table 2.3 Composition of 5x DNA loading dye buffer.

Components	**Final concentration (5X)**
Tris-HCl (pH 8.0)	50 mM
Glycerol	25% (w/v)
EDTA	5.0 mM
Bromophenol blue	0.2% (w/v)
Xylene cyanol	0.2% (w/v)

2.2.6 Extraction of DNA from agarose gel

The PCR amplified DNA or other plasmids were purified from agarose gel by using a gel extraction kit (Sigma GenElute), following the protocol provided by the manufacturer as described further in this section. To start with extraction, 1.5 ml sterile microcentrifuge tube was weighed and the weight was noted. After running the DNA on agarose gel, the desired band was excised using a sterilized scalpel by placing the gel on a UV transilluminator and visualizing at 302 nm wavelength by using UV protecting spectacles and gloves. The excised gel piece was transferred to a sterile preweighed microcentrifuge tube and then weighed again. The weight of the gel piece was determined by subtracting the weight of the empty tube from the weight of the tube with gel piece. Three volumes of gel solubilisation solution was added to 1 volume of gel (100 mg ~ 100 µl). The tube was incubated at 50°C for 10 min and was vortexed after every 2 min for complete dissolution the gel. Further isopropanol (equivalent to the initial weight of the gel, 1/3rd volume of QG buffer added) was added to the solution. To prepare the gel extraction column, GenElute binding column G was placed in a 2 ml collection tube provided with the kit and 500 µl of column preparation solution was added over the column membrane and centrifuged at 13000*g* for 1 min. The flow through was discarded and the mixture containing DNA (~700 µl) was added to the DNA binding column and centrifuged at 13000*g* for 1 min at 25°C. The flow through obtained was again discarded. If the volume was more than 700 µl, the remaining solution was centrifuged similarly and again the flow through was discarded. The column was then washed with 700 µl of wash solution by centrifugation at 13000g for 1 min at 25°C, discarding the flow through. To completely remove the traces of wash buffer an additional empty spin of 1 min at

13000*g* was given to the column. The column containing bound DNA was placed on a fresh sterilized microcentrifuge tube and 30 µl of pre-warmed nuclease-free water Sigma-Aldrich Co. LLC., USA or pre-warmed eluent solution (10 mM Tris-Cl, pH 8.5) was added at the centre of the column. The column was then left for 2 min to set at 25°C and DNA was eluted in the tube by spinning the column at 13000*g* for 1 min. The eluted DNA was then analyzed on a 0.8% (w/v) agarose gel and stored at -20°C till further use.

2.2.7 Preparation of culture medium

In the entire study, LB medium was used for growing the *E. coli* DH5α and BL-21 (DE3) cells containing recombinant plasmid. The medium was prepared by dissolving the ingredients (Table 2.4) in 800 ml of deionized water. The pH was adjusted to 7.2 and then the final volume was made up to 1 litre. 100 ml of LB medium was then transferred to 250 ml conical flask and autoclaved at 121°C at 15 psi for 20 min. The filter sterilized antibiotic (Kanamycin; 50 µg/ml) was added to autoclaved and cooled LB medium prior to culture inoculation.

Table 2.4 Composition of Luria-Bertani medium (Sambrook et al., 1989)

Components	**Final concentration (%, w/v)**
Tryptone	1.0
Yeast extract powder	0.5
Sodium chloride	1.0

2.2.7.1 Preparation of LB-agar medium

LB agar medium was prepared by adding 2% (w/v) Agar type I in LB broth medium and autoclaving as described in Section 2.2.7. The medium was cooled to around 50-55°C and appropriate amount of antibiotic (kanamycin; 50 µg/ml) was added under laminar air flow. Nearly 25 ml of above prepared medium

supplemented with antibiotic was poured in sterile petri plates under laminar air flow and allowed to solidify for 30 min.

2.2.8 Preparation of *E. coli* DH5α competent cells

Day 1: Primary culture

A single colony of *E. coli* DH5α cells picked from freshly streaked plate was inoculated in a test tube containing 5.0 ml LB medium (Sambrook et al., 1989). The culture was grown overnight at 37ºC and 180 rpm.

As the preparation for next day, 0.1 M $CaCl_2$ solution was sterilized by autoclaving after filter by whatman No.1 filter paper and kept in refrigerator. 1.5 ml micro-centrifuge tubes, 50 ml centrifuge tubes (round bottom) and micro tips were autoclaved and kept in laminar hood.

Day 2: Secondary culture

Next day, 1.0 ml culture from primary culture was inoculated in 100 ml LB medium prepared in 250 ml conical flask and incubated at 37°C in a shaking incubator at 180 rpm till its OD_{600} reached ~0.4. The culture was chilled on ice for 30 min and then 40 ml culture was transferred aseptically to round bottom centrifuge tubes and harvested by centrifugation at 2710*g* at 4ºC for 10 min. The supernatant was discarded and the cell pellet was resuspended in 20 ml of ice-cold 0.1 M $CaCl_2$ solution and kept on ice for 10 min subjected to centrifugation at 2710*g* at 4ºC for 10 min. The supernatant was carefully removed and the cell pellet was resuspended in 3.0 ml of sterile ice chilled 0.1 M $CaCl_2$ solution. Aliquots of 100 µl of competent cells were made in sterile 1.5 ml microcentrifuge tubes containing 10% (v/v) glycerol (final concentration) and kept at -80ºC for further use. Similarly, competent cells of *E. coli* BL-21 (DE3) bacterial strain were made.

2.2.9 Cloning of gene encoding *Ps*GH43_12 into pET28a(+) vector

The pET-28a(+) is a modified form of pBR322 plasmid. It is a frequently used vector for cloning and expression of recombinant proteins in *E. coli* cells. pET-28a(+) vector has a T7 promoter system originally developed by Studier and colleagues (Studier and Moffatt, 1986; Studier et al., 1990). The expression of genes cloned in pET plasmids is under the control of T7 bacteriophage promoter. The cloned genes are transcribed by T7 RNA polymerase of the host cell. The genes cloned in pET vectors remain transcriptionally silent in the uninduced state. The proteins encoded by the cloned genes contain a His_6-Tag which involves single step purification method using affinity chromatography. The pET-28a(+) vector allows for incorporation of expressed protein with an N-terminal His_6-Tag/thrombin/T7-Tag in addition to an optional C-terminal His_6-Tag sequence (Fig. 2.1). The location of sequence encoding His-Tag, T7 promoter, T7 terminator, kanamycin resistance and f1 origin are indicated in the Fig. 2.1.

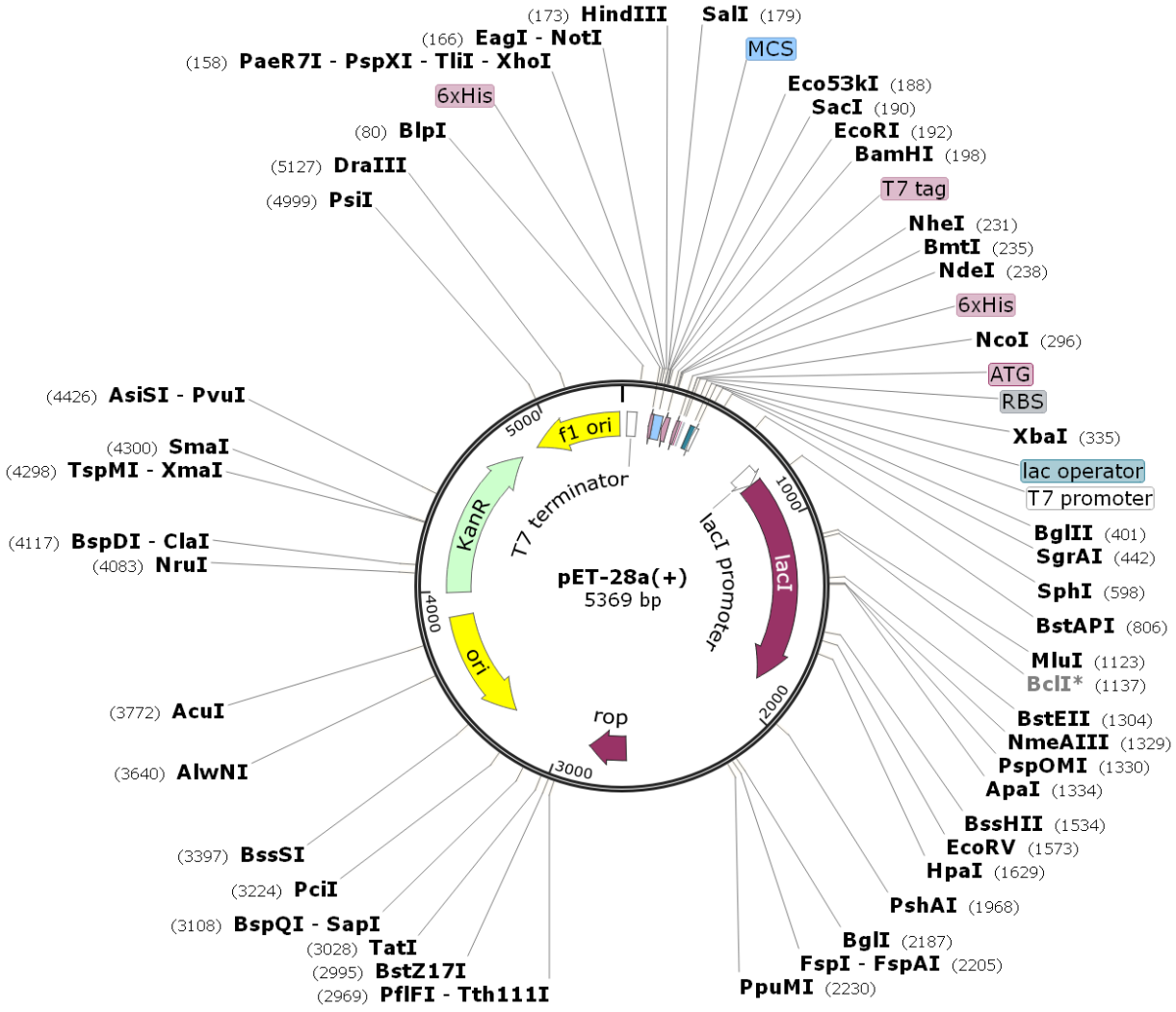

Fig. 2.1 Restriction map of the pET-28a(+) expression vector showing multiple cloning site (158-203 bp), restriction enzyme sites, N-terminal His_6-Tag coding sequence (270-287 bp), C-terminal His_6-Tag coding sequence (140-157 bp), T7 promoter (370-386), T7 terminator (26-72 bp), pBR322 origin (3286 bp), kanamycin marker (3995-4807 bp) and a f1 origin (4903-5358). *Nhe*I cuts at 231 and *Xho*I at 158.

2.2.10 Restriction digestion of PCR amplified gene encoding for *Ps*GH43_12 and pET28a(+) vector DNA

The DNA concentration was measured by using Nano drop (Implen, Germany). One unit of the restriction enzyme/µg of the DNA was used for the desired DNA along with the appropriate reaction buffer. The reaction volume was finally

made up by using filter sterilized nuclease-free water. For vector preparation, pET-28a(+) was digested with *Nhe*I-*Xho*I restriction enzymes (Table 2.5). PCR amplified gene encoding *Ps*GH43_12 was also digested with *Nhe*I-*Xho*I enzyme to prepare the insert (Table 2.5) for ligation. The digestion reactions were incubated in a water bath at 37°C for 90 min. The *Nhe*I-*Xho*I digested pET-28a(+) vector DNA and PCR amplified DNA were extracted and purified from agarose gel as described in Section 2.2.6.

Table 2.5 Restriction enzyme digestion of pET-28a (+) plasmid DNA and PCR amplified genes encoding *Ps*GH43_12.

Reaction components	**For pET-28a(+) (µl)**	**For gene encoding *Ps*GH43_12 (µl)**
Plasmid DNA (approx. 13 ng/ µl)	10	-
PCR amplified product	-	15
10x buffer	1.5	2
Nuclease free water	2.3	1
*Nhe*I (10 U/µl)	0.6	1
*Xho*I (10 U/µl)	0.6	1
Total	15	20

2.2.11 Ligation of restriction digested gene encoding *Ps*GH43_12 insert into pET-28a(+) vector

The insert and vector DNA were ligated using T4 DNA Ligase (NEB, USA) for constructing the recombinant plasmid. The *Nhe*I-*Xho*I digested gene encoding *Ps*GH43_12 was ligated into pET-28a(+) vector, which was also digested with same restriction enzymes as described in Section 2.2.10. A 16 µl ligation reaction mixture was set up that contained the insert and vector in molar ratio 3:1 in 10x T4 DNA Ligase buffer and T4 DNA Ligase. The concentration and volume of reaction components used are mentioned in Table 2.6. The ligation mixture was incubated at 16°C overnight (~12h) to get maximum number of transformants. The concentration of

insert to be used in ligation was calculated by using the mentioned ligation formula below:

$$\text{ng of insert} = \frac{[\text{ng of vector x kb size of insert}]}{[\text{kb size of vector}]} \text{ x molar ratio of } \frac{[\text{insert}]}{[\text{vector}]}$$

$$\frac{27.6 \text{ ng} \times 1.7 \text{ (kb)}}{5.369 \text{ (kb)}} \times \frac{3}{1} = 26.4 \text{ ng (}Ps\text{GH43\_12)}$$

Table 2.6 Components of reaction for ligation of the gene encoding *Ps*GH43_12 and pET-28a(+) expression vector.

Reaction component	(µl)
Restriction digested product (3.1 ng/ µl)	8.8
pET-28a (+) Vector (27.6 ng/ µl)	4.6
10x Rapid T4 DNA Ligation Buffer	1.6
T4 DNA Ligase (3 Units/µl)	1.0
Total	16

2.2.12 Transformation of ligated recombinant DNA into *E. coli* DH5α cells

The ligation reaction mixture was transformed using the *E. coli* DH5α competent cells, which were prepared as mentioned in Section 2.2.8. The transformation was performed by heat shock method. 15 µl of ligation mixture was added to 100 µl *E. coli* DH5α competent cells under laminar air flow (competent cells were taken out from -80°C and kept on ice for 5 min before adding the DNA) and was incubated for 30 min on ice. The cells were occasionally gently tapped during 30 min incubation. Heat shock at 42°C for 40 sec was given to the cells followed by immediate incubation on ice for 5 min. Autoclaved LB (0.9 ml) medium was added to the competent cells and the microcentrifuge tube was incubated at 37°C with shaking in the incubator shaker at 37°C for 60 min at 180 rpm. After the completion of regeneration time, the cells were centrifuged at 2000 rpm for 5 min at 25°C. 800 µl of supernatant was discarded and the cell pellet was re-suspended in

remaining 200 µl supernatant and spread plated on LB agar plates supplemented with the (kanamycin (50 µg/ml) and incubated at 37°C for 16h.

The transformation efficiency was calculated by using the following formula,

$$\text{Transformation efficiency} = \frac{\text{No. of colonies on LB plate}}{\text{Amount of insert (µg)}} = \text{cfu/µg}$$

2.2.13 Isolation of plasmid DNA from transformed colonies by miniprep kit

The LB agar medium plates incubated for overnight were observed for colonies. Colonies preferably from the centre of the plate were randomly picked in a laminar air flow and grown overnight (12h) in 5 ml LB medium supplemented with kanamycin (50 µg/ml). The plasmid DNA from this 5 ml culture was isolated by miniprep kit (Sigma-Aldrich Co. LLC., USA) following the manufacturer's protocol.

The cells were harvested in a 1.5 ml sterilized microcentrifuge tube by centrifugation at 13000*g* for 1 min. The supernatant was discarded and the process was repeated till the entire 5 ml culture was harvested. The resulting cell pellet containing recombinant plasmid was re-suspended in 200 µl resuspension solution by vortexing. RNAse at final concentration of 0.3 mg/ml was added to the re-suspension solution prior to use. To the resuspension, 200 µl of lysis solution was added and the tubes were inverted gently 5-6 times to ensure mixing and allowed to stand for 5 min. To the lysate, 350 µl of neutralization solution was added and the tubes were gently inverted again 4-6 times for proper mixing. The mixture was then centrifuged at 13000***g*** for 10 min. The DNA binding column was prepared and activated by adding 500 µl of column preparation solution to the binding column and then centrifuged at 13000***g*** for 1 min. The flow through accumulated in collection tube was discarded. The clear cell lysate was then transferred to the activated DNA binding column and

centrifuged at 13000***g*** for 1 min. The flow through was discarded again and the plasmid DNA bound to the column was washed with wash solution and centrifuged at 13000***g*** for 1 min. The flow through was discarded and the column was given another 1 min spin at 13000***g*** for removing the residual wash solution completely. Now the column was placed on a fresh sterilized 1.5 ml microcentrifuge tube and 30 µl nuclease- free water was added at the centre of binding column. The column was incubated for 5 min at 25°C. Plasmid DNA was then collected by spinning the column for 1 min at 13000***g***. The eluted plasmid was stored at -20°C for further use.

2.2.14 Screening of recombinant plasmid DNA for positive clone by restriction digestion

The confirmation of pET-28a(+) plasmid containing the gene encoding for *Ps*GH43_12 was done by restriction digestion. 15 µl of recombinant plasmid isolated harbouring the gene encoding *Ps*GH43_12 was taken in separate fresh sterile micro-centrifuge tube. The recombinant plasmid DNA was digested with restriction enzymes, *Nhe*I and *Xho*I, to check for the positive clone in a 10 µl reaction mixture, as mentioned in Table 2.7.

Table 2.7 Restriction enzyme digestion of recombinant plasmid DNA containing gene encoding *Ps*GH43_12.

Reaction components	(µl)
Plasmid DNA (approx. 29 ng/ µl)	5.0
10x reaction buffer	1.0
Nuclease free water	3.5
*Nhe*I (10 U/µl)	0.25
*Xho*I (10 U/µl)	0.25
Total	10

2.2.15 Transformation and expression of protein *Ps*GH43_12 in *E. coli* BL-21(DE3)

The expression of *Ps*GH43_12 was observed through transformation of confirmed recombinant plasmid in *E. coli* BL-21(DE3) competent cells. 2 µl of the recombinant plasmid with gene encoding (*Ps*GH43_12) isolated in Section 2.2.13 was transformed in 200 µl *E. coli* BL-21(DE3) competent cells by heat shock method according to the protocol described in section 2.2.12. The cells were spreaded on LB agar plate supplemented with kanamycin (50 µg/ml) and grown overnight (12h) at 37°C. *E. coli* BL-21(DE3) cells containing the gene encoding *Ps*GH43_12 were cultured in 5 ml of LB medium supplemented with kanamycin (50 µg/ml) at 37°C, 180 rpm. After the cell growth reached mid exponential phase (A_{600} = 0.4) were cooled to 24°C and induced by adding isopropyl-β-D-thiogalactopyranoside (IPTG) at a final concentration varying from 0.25 to 1.0 mM. After IPTG induction, the cells were further incubated at 24°C for 18 h at 180 rpm. From each tube 200 µl of culture medium was collected and centrifuged at 13000*g* for 5 min. The supernatant was discarded and the cells were resuspended in 200 µl water by vortexing. The tubes were again centrifuged at 13000*g* for 5 min. The supernatant was discarded and the cells were resuspended in 40 µl water. The expression of recombinant protein was confirmed by comparing the uninduced and induced cell samples on polyacrylamide gel electrophoresis (SDS-PAGE)

2.2.16 Recombinant *Ps*GH43_12 protein expression analysis by SDS-PAGE

The recombinant protein expression was analyzed by Sodium dodecyl sulphate-Polyacrylamide gel electrophoresis (SDS-PAGE) on 12% (w/v) gel. The hyper-expression of protein was confirmed by comparing the induced and uninduced

E. coli BL-21(DE3) cells on the gel. SDS-PAGE was used by following the method of Laemmli, (1970) and Sambrook et al., (1989) and 12% (w/v) gel was prepared by using ingredients as mentioned in Table 2.8.

Table 2.8 Components for preparation of resolving and stacking gel for SDS-PAGE.

Component	Volume (ml) for 12% resolving gel	Volume (ml) for 4% stacking gel
Acrylamide solution *(30%,w/v)	4.0	0.7
Deionized water	0.6	2.8
SDS (10%, w/v)	1.0	0.5
Glycerol (50%, v/v)	1.0	-
1.5 M Tris-HCl (pH 8.8)	3.3	-
0.5 M Tris-HCl (pH 6.8)	-	1.0
APS (10%, w/v)	0.1	0.05
TEMED	0.01	0.005
Total	10.0	5.0

**mixture of 29.2% (w/v) acrylamide and 0.8% (w/v) N,N'-Methylenebisacrylamide*

SDS-PAGE was run by using 1x Tris-Glycine (25 mM Tris, 192 mM glycine and 0.1% SDS; pH 8.3) running buffer at constant current 40 mA. The expressed and purified protein samples were visualised after staining the gel with staining solution containing (0.25%, w/v) Coomassie Brilliant Blue (CBB) R-250 dye 100 ml solution of deionized water, methanol and glacial acetic acid in 5:4:1 ratio. The gels were de-stained by immersing the gel in de-staining solution containing deionized water, methanol and glacial acetic acid in 5:4:1 ratio. The gels were subjected to gentle shaking under de-staining solution with periodic change of buffer until the protein bands were clearly visible.

2.2.17 Purification of recombinant *Ps*GH43_12 protein

A single-step purification method by using the immobilized metal ion affinity chromatography (IMAC) was employed for purification of His_6-tag linked *Ps*GH43_12. The *E. coli* BL-21 (DE3) cells harbouring the recombinant plasmid

pET-28a(+)-*Ps*GH43_12 were grown in 100 ml LB medium supplemented with kanamycin (50 µg/ml) and induced with optimized concentration 0.25 mM of IPTG when the cell growth reached mid exponential phase (OD_{600}-0.6) for protein expression. The bacterial cells were harvested from the broth by centrifuging at 6000*g* for 15 min. The cell pellet was resuspended in 50 mM sodium phosphate buffer, pH 7.5 and subjected to sonication for 10 min (10s on and 10s off 30 MHz). 1 ml HiTrap gravity column (GE Healthcare, USA) was activated with Ni^{2+} ions using 0.1M $NiSO_4$. The cell free extract obtained after sonication and centrifugation (16000*g*, 40 min) was loaded on to the 1 ml column. The column was washed with 40 ml of equilibration buffer and the bound protein was eluted by elution buffer as mentioned in Table 2.9. The column was cleaned by using cleaning buffer as mentioned in Table 2. 9, further washed with 5 column volumes of water and incubated in 1N NaOH at 4°C for 2h. The column was then washed with 20 column volumes of water to remove NaOH, and finally stored in 20% (v/v) ethanol at 4°C. The eluted protein was dialyzed against 50 mM sodium phosphate buffer, pH 7.5 (1 litre x 4) for 2h. The concentration of protein was determined by Bradford method (Bradford 1976). The purity and molecular mass of recombinant purified protein were verified by running SDS-PAGE using 12% (w/v) gel. The protein samples were boiled for 5 min and loaded on the gel. The gel was stained with Coomassie brilliant blue (Neuhoff et al., 1985). The composition of various buffers used for affinity column purification is mentioned in Table 2.9.

Table 2.9 Composition of buffers required for purification of *Ps*GH43_12 by IMAC.

Buffer	Composition
Resuspension buffer	50 mM sodium phosphate buffer, pH 7.5
Equilibration buffer	50 mM sodium phosphate buffer, pH 7.5 300 mM NaCl, 60 mM imidazole
Elution buffer	50 mM sodium phosphate buffer, pH 7.5 300 mM NaCl, 300 mM imidazole
Dialysis buffer	50 mM sodium phosphate buffer, pH 7.5
Cleaning buffer	50 mM sodium phosphate buffer, pH 7.5 500 mM NaCl, 20 mM EDTA

2.2.18 Protein concentration determination of purified *Ps*GH43_12 protein by UV method

The concentration of purified *Ps*GH43_12 protein was determined by taking absorbance at 280 nm (A_{280}) and by using the equation below (Layne, 1957; Stoscheck, 1990). The absorbance was measured after appropriate dilution of the protein by using a spectrophotometer (Gene Quant, GE) having a path length of 1 cm. The molar extinction co-efficient 77240 $M^{-1}cm^{-1}$ for *Ps*GH43_12 was used.

$$\text{Concentration of protein (mg/ml)} = \frac{\text{Absorbance at 280 nm x Mol. mass (Da)}}{\text{Extinction coefficient } (M^{-1}cm^{-1}) \text{ x Path length (1 cm)}}$$

2.2.19 Protein concentration determination of purified protein *Ps*GH43_12 by Bradford method

The concentration of the recombinant protein was determined by the Bradford method measuring the absorbance at wavelength, 595 nm (A_{595}) (Bradford, 1976). Bovine serum albumin (BSA) purchased from Sigma-Aldrich Co. LLC., USA. was used as standard protein. A standard plot of A_{595} versus different concentration of BSA (1–10 μg/ml) was prepared. The amount of protein was estimated by using the following equation,

$$[\text{Protein}] = \frac{\Delta A_{595} \times V \times C}{v}$$

Where,

ΔA_{595} = change in absorbance of the sample

V = volume of the reaction mixture (ml)
C = 1 OD equivalent of BSA from standard plot (mg/ml)

2.3 Results and Discussion

2.3.1 Sequence analysis of *Ps*GH43_12

A schematic representation of the molecular architecture of *Ps*GH43_12 is given in Fig. 2.2. The amino acid sequence of *Ps*GH43_12 with locus tag Pedsa_2580 from *Psuedopedobacter saltans* was retrieved from NCBI. CDD search analysis of Pedsa_2580 revealed the presence of catalytic module with putative α-L-arabinofuranosidase activity belonging to family 43 glycoside hydrolase. BLASTp analysis of *Ps*GH43_12 displayed the sequence similarity with β-1,4-xylosidase from *Geobacillus thermoleovorans* (35.6% identity, PDB ID 5Z5D) and α-L-arabinofuranosidase (*Bo*GH43) from *Bacteroides ovatus* ATCC 8483 (35.4% identity, PDB ID 5JOW). The subcellular localization of *Ps*GH43_12 revealed that it contains 29 amino acid long signal peptide and predicted a cleavage site between Ser29 and Val30 followed by a catalytic module of 557 amino acids (Fig. 2.2). The predicted theoretical molecular mass, pI and molecular extinction coefficient of *Ps*GH43_12 was found to be 65.02 kDa, 8.35 and 77240 $M^{-1}cm^{-1}$, respectively.

MRRKSVFHPLKFYSSCLLVLSCFTQSCKSVEPQDTKERTNEPIFSNFAYKGDDKVYRENPVSSNKFYTSILQGCYP
DPAITRKGDDYFLVNSSFTFFPGVPIFHSKDLVNWRQIGHVLDRPSQLKVENTLMNFGVYAPAIKYNQYNDTFYMI
TTQFSGGFGNIVVKTKDPFKGWSDPIKLQFDGIDPSMFFDDNGKAYVVHNDAPAKGAELYNGHRVIKIWDYDLEND
RVVPGTDKIIVNGGVDISKKPIWIEAPHIYKKNGRYYLMCAEGGTGGAHSEVIFSSDNPRGPYTPAPKNPILTQRH
LPANRPDKVDWAGHADLVEGPDGKYYGVFLGIRPNEKDRVNTGRETFILPVDWTGEFPVFENGLEPMPATIKTPAG
VVNKKGDEGFFPSGNFEFKDNFDNEKLDYRWIGVRGPREHFVHSDKKGGLRIKPFTVNISEVKPTSTLFYRQQHNN
FSAEVAINYQPNSEKDLAGLVCMQNEKFNYVFGVTKKGKTNYIVLQRTQNGIKTIVASEKVDINKPLRLQVKANGD
NYEFAFKSGNAGYKMLGGIVSGDILSTNVAQGFTGNLIGLYATLNNNMDLSVIK

Fig. 2.2 Molecular architecture and sequence of protein Pedsa_2580.

2.3.2 PCR amplification of gene encoding *Ps*GH43_12

The gene encoding *Ps*GH43_12 was amplified from the genomic DNA of *Pseudopedobacter saltans* DSM-12145 by using the conditions mentioned in Section 2.2.3. The amplicon was checked on 0.8% (w/v) agarose gel and is displayed in Fig. 2.3. The PCR product was purified from gel using gel extraction kit as mentioned in section 2.2.6 and stored at -20°C.

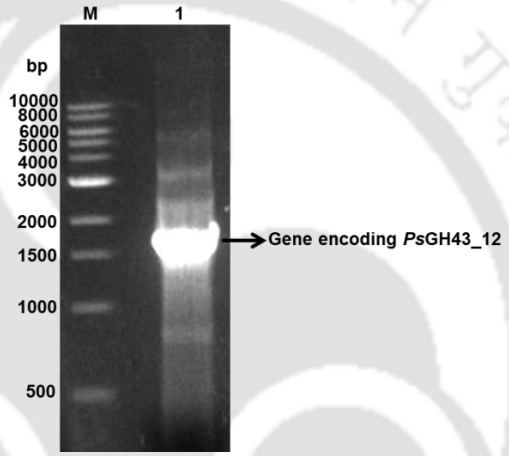

Fig. 2.3 Agarose gel (0.8%, w/v) showing Lane M- DNA marker (1 kb DNA ladder, NEB) and Lane 1- PCR amplified gene encoding *Ps*GH43_12 of size around 1.7 kb.

2.3.3 Digestion of PCR insert DNA and vector DNA by restriction enzyme

The PCR insert DNA and Vector DNA were digested by using the protocol described in section 2.2.10. The double digested insert DNA and Vector DNA were loaded on 0.8% (w/v) agarose gel and purified from gel by using the gel extraction kit as mentioned in section 2.2.6. Agarose gels showing the digested pET-28a(+) vector of approximately, 5.3 kb and the gene encoding *Ps*GH43_12 of 1.7 kb are displayed in Fig. 2.4.

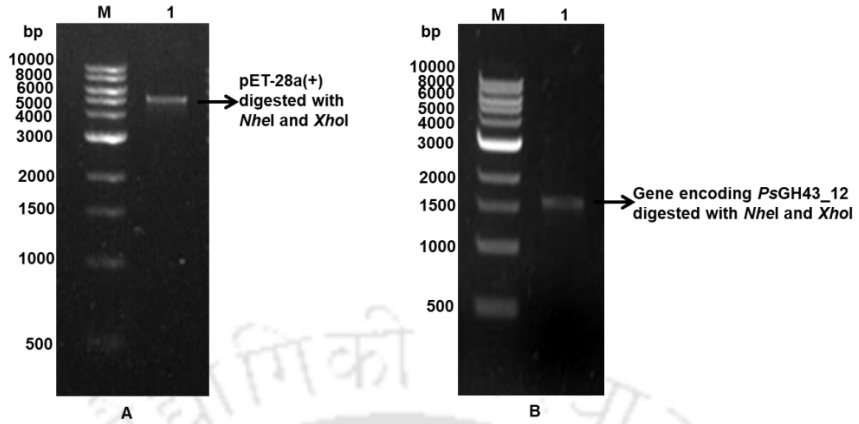

Fig. 2.4 Agarose gels (0.8%, w/v) showing (A) Lane M- DNA marker (1 kb DNA ladder, NEB) and Lane 1- vector preparation by restriction digestion of pET-28a(+) with *Nhe*I and *Xho*I enzymes (B) Lane M- DNA marker (1 kb DNA ladder, NEB) and Lane 1- insert preparation by restriction digestion of PCR amplified gene with *Nhe*I and *Xho*I enzymes

2.3.4 Cloning of gene encoding *Ps*GH43_12 into pET-28a (+) vector

The ligation was performed after the preparation of insert and vector. The restriction enzyme digested gene encoding *Ps*GH43_12 was ligated with the linearized fragment of pET-28a (+) vector by following the protocol mentioned in Section 2.2.11. The ligated product was transformed into *E. coli* DH5α competent cells and grown overnight (12h) on LB agar plates grown at 37°C under stationary condition. The *E. coli* DH5α competent cells having transformation efficiency $1.7x10^7$ cfu/µg were used.

2.3.4.1 Isolation of recombinant plasmid DNA

The plasmid DNA from *E. coli* DH5α colonies transformed with the gene encoding *Ps*GH43_12 into pET-28a(+) was isolated by Plasmid miniprep kit following the protocol mentioned in Section 2.2.13. The isolated plasmid was visualized by electrophoresis on 0.8% (w/v) agarose gel (Fig.2.5). Positive clone was confirmed by restriction digestion of this isolated plasmid DNA.

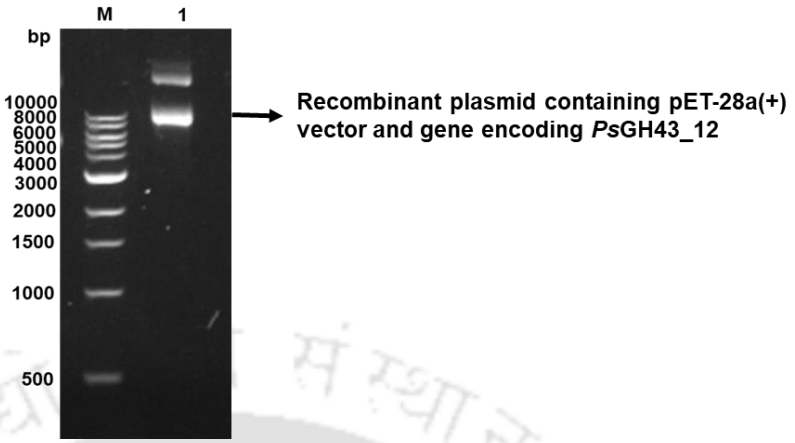

Fig. 2.5 Agarose gels (0.8%, w/v) showing (A) Lane M- DNA marker (1 kb DNA ladder, NEB) and Lane 1- Recombinant plasmid DNA.

2.3.4.2 Restriction digestion of isolated plasmid DNA for confirmation of positive clone

The isolated plasmid was digested with *Nhe*I and *Xho*I restriction enzymes for confirming the positive clone. The plasmid map of positive clone is shown in Fig. 2.5A. The plasmid after restriction digestion was electrophoresed on 0.8% (w/v) agarose gel. *Nhe*I and *Xho*I digested fragment of gene encoding *Ps*GH43_12 (Fig. 2.6B; Lane 1) was visualized on agarose gel at around 1.7 kb and linearized pET-28a(+) vector was visualized at around 5.3 kb. The positive clone was sequenced (AgriGenome Labs Pvt Ltd., India) and no mutation was detected. (Fig. 2.7).

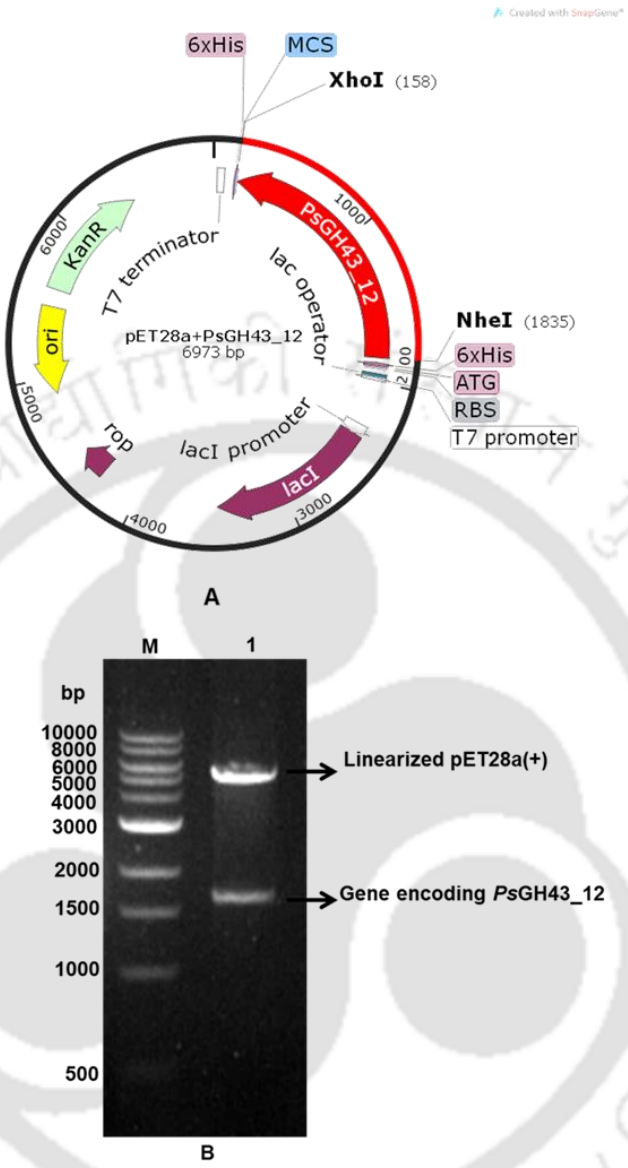

Fig. 2.6 (A) Plasmid map of positive clone pET-28a(+) *Ps*GH43_12, (B) Agarose gel (0.8%, w/v) Lane M- DNA marker (1 kb DNA ladder, NEB), Lane 1- showing *Nhe*I-*Xho*I digested recombinant plasmid containing gene encoding *Ps*GH43_12 (~1.7 kb).

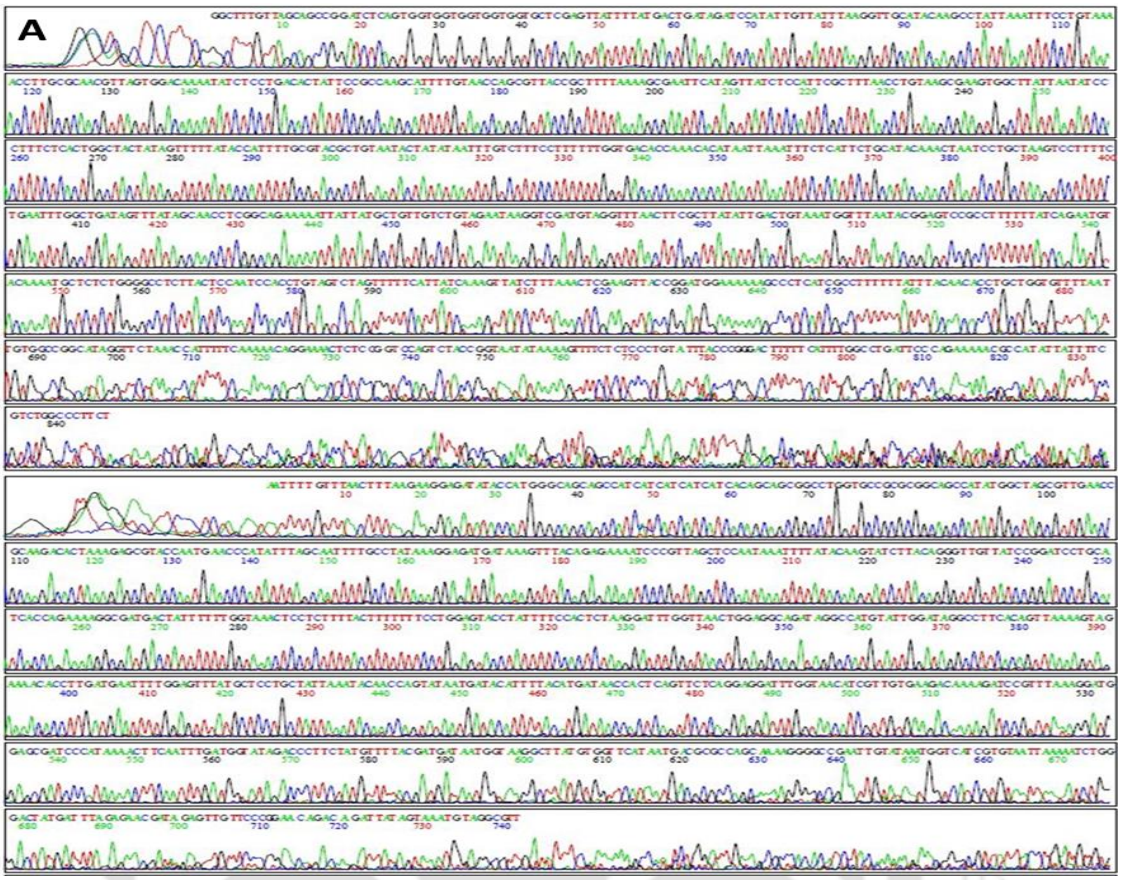

B

CGGGGGGACATTACGTGTTCATTCCCCTCTAGAAATAATTTTGTTTAACTTTAAGAAGGAGATATACCATGGGCAGCAGCC
ATCATCATCATCATCACAGCAGCGGCCTGGTGCCGCGCGGCAGCCATATGGCTAGCGTTGAACCGCAAGACACTAAAGAG
CGTACCAATGAACCCATATTTAGCAATTTTGCCTATAAAGGAGATGATAAAGTTTACAGAGAAAATCCCGTTAGCTCCAAT
AAATTTTATACAAGTATCTTACAGGGTTGTTATCCGGATCCTGCAATCACCAGAAAAGGCGATGACTATTTTTTGGTAAAC
TCCTCTTTTACTTTTTTTTCCTGGAGTACCTATTTTCCACTCTAAGGATTTGGTTAACTGGAGGCAGATAGGCCATGTATTGGA
TAGGCCTTCACAGTTAAAAGTAGAAAACACCTTGATGAATTTTGGAGTTTATGCTCCTGCTATTAAATACAACCAGTATAA
TGATACATTTTACATGATAACCACTCAGTTCTCAGGAGGATTTGGTAACATCGTTGTGAAGACAAAAGATCCGTTTAAAGG
ATGGAGCGATCCCATAAAACTTCAATTTGATGGTATAGACCCTTCTATGTTTTACGATGATAATGGTAAGGCTTATGTGGTT
CATAATGACGCGCCAGCAAAAGGGGCCGAATTGTATAAATGGTCATCGTGTAATTAAAAATCTGGGACTATGATTTAGAG
AACGATAGAGTTGTTCCCGGAACAGACAGATTATAGTAAATGTAGGCGTTTGATATTTCAAAAAAGCCAATCTGGATTGA
AGCGCCACACATCTACAAAAGAACGGGCGTTATTACCTGAATGTGTGCAGAAAGAGGTACAGGAGGAGCGCACTGTGAA
AAAAGAAGTCGCTTCTTTCGGGCTTTGTTAGCAGCCGGATCTCAGTGGTGGTGGTGGTGGTGCTCGAGTTATTTTATGACTG
ATAGATCCATATTGTTATTTAAGGTTGCATACAAGCCTATTAAATTTCCTGTAAAACCTTGCGCAACGTTAGTGGACAAAA
TATCTCCTGACACTATTCCGCCAAGCATTTTGTAACCAGCGTTACCGCTTTTAAAAGCGAATTCATAGTTATCTCCATTCGC
TTTAACCTGTAAGCGAAGTGGCTTATTAATATCCACTTTCTCACTGGCTACTATAGTTTTTATACCATTTTGCGTACGCTGTA
ATACTATATAATTTGTCTTTCCTTTTTTGGTGACACCAAACACATAATTAAATTTCTCATTCTGCATACAAACTAATCCTGCT
AAGTCCTTTTCTGAATTTGGCTGATAGTTTATAGCAACCTCGGCAGAAAAATTATTATGCTGTTGTCTGTAGAATAAGGTCG
ATGTAGGTTTAACTTCGCTTATATTGACTGTAAATGGTTTAATACGGAGTCCGCCTTTTTTATCAGAATGTACAAAATGCTC
TCTGGGGCCTCTTACTCCAATCCACCTGTAGTCTAGTTTTTCATTATCAAAGTTATCTTTAAACTCGAAGTTACCGGATGGA
AAAAAGCCCTCATCGCCTTTTTTATTTACAACACCTGCTGGTGTTTTAATTGTGGCCGGCATAGGTTCTAAACCATTTTTCA
AAAACAGGAAAACTCTCCGGTCCAGTCTACCGGTAATATAAAAGTTTTCTCTCCCTGTATTTACCCGGGACTTTTTCATTTT
GGCCTGATTCCCAGAAAAACGCCATATTATTTTCCGTCTGGCCCTTCTAATAATTCTGCATGTCCGGCCCAGTCTACCCTTA
TCAGGCCTATTTGCCGGCAATGTCTTTGCGTTAGAATAGGATTTTTTGGAGCCGGTGAATTA

Fig. 2.7 DNA Sequencing results of gene encoding *Ps*GH43_12 by using T7 promoter gene specific primers. (A**)** Electropherogram showing the DNA sequencing result for cloned gene encoding *Ps*GH43_12. Sequencing was done by using T7 forward and T7 reverse primers, (B) The *Ps*GH43_12 deduced sequence.

2.3.5 Expression and purification of recombinant protein

The *E. coli* BL-21 (DE3) competent cells were transformed with recombinant pET28a(+) plasmid containing gene encoding *Ps*GH43_12. The transformation efficiency of *E. coli* BL-21 (DE3) competent cell was $1.8x10^7$ cfu/µg. The colonies were picked randomly and grown in 5 ml LB medium supplemented with kanamycin (50 µg/ml). The cells were induced for protein expression at mid exponential stage as described in Section 2.2.15. Protein expression was analysed by SDS-PAGE using 12% w/v gel as depicted in Fig. 2.8. The expressed *Ps*GH43_12 showed molecular weight of approximately, 65 kDa size. The cells induced with isopropyl-β-D-thiogalactopyranoside (IPTG) at final concentrations 0.25, 0.50 and 1.0 mM are shown in Fig. 2.8. The optimum concentration of IPTG for protein hyper-expression was optimized to be 0.25 mM.

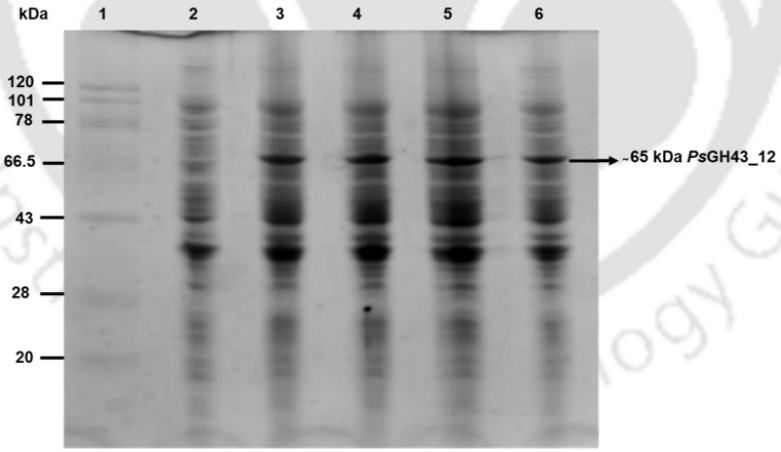

Fig. 2.8 SDS-PAGE (12% w/v gel) showing hyper-expression of *Ps*GH43_12. Lanes 1- Protein marker (BioBharti, India), 2- Uninduced cells, 3- Induced cells (0.25 mM), lane 4- Induced cells (0.5 mM)**,** 5- Induced cells (0.75 mM) and 6- Induced cells (1 mM IPTG)

The recombinant protein was purified by IMAC as described in Section 2.2.17 and then dialysed for removal of imidazole and sodium chloride. The recombinant

*Ps*GH43_12 expressed as a soluble protein and after purification displayed homogeneous single band on 12% (w/v) gel after SDS-PAGE analysis (Fig. 2.9). The purified *Ps*GH43_12 containing Hexa-Histidine tag (MGSSHHHHHHSSGLVPRGSHMAS) at N-terminal in the pET28a- *Ps*GH43_12 constructs, gave the molecular mass of approximately, 65 kDa, which was in the agreement with the size obtained from protein primary sequence analysis by expasy protparam.

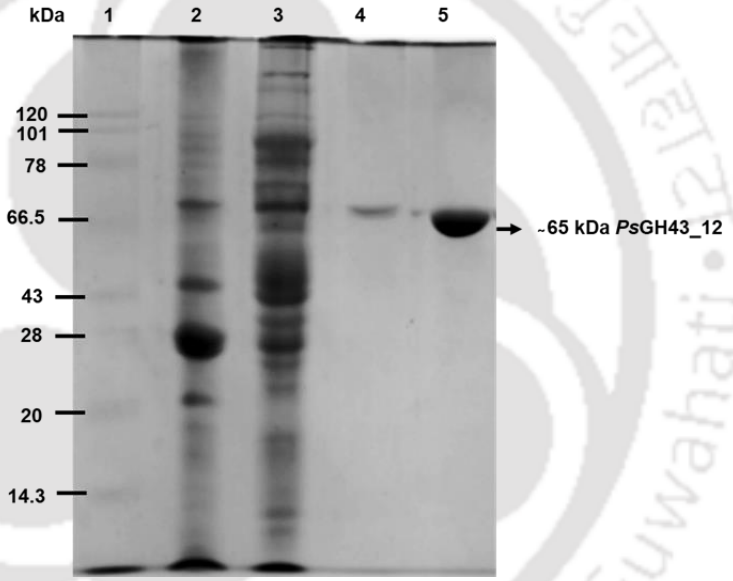

Fig. 2.9 SDS-PAGE (12% w/v) gel showing purification of *Ps*GH43_12. Lanes 1- Protein marker (BioBharti, India), 2- cell pellet (after sonication), 3- cell free supernatant, 4- Last column wash, 5- purified *Ps*GH43_12 (~65 kDa).

2.3.6 Protein Estimation of purified *Ps*GH43_12 recombinant

The amount of purified recombinant protein obtained from 100 ml of grown *E. coli* BL-21(DE3) cells was calculated by using the formula mentioned in Section 2.2.18. Both UV and Bradford method obtained approximately, 3.5 mg of *Ps*GH43_12 protein from 100 ml LB medium.

2.4 Conclusions

The gene encoding *Ps*GH43_12 of Glycoside hydrolase family 43 (GH43) in *Pseudopedobacter saltans* DSM12145 (GenBank Accession No: ADY53124.1) was cloned, expressed and purified. The molecular architecture revealed a signal peptide (29 amino acid residues) at N-terminal followed by a catalytic module *Ps*GH43_12 of 557 amino acid residues. The PCR amplified gene fragment encoding *Ps*GH43_12 showed a band of ~1.7 kb. The restriction enzyme digested fragments of gene encoding *Ps*GH43_12 was ligated with linearized pET-28a(+) expression vector. The ligated mixture was transformed into *E. coli* DH5α competent cells. The positive clones containing recombinant plasmid DNA were screened by restriction enzyme digestion using enzymes, *Nhe*I and *Xho*I. The restriction enzyme digested products were electrophoresed and the band of ~ 5.3 kb was produced for pET-28a(+) vector and corresponding band of ~1.7 kb was produced from the insert fragment for gene encoding *Ps*GH43_12. The recombinant plasmid DNA containing gene encoding *Ps*GH43_12 was transformed into *E. coli* BL-21 (DE3) cells. The recombinant, *Ps*GH43_12 was expressed as soluble homogenous protein. The purified recombinant *Ps*GH43_12 displayed a single band of molecular mass approximately, 65 kDa by SDS-PAGE analysis. The amount of purified recombinant *Ps*GH43_12 obtained from 100 ml *E. coli* BL-21 (DE3) cells was 3.5 mg.

2.5 References

Ahmed, S., Luis, A. S., Bras, J. L., Ghosh, A., Gautam, S., Gupta, M. N., & Goyal, A. (2013). A novel α-L-arabinofuranosidase of family 43 glycoside hydrolase (*Ct*43Araf) from *Clostridium thermocellum*. *PLoS One*, 8(9), e73575.

Balasubramaniam, K., Sharma, K., Rani, A., Rajulapati, V., & Goyal, A. (2018). Deciphering the mode of action, structural and biochemical analysis of heparinase II/III (PsPL12a) a new member of family 12 polysaccharide lyase from *Pseudopedobacter saltans*. *Annals of Microbiology*, *68*(6), 409-418.

Bradford, M. M. (1976). A rapid and sensitive method for quantitation of microgram quantities of protein utilizing the principle of protein-dye binding. *Analytical Biochemistry*, *72*, 248-254.

Hespell, R. B., & O'Bryan, P. J. (1992). Purification and characterization of an α-L-arabinofuranosidase from *Butyrivibrio fibrisolvens* GS113. *Applied and Environmental Microbiology*, *58*(4), 1082-1088.

Laemmli, U. K. (1970). Cleavage of structural proteins during the assembly of the head of bacteriophage T4. *Nature*, *227*(5259), 680.

Layne, E. (1957). Spectrophotometric and turbidimetric methods for measuring proteins. Academic Press, New York, (3) 447-454

Liolios, K., Sikorski, J., Lu, M., Nolan, M., Lapidus, A., Lucas, S., & Han, C. (2011). Complete genome sequence of the gliding, heparinolytic *Pedobacter saltans* type strain (113 T). *Standards in Genomic Sciences*, *5*(1), 30.

Lombard, V., Golaconda Ramulu, H., Drula, E., Coutinho, P. M., & Henrissat, B. (2013). The carbohydrate-active enzymes database (CAZy) in 2013. *Nucleic Acids Research*, *42*(D1), D490-D495.

Mewis, K., Lenfant, N., Lombard, V., & Henrissat, B. (2016). Dividing the large glycoside hydrolase family 43 into subfamilies: a motivation for detailed enzyme characterization. *Applied and Environmental Microbiology*, *82*(6), 1686-1692.

Neuhoff, V., Stamm, R., & Eibl, H. (1985). Clear background and highly sensitive protein staining with Coomassie Blue dyes in polyacrylamide gels: a systematic analysis. *Electrophoresis*, *6*(9), 427-448.

Rani, A., & Goyal, A. (2016). A new member of family 8 polysaccharide lyase chondroitin AC lyase (*Ps*PL8A) from *Pedobacter saltans* displays endo-and exo-lytic catalysis. *Journal of Molecular Catalysis B: Enzymatic*, *134*, 215-224.

Saha, B. C. (2000). α-L-Arabinofuranosidases: biochemistry, molecular biology and application in biotechnology. *Biotechnology Advances*, *18*(5), 403-423.

Saha, B. C., & Bothast, R. J. (1997). Enzymes in lignocellulosic biomass conversion, Fuels and Chemicals from Biomass, *ACS Publications 666*, 46-56.

Sambrook, J., & Russell, D. W. (2001). *Molecular cloning: a laboratory manual*. Cold Spring Harbor, NY: Cold Spring Harbor Laboratory. *1*,112

Sambrook, J., Fritsch, E. F., & Maniatis, T. (1989). *Molecular cloning: a Laboratory Manual* (No. Ed. 2). Cold spring harbor laboratory press.

Sharma, K., Antunes, I. L., Rajulapati, V., & Goyal, A. (2018). Molecular characterization of a first endo-acting β-1, 4-xylanase of family 10 glycoside hydrolase (*Ps*GH10A) from *Pseudopedobacter saltans* comb. nov. *Process Biochemistry*, *70*, 79-89.

Sozzi, G. O., Fraschina, A. A., Navarro, A. A., Cascone, O., Greve, L. C., & Labavitch, J. M. (2002). α-L-Arabinofuranosidase activity during development and ripening of normal and ACC synthase antisense tomato fruit. *HortScience*, *37*(3), 564-566.

Stoscheck, C. M. (1990). [6] Quantitation of protein. In *Methods in Enzymology*. Academic Press.*182*, 50-68.

Studier, F. W. (1990). Use of T7 RNA polymerase to direct expression of cloned genes. *Methods in Enzymology* 185, 60-89.

Studier, F. W., & Moffatt, B. A. (1986). Use of bacteriophage T7 RNA polymerase to direct selective high-level expression of cloned genes. *Journal of Molecular Biology*, *189*(1), 113-130.

Thakur, A., Sharma, K., & Goyal, A. (2019). α-l-Arabinofuranosidase: A potential enzyme for the food industry. In *Green Bio-processes*. Springer, Singapore. 229-244

Viborg, A. H., Sørensen, K. I., Gilad, O., Steen-Jensen, D. B., Dilokpimol, A., Jacobsen, S., & Svensson, B. (2013). Biochemical and kinetic characterisation of a novel xylooligosaccharide-upregulated GH43 β-D-xylosidase/α-L-

arabinofuranosidase (BXA43) from the probiotic *Bifidobacterium animalis* subsp. lactis BB-12. *AMB Express*, *3*(1), 1-8.

Wagschal, K., Franqui-Espiet, D., Lee, C. C., Kibblewhite-Accinelli, R. E., Robertson, G. H., & Wong, D. W. (2007). Genetic and biochemical characterization of an α-L-arabinofuranosidase isolated from a compost starter mixture. *Enzyme and Microbial Technology*, *40*(4), 747-753.

Zhou, A., Hu, Y., Li, J., Wang, W., Zhang, M., & Guan, S. (2020). Characterization of a recombinant β-xylosidase of GH43 family from *Bacteroides ovatus* strain ATCC 8483. *Biocatalysis and Biotransformation*, *38*(1), 46-52.

Chapter 3

Biochemical characterization, regioselective and synergistic action of α-L-arabinofuranosidase of family 43 glycoside hydrolase (*Ps*GH43_12) from *Pseudopedobacter saltans*

3.1 Introduction

The plant cell wall has a complex structure consisting of carbohydrate, lignin, lipid and protein. Cellulose, hemicellulose and pectin are the major carbohydrate components. The cellulose is the most abundant polysaccharide and is simple structure, made up of glucose. The complex structure of hemicellulose is because of presence of side chain. Xylan belongs to the second most abundant structural component, the hemicellulose part of the secondary walls of dicot plants. Xylan has a backbone of β-(1→4)-linked xylose residues. Xylans are found with various degrees of substitution based on the plant tissue types and species. The common side chain substitutions on the xylan backbone are arabinose, acetic acid, glucuronic acid, ferulic acid, *p*-coumaric acid or *4-O*-methyl glucuronic acid (Ordaz and Saulnier 2005). Depending on the relative richness of their substitutions within the xylans, further categorized into Glucuronoxylan, Arabinoxylans and Xyloglucans etc. Arabinoxylan

is a non-starch polysaccharide, mainly found in cereal plants, considered as dietary fiber. Arabinoxylans have the β-(1→4)-linked xylose backbone with the substitution of one or more L-arabinofuranosyl units, at position 2 or 3 (Thakur et al., 2019). Arabinoxylan is located in primary cell walls of grasses and monocot plants cereals like wheat, rye, barley, oat, rice, corn and sorghum (Brett and Waldron 1990). L-Arabinosyl residues are extensively found in these polymers as side chains. The presence of L-arabinosyl side chain hinders the enzymes, in the hydrolysis of hemicelluloses and pectins causing a technological bottleneck for the advancement of various industrial processes (Saha 2000). α-L-Arabinofuranosidase is one of the important hemicellulases, which cleaves α-L-arabinofuranosidic bond (1→2, 1→3 and 1→5) and plays a vital role towards complete degradation of hemicellulose and pectins by acting synergistically with other hemicellulases and pectic enzymes (Margolles et al., 1996). α-L-Arabinofuranosidase cleaves the arabinose side chain from arabinose substituted polysaccharides (Wilkens et al., 2017). The mode of action of hydrolysis by α-L-arabinofuranosidase is overall inversion of the anomeric configuration (Saha 2000).

Exo α-L-arabinofuranosidase (EC 3.2.1.55) are found in glycoside hydrolase (GH) families 2, 3, 43, 51, 54 and 62 (http://www.cazy.org/) (Lombard et al., 2013). Family 43 glycoside hydrolase contains β-xylosidase, α-L-arabinofuranosidase, xylanase, α-1,2-L-arabinofuranosidase, exo-α-1,5-L-arabinofuranosidase, exo-α-1,5-L-arabinanase, β-1,3-xylosidase, exo-α-1,5-L-arabinanase, endo-α-1,5-L-arabinanase, exo-β-1,3-galactanase and β-D-galactofuranosidase. Total 16079 enzymes (182 characterized) are reported in family 43 glycoside hydrolase. On the basis of sequence similarity family 43 glycoside hydrolase is further sub classified into 37 subfamilies

(Mewis et al., 2016). *Ps*GH43_12 belongs to subfamily 12 of family 43 glycoside hydrolase. In the present study, biochemical characterization, regioselective analysis and synergistic action of the purified protein *Ps*GH43_12 is studied.

3.2 Materials and Methods

3.2.1 Microbes, plasmids and chemicals

All reagents, buffer components and salts were purchased from Sisco Research Laboratories Pvt. Ltd. Mumbai, India. Rye arabinoxylan, wheat arabinoxylan and 4-nitrophenyl-glycoside *(p*NPG) substrates were purchased from Megazyme (Ireland). TLC plates were from Merck, Germany. Oat spelt xylan, beechwood xylan and carboxymethyl cellulose were procured from Sigma-Aldrich Co. LLC., USA.

3.2.2 Enzyme assay

3.2.2.1 Against natural substrates

Arabinofuranosidase activity was checked by using 1% (w/v) rye arabinoxylan dissolved in citrate phosphate buffer (50 mM, pH 6.5). The reaction volume, 100 µl contained 90 µl of the substrate and 10 µl of the enzyme (*Ps*GH43_12, 50 µg/ml). The reaction mixture was incubated at 50°C for 5 min. The method of Nelson (Nelson 1944) and Somogyi (Somogyi 1945) for estimating the reducing sugar concentration was followed by using the standard curve of L-arabinose. The specific activity of *Ps*GH43_12 was defined as number of µmole of arabinose released from arabinoxylan per min per mg of enzyme (µmol/min/mg) under the optimum conditions of enzyme.

3.2.2.2 Against synthetic substrates

The enzyme activity was checked against synthetic substrates *viz*, *p*-nitrophenyl-glycosides (*p*NP-α-L-arabinopyranoside, *p*NP-α-L-arabinofuranoside, *p*NP-β-D-glucoside, *p*NP-β-L-arabinopyranoside and *p*NP -β-D-xylopyranoside), 500 µl of the reaction mixture was prepared by taking 480 µl of the substrate (4 mM)

dissolved in 50 mM citrate phosphate buffer (pH 6.5), 20 µl of buffer for blank and 20 µl of the enzyme (*Ps*GH43_12, 50 µg/ml) for assay. The reaction was stopped after 5 min of incubation by adding 500 µl of 0.5 M sodium carbonate solution. The released *p*NP was quantified by taking the absorbance at 410 nm (A_{410}) and the enzyme activity was calculated by using a standard plot of *p*NP (Margolles and Clara 2003). All assays were carried out in triplicate.

3.2.3 Biochemical characterization of α-L arabinofuranosidase (*Ps*GH43_12)

3.2.3.1 pH and Temperature optimization

The pH optimization of *Ps*GH43_12 activity was carried out by incubating, the reaction mixtures (100 µl) containing final 1.0% (w/v) rye arabinoxylan dissolved in 50 mM citrate phosphate buffer pH (3.0-7.0), 50 mM sodium phosphate buffer pH (6.0-8.0) or 50 mM bicine buffer pH (7.5-9.0) and 10 µl of *Ps*GH43_12 (50 µg/ml) at 50°C for 5 min. The method of Nelson (Nelson 1944) and Somogyi (Somogyi 1945) was used for estimation of the reducing sugar. The percent relative activity was calculated and plotted against the range of pH tested.

The optimum temperature of *Ps*GH43_12 activity was determined by incubating, the 100 µl reaction mixture containing final 1.0% (w/v) rye arabinoxylan (90 µl) in 50 mM citrate phosphate buffer, (pH 6.5) at different temperatures ranging from 5°C to 70°C. The volume of the enzyme was 10 µl (50 µg/ml). The reducing sugar released was estimated by method of Nelson (Nelson 1944) and Somogyi (Somogyi 1945). The relative activity (%) of *Ps*GH43_12 was calculated and plotted against the different temperature.

3.2.3.2 pH and Temperature stability

The pH stability of *Ps*GH43_12 was studied by incubating the enzyme (50 µg/mL) at 30°C for 90 min in a wide pH range, 3-8.5 with different buffers: 50 mM citrate-phosphate (pH 3.0-6.5), 50 mM sodium phosphate (pH 6-8), 50 mM and HEPES (pH 7.5-8.5). The thermal stability study of *Ps*GH43_12 was carried out by incubating 100 µl of the enzyme (50 µg/mL) in 50 mM sodium phosphate buffer (pH 8.0) at a different temperature ranging between 30°C-60°C for 90 min. The thermal stability of *Ps*GH43_12 for longer duration *i.e.* 3 months was determined by incubating the enzyme (50 µg/mL) at 4°C, 30°C, 50°C and 55°C. The reaction was set up as explained in section 2.5.1. The released of reducing sugar concentration was estimated by the method of Nelson (Nelson 1944) and Somogyi (Somogyi 1945) and the residual activity (%) was calculated and plotted against pH or temperature. The half-life $t_{1/2}$ of *Ps*GH43_12 at different temperatures were calculated by following an earlier report (Margolles and Clara 2003).

3.2.3.3 Substrate specificity and kinetic parameters of *Ps*GH43_12

The hydrolytic action of *Ps*GH43_12 was assayed against natural substrates (rye arabinoxylan, wheat arabinoxylan, arabinogalactan, insoluble wheat arabinoxylan, oat spelt xylan, galactomannan, beechwood xylan and avicel) and synthetic *p*NP glycosides (*p*NP-α-L-arabinopyranoside, *p*NP-α-L-arabinofuranoside, *p*NP-β-D-glucuronide, *p*NP-β-L-arabinopyranoside and *p*NP -β-D-xylopyranoside). The released reducing sugar from natural substrates was estimated by the method of Nelson (Nelson 1944) and Somogyi (Somogyi 1945) for estimation of *p*NP glycosides, the A_{410} was used as explained in section 2.5.2. The optimized conditions of temperature, 50°C, pH, 6.5 of 50 mM citrate phosphate) and the reaction time of 5

min were used for assaying the enzyme activity of *Ps*GH43_12. The kinetic parameters of *Ps*GH43_12 (V_{max}, K_m and k_{cat}) were determined against rye arabinoxylan, wheat arabinoxylan and *p*NP-α-L-arabinofuranoside. The specific activities versus substrate concentration were plotted using GraphPad Prism v8.0 software and kinetic parameters were determined.

3.2.3.4 Effect of metal ion on *Ps*GH43_12 activity

The effects of different metal ions on the activity of *Ps*GH43_12 were determined. The enzyme (0.05 mg/ml) in 100 µl reaction mixture containing 0.9% (w/v) wheat arabinoxylan in 50 mM HEPES buffer, pH 6.5 and metal salt at low molar concentrations (up to 20 mM) was incubated at 50°C for 5 min. The reaction without any metal ion was run in parallel and used as a control. The residual enzyme activity was calculated by estimating the reducing sugars by the method reported by Nelson (Nelson 1944) and Somogyi (Somogyi 1945). The residual activity of *Ps*GH43_12 was determined, by considering the specific activity of *Ps*GH43_12 without any metal ion as 100%.

3.2.3.5 Mode of action analysis of *Ps*GH43_12 by TLC, mass spectrometry and HPLC

The qualitative analysis of *Ps*GH43_12 hydrolysed products of natural substrates was performed by thin layer chromatography (TLC) using silica gel-coated aluminum plate (Merck, Germany). 180 µl of 1% (w/v) rye arabinoxylan in 50 mM citrate phosphate buffer, pH 6.5 containing with 20 µl of *Ps*GH43_12 (0.05 mg/ml) was incubated at 50°C for 5 min, 30 min and 1 h. The reaction was stopped by adding 3 volume *i.e.* 600 µl of absolute ethanol and subjected to centrifugation at 13000*g* for 5 min. The supernatant was transferred to fresh microcentrifuge tube and kept in the

hot air oven at 75°C for 7 h. 0.6 µl of each sample was loaded on TLC plate along with the standards, xylose (1 mg/ml) and arabinose (1 mg/ml). Chloroform: glacial acetic acid: water (6:7:1) was used as mobile phase and solution containing 0.5% α-naphthol in sulfuric acid: ethanol (5:95) was used for visualizing (Sharma et al., 2018). The concentrated *Ps*GH43_12 hydrolysed products were subjected to mass spectrometric analysis as reported earlier (Sharma et al., 2018). *Ps*GH43_12 hydrolysed products dissolved at a concentration of 0.6 mg/mL in water was used for analysis by Electron Spray Ionization (ESI) mass spectrometer (Waters, Q-TOF Premier) in positive mode for ESI–MS mode. L-arabinose at a final concentration of 2 mg/mL was used ESI-MS analysis and for further comparing with *Ps*GH43_12 hydrolysed products. D-Xylose and L-arabinose are of similar molecular mass *i.e.* 150 Da therefore, the *Ps*GH43_12 hydrolysed product was subjected to HPLC analysis for further confirmation of the released L-arabinose from the side chain of arabinoxylan The analysis was carried out by using HPLC system (LC-20AD, Shimadzu corporation, Japan) coupled with an autosampler (SIL-20AHT, Shimadzu corporation, Japan) and RI detector (RID-10A, Shimadzu corporation, Japan). Standard arabinose procured from Sigma Aldrich, USA were used at concentration 1 mg/mL. The HPLC column (Phenomenex Rezex ROA (H+) organic acid and monosaccharide column (300 x 7.8 mm)) coupled with a guard column (50 x7.8 mm) was used. A mobile phase of 0.005 N H_2SO_4 was run through the column at a flow rate of 0.5 mL/min.

3.2.4 Regioselectivity analysis of *Ps*GH43_12 towards rye arabinoxylan

The regioselectivity of *Ps*GH43_12 towards arabinose substitutions present at O2, O3 or O2/O3 position in rye arabinoxylan was evaluated by performing the ^{1}H NMR analysis of *Ps*GH43_12 hydrolysed rye arabinoxylan sample. The reaction

mixture (2 ml) containing rye arabinoxylan (1%, w/v) dissolved in 50 mM citrate phosphate buffer (pH 6.5) and 200 µl of 50 µg/ml *Ps*GH43_12 was mixed and incubated at 50°C for 12h. The resulting polysaccharide without arabinose side chain was precipitated by the addition of 3 volume (1200 µl) ice-cold ethanol (95%) to the reaction mixture and then centrifuged at 13,000*g* for 10 min. The precipitated polysaccharide was washed with 200 µl of ice-cold ethanol (95%) and freeze-dried by lyophilization (ScanVac, Labogene, Denmark) for 12h. The similar protocol was followed for the preparation of control rye arabinoxylan (Untreated) sample. The freeze-dried samples were resuspended in 0.6 ml of D_2O and their ^{1}HNMR spectra were recorded at 25ºC using 600 MHz Nuclear Magnetic Resonance (NMR) Spectrometer (Bruker, ASCEND 600, Karlsruhe, Germany) fitted with a 5-mm probe and analyzed using topspin NMR software (Bruker, Karlsruhe, Germany)**.** The regioselectivity of *Ps*GH43_12 was further confirmed by hydrolysing the arabino-xylooligosaccharide (AXOS) standards substituted at O2 or O3 positions by *Ps*GH43_12. The AXOS *viz.*, 3^2-α-**L**-Arabinofuranosyl-xylobiose (A^3X), 2^3-α-**L**-Arabinofuranosyl-xylotriose (A^2XX) and 3^3-α-**L**-Arabinofuranosyl-xylotetraose (XA^3XX) were subjected to *Ps*GH43_12 mediated hydrolysis and to confirm the selectivity of linkage for *Ps*GH43_12 hydrolysis. The resulting products were identified and compared with arabinose and other standards by running the hydrolysed mixture on TLC plate by following the protocol mentioned in section 3.2.3.5.

3.2.5 Synergistic behaviour of *Ps*GH43_12

The complete degradation of hemicellulose requires the synergistic action of xylanolytic enzymes. Endo-β-xylanase (*Ct*Xyn11A) from *Clostridium thermocellum*

and exo-β-xylosidase (*Bo*GH43) from *Bacteroides ovatus* were expressed, purified and assayed as reported earlier (Jamaldheen et al., 2019). *Ct*Xyn11A acts on the main chain of xylan polysaccharide and produces xylo-oligosaccharides and *Bo*GH43 acts on xylo-oligosaccharides to produce xylose. The individual enzymes, *Ps*GH43_12 (50 U/g), *Bo*GH43 (50 U/g) or *Ct*Xyn11A (200 U/g) separately or in different combinations *viz.* *Ps*GH43_12+*Bo*GH43, *Ps*GH43_12+*Ct*Xyn11A, *Ct*Xyn11A+*Bo*GH43 and *Ps*GH43_12+*Ct*Xyn11A+*Bo*GH43 were used for the enzymatic hydrolysis of pretreated FMS and commercially available insoluble wheat arabinoxylan. The pretreated Finger millet stalk (FMS) by 1%, w/v NaOH + autoclave was used as reported earlier (Jamaldheen et al., 2019). 3% (w/v) of pretreated FMS and 3% (w/v) insoluble wheat arabinoxylan in 50 mM sodium phosphate buffer, pH 7.0 were separately incubated in 2 ml reaction mixture containing total 200 µl enzyme(s) alone or in combinations at 50°C for 24 h. The pretreated 3% (w/v) FMS biomass and 3% (w/v) insoluble wheat arabinoxylan in 1 ml 50 mM sodium phosphate buffer (pH 7.0) was used as blank. The released reducing sugar was estimated by the method of Nelson (Nelson 1944) and Somogyi (Somogyi 1945). The hydrolysed products were further analysed for confirmation for the presence of monosaccharides and oligosaccharides by TLC (spotting 0.5 µl of the reaction mixture on TLC plate as described earlier in section 3.2.3.5).

3.3 Results and Discussion

3.3.1 pH and temperature optimization of *Ps*GH43_12

*Ps*GH43_12 was active in a pH range from 5 to 9, showing optimum activity at pH 6.5 in 50 mM citrate phosphate buffer (Fig. 3.1A). *Ps*GH43_12 was active in the temperature of 35-55°C, displaying maxima at 50°C (Fig. 3.1B). The enzyme activity sharply decreased at or beyond 60°C. The optimum temperature and pH for maximum activity of *Ps*GH43_12 observed in this study similar to other arabinofuranosidases. AbfB from *Bifidobacterium longum* B667, showed optimum temperature of 45°C and pH 6.0 (Margolles and Clara 2003), α-L-arabinofuranosidase from *B. breve* K-110 optimum temperature 45°C and pH 4.5 (Shin et al., 2003), *Rj*Axh43B from *Ruminiclostridium josui* displayed optimum temperature of 45°C and pH 7 (Zhou et al., 2012) and *Ct*43Ara*f* from *Clostridium thermocellum showed* optimum temperature 50°C and pH 5.7 (Ahmed et al., 2013). However, arabinofuranosidase of family 51 from *Clostridium thermocellum* showed maximum activity at 82°C (Taylor et al., 2006).

3.3.2 pH and temperature stability of *Ps*GH43_12

*Ps*GH43_12 showed stability in the pH range of 7-8 of 50 mM sodium phosphate and HEPES buffer (Fig. 3.1C). It displayed 100% activity up to 45°C and the beyond this, the enzyme activity decreased gradually with 80% of residual activity at 55°C after 90 min of incubation (Fig. 3.1D). The thermal stability analysis at different temperature for long duration reveals that the *Ps*GH43_12 showed 50% residual activity after incubation at 50°C for 24h and at 55°C for 4h (Fig. 3.1E). *Ps*GH43_12 displayed 89% residual activity on incubation at 30°C for 72h and 76 % residual activity on incubation at 4°C for 90 days (Fig. 3.1F) confirming that the

enzyme is fairly stable for long durations. *Ps*GH43_12 displayed $t_{1/2}$ of 102 min, 18.7 h, 52.7 h and 89 days at 55°C, 50°C, 30°C and 4°C respectively. *Ct*43Ara*f* was also reported to be stable at 50°C but its pH stability was in the range of pH 5-6.5 for 1h (Ahmed et al., 2013). AbfB showed 100% activity at 55°C and pH stability in the range of pH 5.5-7.5 after incubation of 10 min (Margolles and Clara 2003). Arabinofuranosidases, *Ru*Xyn1 and *Ru*Xyn2 from rumen bacterial metagenome were stable up to 40°C and 50°C for 10 min, respectively (Zhou et al., 2012).

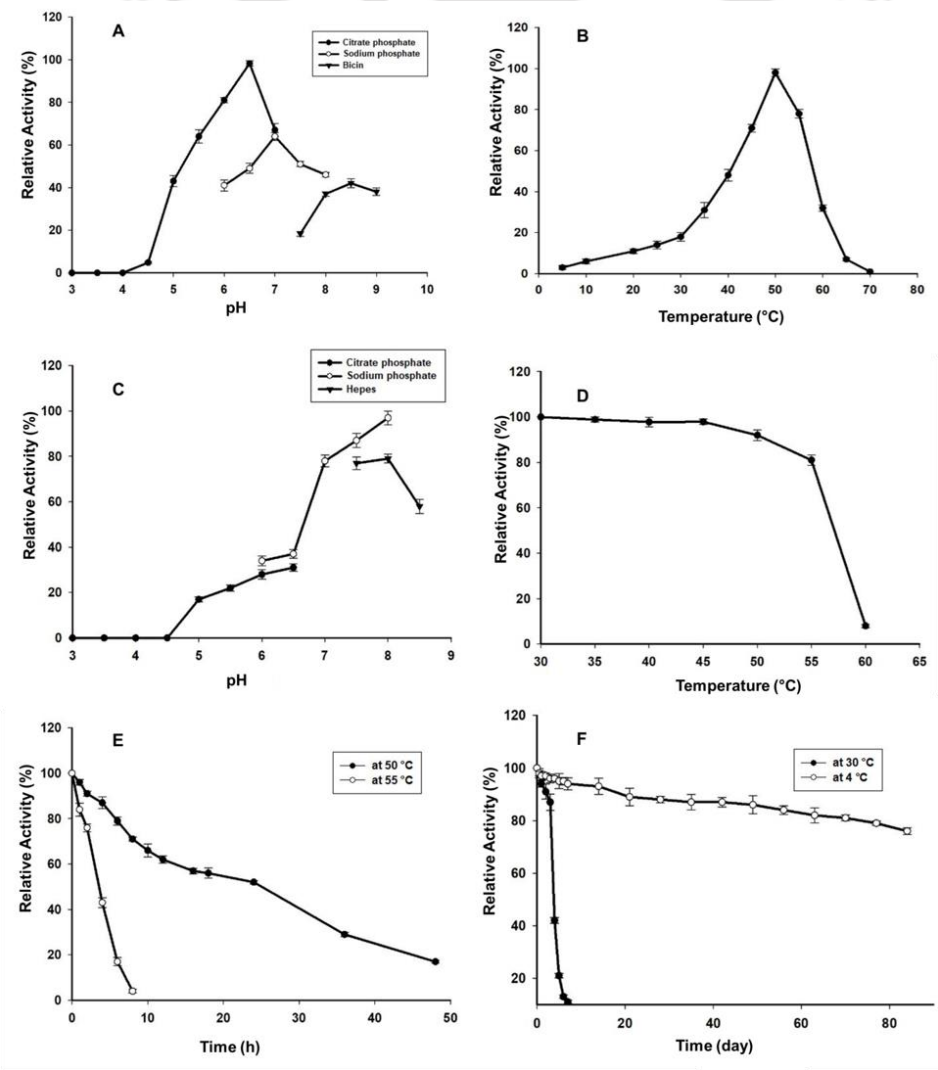

Fig. 3.1 Biochemical characterization of *Ps*GH43_12. A) Temperature optimization, B) pH optimization, C) temperature stability D) pH stability, E) stability at 50°C and 55°C and F) stability at 4°C and 30°C.

3.3.3 Substrate specificity and kinetic parameters of *Ps*GH43_12

*Ps*GH43_12 showed activity against both natural and synthetic substrates (Table 3.1). *Ps*GH43_12 displayed maximum activity against rye arabinoxylan (88.7 U/mg) followed by wheat arabinoxylan (78.9 U/mg), insoluble wheat arabinoxylan (2.19 U/mg) and Oat spelt xylan (1.37 U/mg) under optimized conditions. *Ps*GH43_12 showed activity against only *p*NP-α-L-arabinofuranoside (77.11 U/mg) and no activity against *p*NP -β-D-xylopyranoside. These results indicated that *Ps*GH43_12 is specific for α-L-arabinofuranoside. The activity of *Ps*GH43_12 was 5 times higher than RuXyn1 from rumen bacterial metagenome (14.2 U/mg) (Zhou et al., 2012), 1285 fold higher than β-1,3-D-xylosidase from *Streptomyces sp*. SWU10 (0.06) against *p*NP-α-L-arabinofuranoside (Phuengmaung et al., 2018), 18 times higher than Ct*43Araf* (5.0 U/mg) (Ahmed et al., 2013) against rye arabinoxylan and 2.7 times higher than BiXyn10B/Ara43A from *Bacteroides intestinalis (*28 U/mg) against wheat arabinoxylan (Wang et al., 2016). Several previously reported bacterial arabinofuranosidase displayed less specific activity in comparison to *Ps*GH43_12 such as *R. josui* (62.3 U/mg) (Orita et al., 2017), *B. fibrisolvens (*52.9 U/mg) (Hespell and *O'Bryan 1992*), *R. ginsenosidimutans* (27.1 U/mg) (An et al., 2012), *B. breve K*-110 (6.46 U/mg) (Shin et al., 2003), *B. ovatus* (7.41 U/mg) (Zhou et al., 2020), *S. avermitilis* (2.92 U/mg) (Ichinose et al., 2008), *B. animalis* subsp. lactis BB-12 (1.8 U/mg) (Viborg et al., 2013) and Uncultured bacterium clone LCC-1 (0.68 U/mg) (Wagschal et al., 2007).

Table 3.1 Substrate specificity of *Ps*GH43_12.

Substrate	Specific Activity (U/mg)
Natural polysaccharides	
Rye Arabinoxylan high viscosity (Megazyme)	88.7 (±2.8)
Wheat arabinoxylan low viscosity (Megazyme)	76.9 (± 3.1)
Wheat arabinoxylan (insoluble)	2.19 (± 0.5)
Oat Spelt Xylan	1.37 (± 0.1)
Galactomannan	--
Avicel (Merck)	--
Xylan from corn cob	--
Xylan beechwood (Sigma)	--
Carboxy methyl cellulose	--
Synthetic pNP-glycosides	
*p*NP-α- L-arabinopyranoside	--
*p*NP -α- L-arabinofuranoside	77.11 (± 1.6)
*p*NP -β-D-glucuronide	--
*p*NP -β- L-arabinopyranoside	--
*p*NP -β-D-xylopyranoside	--

- - No activity detected

The kinetic parameters of *Ps*GH43_12 are mentioned in Table 3.2. *Ps*GH43_12 displayed the K_m, 3.02 mg/ml and V_{max}, 102.0 U/mg against rye arabinoxylan (Table 3.2). It gave K_m, 3.04 mg/ml and V_{max}, 99.3 U/mg for wheat arabinoxylan and K_m, 2.17 mM and V_{max}, 100.7 U/mg for 4-nitrophenyl-α-L-arabinofuranoside (Table 3.2). The catalytic efficiency (K_{cat}/K_m) of *Ps*GH43_12 for 4-nitrophenyl-α-L-arabinofuranoside (50.27 s^{-1} mM^{-1}) was significantly higher than the α-L-arabinofuranosidase, *Ct*43Ara*f* from *Clostridium thermocellum* ATCC27405 (26.2 s^{-1} mM^{-1}) (Ahmed et al., 2013), but much lower than α-L-arabinofuranosidase from *Thermobacillus xylanilyticus* (79526.2 s^{-1} mM^{-1}) (Arab-Jaziri et al., 2012).

Table 3.2 Kinetic parameters of *Ps*GH43_12.

Substrate	K_m	V_{max} (U/mg)	k_{cat} (s^{-1})	k_{cat}/K_m
Rye arabinoxylan	3.02 (± 0.12) mg/ml	102 (± 2.1)	110	36.4 ml mg^{-1} s^{-1}
Wheat arabinoxylan	3.04 (± 0.11) mg/ml	99.3 (± 1.9)	108	35.5 ml mg^{-1} s^{-1}
*p*NP-α- L-arabinofuranoside	2.17 (± 0.11) mM	100.7 (± 1.7)	109	50.27 s^{-1} mM^{-1}

3.3.4 Effect of metal ions on *Ps*GH43_12 activity

The effect of metal ions and chelating agents on *Ps*GH43_12 were investigated by using wheat arabinoxylan as substrate and the results are shown in Table 3.3. The enzyme activity of *Ps*GH43_12 without any metal ion or chelating agent was considered as 100%. The presence of 10 mM Mg^{2+}, Ca^{2+}, Li^{+} or Na^{+} enhanced the activity of *Ps*GH43_12 by 54%, 27% 11% or 15%, respectively (Table 3.3). It was earlier reported that the addition of 5-10 mM of Mg^{2+} and Ca^{2+} enhances the arabinofuranosidase activity by 2-fold (Ahmed et al., 2013). The addition of 1 mM Fe^{3+}, Co^{2+}, Zn^{2+}, Cu^{2+}, Ni^{2+}, Hg^{2+} and Ag^{+} drastically decreased the activity of *Ps*GH43_12. Similar effect of these metal ions were reported for α-L-arabinofuranosidase from *C. thermocellum* (Ahmed et al., 2013). Previous reports have shown that Hg^{2+} or Ag^{+} ions chemically react with SH group of cysteine or tryptophan residue, which are involved in substrate binding, thereby inactivate the enzyme (Sharma et al., 2018; Zhang et al., 2012). The *Ps*GH43_12 sequence analysis displayed that it contains 3 cysteine and 7 tryptophan residues which may be interacting with the Hg^{2+} or Ag^{+} and inhibiting its activity. EDTA showed no effect on the activity of *Ps*GH43_12 whereas, EGTA showed marginal (17%) decrease of activity, which may be due to removal of inherent Ca^{2+} ions present.

Table 3.3 Metal ion effect on the activity of *Ps*GH43_12.

Metal ion/Reagent	Concentration of additives (mM)	Relative activity (%)	Concentration of additives (mM)	Relative activity (%)
Control	--	100	--	100
Mg^{2+}	01	104	10	154
Ca^{2+}	01	131	10	127
Na^{+}	01	102	10	115
Li^{+}	01	100	10	111
Mn^{2+}	01	83	10	52
Fe^{3+}	01	69	10	23
Co^{2+}	01	24	10	18
Zn^{2+}	01	13	10	04
Cu^{2+}	01	00	10	00
Ni^{2+}	01	00	10	00
Hg^{2+}	01	00	10	00
Ag^{+}	01	00	10	00
EDTA	01	100	10	100
EGTA	01	94	10	83

3.3.5 Mode of action analysis of *Ps*GH43_12 by Thin layer chromatography

The relative migration of hydrolysed product of rye arabinoxylan and the standards, xylose and arabinose indicated that *Ps*GH43_12 released L-arabinosyl residue from the side chain of arabinoxylan (Fig. 3.2A). The spot obtained on TLC indicated the released sugar is arabinose and the substrate specificity on synthetic substrate also justified that *Ps*GH43_12 is specific for α-L-arabinofuranoside. The supernatant containing *Ps*GH43_12 hydrolysed product was analyzed by HPLC. The HPLC analysis of hydrolysed product displayed the single peak with a retention time of 16.207 min (Fig. 3.2B), which matches with the retention time of arabinose standard (16.27 min) (Fig. 3B). These results confirmed that, *Ps*GH43_12 hydrolyses only the side chain and releases arabinose from arabinoxylan. The ESI-MS analysis of 1 h sample confirmed the presence of L-arabinose (m/z 173.03) (Fig. 3.2C). The m/z value obtained from the mass spectrometric analysis of *Ps*GH43_12 assisted rye

arabinoxylan hydrolyzed products corroborated well with the m/z value obtained for standard L-arabinose residue (Fig. 3.2D).

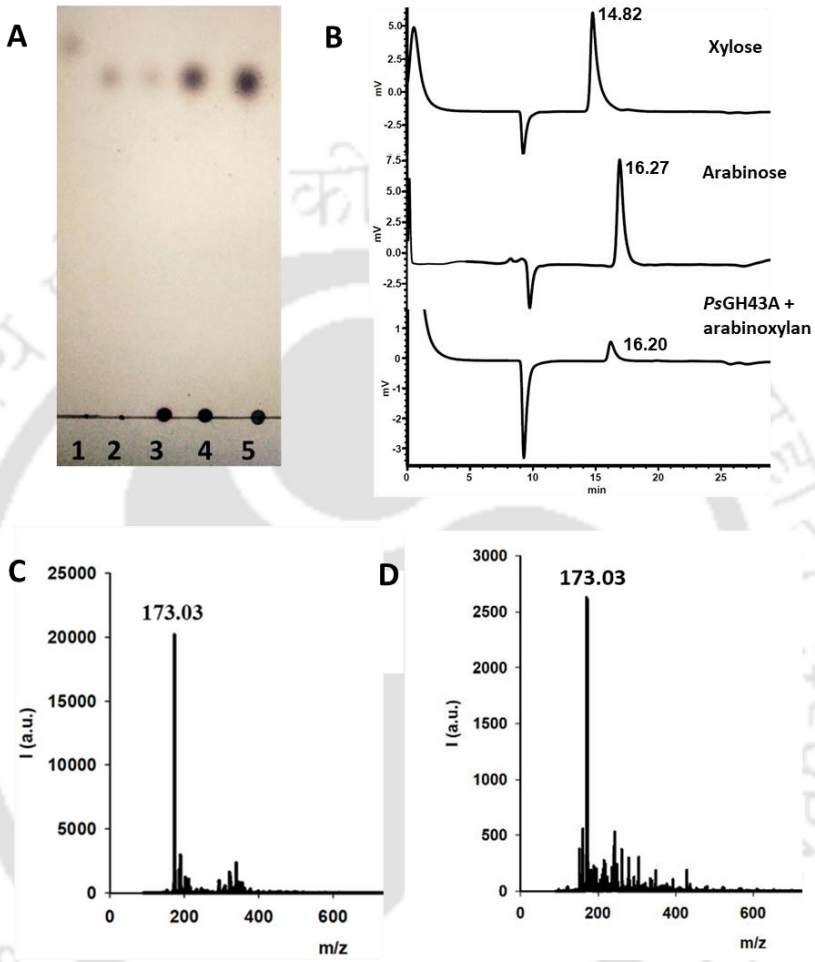

Fig. 3.2 A) TLC analysis of *Ps*GH43_12 hydrolysed products of rye arabinoxylan. Lanes: 1- Xylose, 2- Arabinose, 3- 5 min, 4- 30 min and 5- 60 min hydrolysed product, B) HPLC analysis of *Ps*GH43_12 hydrolysed product and standard xylose and arabinose, C) Mass spectrometric analysis of *Ps*GH43_12 hydrolysed product of rye arabinoxylan and D) Mass spectrometric analysis of L-arabinose standard.

3.3.6 Regioselectivity analysis of *Ps*GH43_12 towards rye arabinoxylan

α-L-Arabinofuranosidases, based on their modes of action on arabinose substitutions are classified into three types. Type-I arabinofuranosidases are active on L-arabinose residues linked to O-2 or O-3 of mono-substituted (m) arabinoxylans.

While, the type-II arabinofuranosidases release L-arabinose linked to O-3 position of di-substituted (d) arabinoxylans. The type-III arabinofuranosidases are able to hydrolyze both mono- and di-substituted **L**-arabinose side chains present in arabinoxylans. Therefore, *Ps*GH43_12 hydrolysed arabinose free and untreated rye arabinoxylan were subjected to ^{1}H NMR analysis to evaluate its mode of action towards specific linkage. The untreated rye arabinoxylan displayed the ^{1}H NMR chemical shift signals corresponding to three different α- L-arabinose substitutions *viz*. m-α-(1→3)-**L**-Araf at 5.23 ppm, d-α-(1→2)-**L**-Araf at 5.11 ppm and d-α-(1→3)-**L**-Araf at 5.06 ppm (Fig. **3.**3A). The ^{1}H NMR analysis also displayed the chemical shift signals at 4.32 ppm and 4.12 ppm corresponding to the with xylose substituted at O2 or O3 positions. The ^{1}H NMR analysis of *Ps*GH43_12 hydrolysed arabinose free rye arabinoxylan revealed that the chemical shift signals at 5.23 ppm, 5.11 ppm and 5.06 ppm corresponding to O3 and O2, O3 were removed (Fig. 3.3B). Similarly, the peaks at 4.32 ppm and 4.12 ppm was also removed after *Ps*GH43_12 mediated hydrolysis of rye arabinoxylan (Fig. **3.**3B). These results indicated that *Ps*GH43_12 was able to cleave both substitutions, as shown in schematic representation (Fig. 3.3C) therefore it belongs to the type III class of arabinofuranosidases. α-**L**-Arabinofuranosidases from *Streptomyces sp*. **(**Phuengmaung et al., 2018) and plant pathogenic fungi (Sarch et al., 2019) of family 62 glycoside hydrolases are of type-I and remove **L**-arabinose from O3 position from wheat arabinoxylan. The TLC analysis of *Ps*GH43_12 hydrolysed O2 or O3 substituted arabino-xylooligosaccharides displayed two spots in Lane 4,6 and 8 (Fig. 3.3D). The relative migration of these two spots corroborated well with the relative migration of arabinose standard and xylooligosaccharides confirming that the *Ps*GH43_12 can act on arabinoxylans substituted at O2 or O3 positions and

releases the arabinose sugar. These results displayed that *Ps*GH43_12 along with other hydrolytic enzymes can be used for enzymatic saccharification of lignocellulosic biomass.

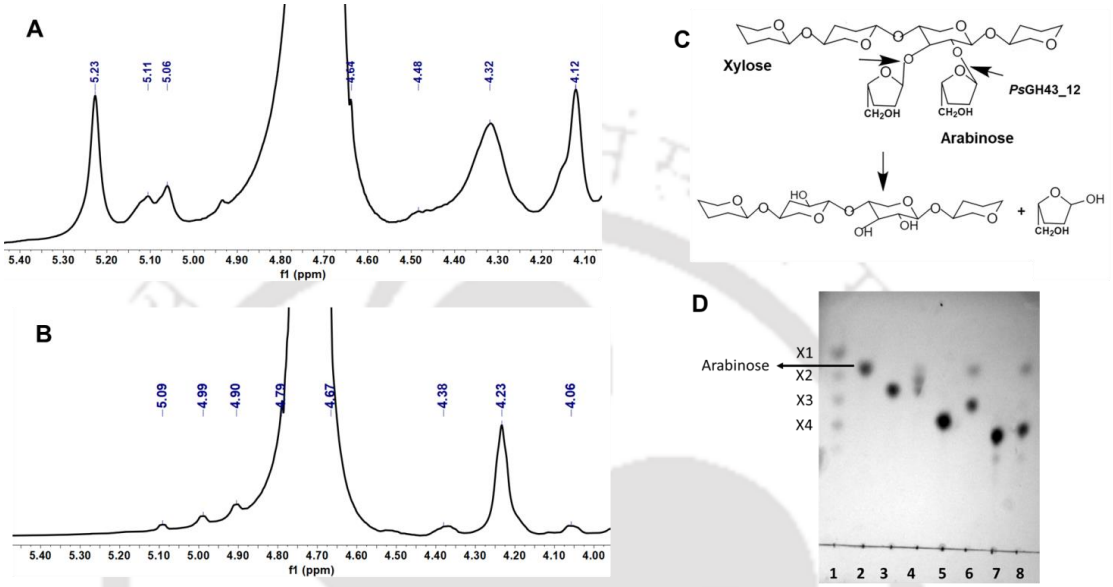

Fig. 3.3 Regioselectivity analysis of *Ps*GH43_12. A) ^{1}H NMR of native Rye arabinoxylan B) *Ps*GH43_12 treated arabinose free rye arabinoxylan, C) Schematic representation of mode of action of *Ps*GH43_12 towards specific linkage and D) TLC analysis showing regioselectivity of *Ps*GH43_12. Lanes: 1-Standard xylose (X1, X2, X3 and X4), 2-standard arabinose, 3- A^3X, lane 4- A^3X + *Ps*GH43_12, 5- A^2XX, 6- A^2XX + *Ps*GH43_12, 7- XA^3XX and 8- XA^3XX + *Ps*GH43_12.

3.3.7 Synergistic behaviour of *Ps*GH43_12

The complete degradation of heteroxylans requires the action of both endo-β-xylanase and exo-β-xylosidase, but arabinose present as the side chain substitutions hinders their activity. Therefore, the removal of arabinose side chain from heteroxylan before the backbone hydrolysis by xylanase and xylosidase, can be achieved by the action of arabinofuranosidase in order to facilitate the hydrolysis. The synergistic effects between *Ps*GH43_12, *Ct*Xyn11A and *Bo*GH43 were studied by monitoring their hydrolytic action on 3% (w/v) pretreated finger millet stalk and on a commercial

substrate, 3% (w/v) insoluble wheat arabinoxylan by using them, individually and in various combinations for 24 h. The hydrolytic action of individual enzyme, *Ps*GH43_12, *Bo*GH43 and *Ct*Xyn11A, released low amount of total reducing sugar (TRS) as compared with their combinations (Table 3.4). The enzymes, *Ps*GH43_12, *Bo*GH43 and *Ct*Xyn11A individually gave TRS of 1.1, 0.08 and 2.06 mg/ml, respectively. The addition of *Ps*GH43_12 to the mixture of *Ct*Xyn11A and *Bo*GH43 enhanced the hydrolysis of pretreated FMS by 2-fold giving TRS of 4.45 mg/ml) from the TRS of 2.17 mg/ml given by the mixture of *Ct*Xyn11A and *Bo*GH43. Similarly, the addition of *Ps*GH43_12 enhanced the hydrolysis of the commercial insoluble wheat arabinoxylan by 2-fold giving TRS of 5.31 mg/ml when added with *Ct*Xyn11A+ *Bo*GH43 whereas, the only these two enzymes gave TRS of 2.64 mg/ml. The pretreated FMS hydrolysis by *Ct*Xyn11A and *Bo*GH43 resulted in the TRS yield 70 mg/g pretreated FMS as reported earlier (Jamaldheen et al., 2019), However, our results displayed that the addition of *Ps*GH43_12 to above mixture of two enzymes enhances the TRS yield by 2-fold to 148 mg/g pretreated FMS.

Table 3.4 Synergistic effect of xylanolytic enzymes.

Enzyme	**TRS (mg/ml) insoluble wheat arabinoxylan**	**TRS (mg/ml) pretreated FMS**
*Ps*GH43_12	1.48 (± 0.02)	1.1 (± 0.02)
*Bo*GH43	0.09 (± 0.00)	0.06 (± 0.0)
*Ct*Xyn11A	2.28 (± 0.02)	2.06 (± 0.03)
*Ct*Xyn11A + *Ps*GH43_12	3.31 (± 0.03)	2.81 (± 0.03)
*Ct*Xyn11A+*Bo*GH43	2.64 (± 0.03)	2.17 (± 0.04)
*Ct*Xyn11A+*Bo*GH43+*Ps*GH43_12	5.31 (± 0.04)	4.45 (± 0.04)

*Ct*Xyn11A =200 U/g, *Ps*GH43_12 =50 U/g and *Bo*GH43 =50 U/g

Several earlier reports showed the hydrolysis of lignocellulosic biomass by using arabinofuranosidases in combination with other hydrolytic enzymes (Raweesri et al., 2008; Delabona et al., 2013). The hydrolysis of cornhusk by xylanase and

xylosidase resulted in 1.5 mg/ml TRS, whereas the addition of arabinofuranosidase and acetyl esterase from *Streptomyces sp.* PC22 to above mixture resulted in the increase in TRS of 1.5-fold to 2.2 mg/ml after 48h hydrolysis (Raweesri et al., 2008). Similarly, in an another report, the pretreated sugarcane bagasse hydrolysis by cocktail of cellulase and glucosidase produced by *T. harzianum* and later supplemented with accessory enzymes *viz.* arabinofuranosidase and pectinase resulted in the enhanced TRS production from 1.5 mg/ml to 3.3 mg/ml (Delabona et al., 2013). These results clearly demonstrated the potential role played by the accessory enzyme in complete and efficient deconstruction of heteroxylan polysaccharides. The qualitative analysis of pretreated FMS hydrolysed products by all individual and the combinations of enzymes for 24 h as mentioned above was performed by TLC (Fig. 3.4). The TLC analysis showed that the enzymes, *Ps*GH43 released arabinose (Fig. 3.4, Lane 4), *Bo*GH43 did not produce xylose or any other product (Lane 5) and *Ct*Xyn11A gave only xylooligosaccharides (lane 6) on hydrolysis of pretreated FMS. The combination of *Ct*Xyn11A and *Ps*GH43_12 showed spots for xylooligosaccharides, xylobiose and arabinose (Fig. 3.4, Lane 7). The lane 7 also clearly showed higher intensity of xylobiose as compared with only Xyn11A hydrolysed pretreated FMS (Lane 6). This result demonstrated the synergistic action of *Ps*GH43_12 by removing side chain arabinose thereby making it more accessible for *Ct*Xyn11A action on the main chain xylan. The mixture of *Bo*GH43 and *Ct*Xyn11A enzymes showed only xylooligosaccharides and xylose (Fig 3.4, lane 8). However, the combination of all three enzymes, *Ps*GH43_12, *Bo*GH43 and *Ct*Xyn11A displayed predominantly the spots for only xylose and arabinose sugars (Fig. 3.4 lane 9). Therefore, all these results of TRS and TLC analysis confirmed the

synergistic behaviour of the three enzymes. These findings suggested that the α-L-arabinofuranosidase obtained from *P. saltans* could be a more suitable enzyme for complete degradation of heteroxylan by removing L-arabinose and making its main chain accessible for other xylanolytic enzymes. Therefore, it can be used in combination with other enzymes for enzymatic saccharification of lignocellulosic biomass targeting bioethanol production.

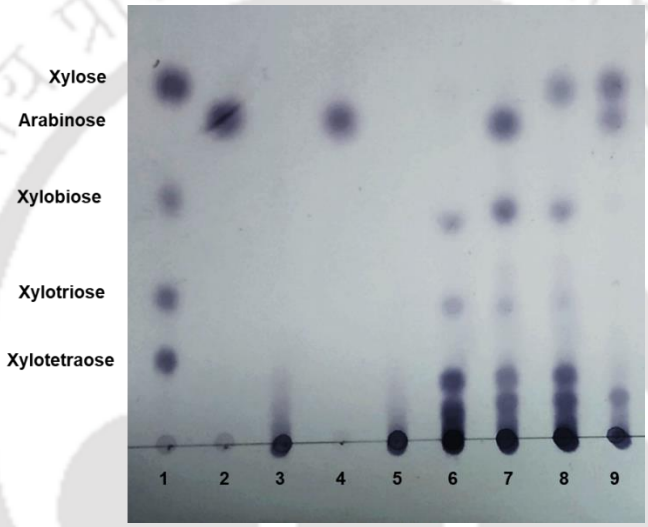

Fig. 3.4 TLC analysis showing synergistic effect of xylanolytic enzymes on pretreated FMS. Lanes: 1-Standard xylose, xylobiose, xylotriose and xylotetraose, 2-standard arabinose, 3-Pretreated FMS Control, 4-Pretreated FMS+*Ps*GH43_12, 5-Pretreated FMS+ *Bo*GH43, 6-Pretreated FMS+*Ct*Xyn11A, 7-Pretreated FMS + *Ct*Xyn11A + *Ps*GH43_12, 8-Pretreated FMS+*Ct*Xyn11A+*Bo*GH43 and 9-Pretreated FMS + *Ct*Xyn11A+*Bo*GH43 +*Ps*GH43_12. All enzyme treatments were carried out for 24 h.

3.4. Conclusion

α-L-Arabinofuranosidase hydrolyses complex polysaccharides such as hemicelluloses. *Ps*GH43_12 displayed the maximum activity at 50°C and pH 6.5. The enzyme *Ps*GH43_12 was more stable than several previously reported arabinofuranosidases as it exhibited activity in a broad pH range (pH 5 - 9) and broad temperature range (35 - 55°C). The substrate specificity analysis of *Ps*GH43_12 revealed higher activity against soluble arabinoxylan substrates. The enzyme displayed specific activities, 88.7 U/mg and 78.9 U/mg, against rye arabinoxylan and wheat arabinoxylan, respectively under optimised conditions. The analysis of the kinetics parameters of *Ps*GH43_12 against rye arabinoxylan gave K_m, 3.02 mg/ml and V_{max}, 103 µmole/min/mg. *Ps*GH43_12 also displayed the activity against *p*NP-α-L-arabinofuranoside with V_{max} 100.7 U/mg, K_m 2.17 mM, and k_{cat}/k_m 50.27 s^{-1} mM^{-1}. The metal ions, Mg^{2+}, Ca^{2+}, Li^{+} or Na^{+} at 10 mM concentration markedly enhanced the activity of *Ps*GH43_12 by 54%, 33%, 15% or 11%, respectively. The TLC analysis displayed the release of only L-arabinosyl moiety from rye arabinoxylan after *Ps*GH43_12 hydrolysis confirming its specificity towards α-L-arabinofuranoside.

The TLC, HPLC and Mass spectrometric analysis of *Ps*GH43_12 hydrolysed products of rye arabinoxylan showed the release of arabinose residue present as side chain substitution in arabinoxylan. The regioselectivity analysis of *Ps*GH43_12 action towards arabinoxylan by NMR revealed the release of α- L-Araf substitution at O3 and O2, O3 position and therefore, it was classified as type III α- L-arabinofuranosidase. The enzymatic saccharification of mild alkali pretreated finger miller stalk (FMS) by *Ps*GH43_12 in combination with xylanase (*Ct*Xyn11A) from *Clostridium thermocellum* and xylosidase (*Bo*GH43) from *Bacteroides ovatus*

resulted in a 2-fold increase in the TRS yield (148 mg/g) in 24 h as compared with TRS yield (70 mg/g) produced by xylanase (*Ct*Xyn11A) and xylosidase (*Bo*GH43) in 56h. *Ps*GH43_12 in combination with both xylanase and xylosidase released the maximum concentration of total reducing sugar from pretreated finger millet stalk displaying the synergistic effect of three enzymes. The TLC analysis of the pretreated FMS hydrolysed by mixture of *Bo*GH43 and *Ct*Xyn11A showed xylooligosaccharides and xylose. However, the addition of *Ps*GH43_12 to above combination gave mostly xylose and arabinose sugars. All these results confirmed the synergistic behaviour of the three enzymes. Thus the utilization of these three enzymes for enzymatic saccharification of lignocellulosic biomass in a synergistic manner can be exploited for higher scale bioethanol production.

3.5 References

Ahmed, S., Luis, A. S., Bras, J. L., Ghosh, A., Gautam, S., Gupta, M. N., & Goyal, A. (2013). A novel α-L-arabinofuranosidase of family 43 glycoside hydrolase (*Ct*43Araf) from *Clostridium thermocellum*. *PLoS One*, 8(9), e73575.

An, D. S., Cui, C. H., Sung, B. H., Yang, H. C., Kim, S. C., Lee, S. T., & Kim, S. G. (2012). Characterization of a novel ginsenoside-hydrolyzing α-l-arabinofuranosidase, AbfA, from *Rhodanobacter ginsenosidimutans* Gsoil 3054 T. *Applied Microbiology and Biotechnology*, *94*(3), 673-682.

Arab-Jaziri, F., Bissaro, B., Barbe, S., Saurel, O., Debat, H., Dumon, C., & O'Donohue, M. J. (2012). Functional roles of H98 and W99 and β2α2 loop dynamics in the α-l-arabinofuranosidase from *Thermobacillus xylanilyticus*. The FEBS journal, 279(19), 3598-3611.

Brett, C., & Waldron, K. (1990). Cell wall structure and the skeletal functions of the wall. In *Physiology and Biochemistry of plant cell walls* Springer, Dordrecht, 4-57.

da Silva Delabona, P., Cota, J., Hoffmam, Z. B., Paixão, D. A. A., Farinas, C. S., Cairo, J. P. L. F., & da Cruz Pradella, J. G. (2013). Understanding the cellulolytic system of *Trichoderma harzianum* P49P11 and enhancing saccharification of pretreated sugarcane bagasse by supplementation with pectinase and α-l-arabinofuranosidase. *Bioresource Technology*, *131*, 500-507.

Hespell, R. B., & O'Bryan, P. J. (1992). Purification and characterization of an α-L-arabinofuranosidase from *Butyrivibrio fibrisolvens* GS113. *Applied and Environmental Microbiology*, *58*(4), 1082-1088.

Ichinose, H., Yoshida, M., Fujimoto, Z., & Kaneko, S. (2008). Characterization of a modular enzyme of exo-1, 5-α-l-arabinofuranosidase and arabinan binding module from *Streptomyces avermitilis* NBRC14893. *Applied Microbiology and Biotechnology*, *80*(3), 399.

Jamaldheen, S. B., Thakur, A., Moholkar, V. S., & Goyal, A. (2019). Enzymatic hydrolysis of hemicellulose from pretreated Finger millet (*Eleusine coracana*) straw by recombinant endo-1, 4-β-xylanase and exo-1, 4-β-

xylosidase. *International Journal of Biological Macromolecules*, *135*, 1098-1106.

Lombard, V., Golaconda Ramulu, H., Drula, E., Coutinho, P. M., & Henrissat, B. (2014). The carbohydrate-active enzymes database (CAZy) in 2013. *Nucleic Acids Research*, *42*(D1), 490-495.

Margolles, A., & Clara, G. (2003). Purification and functional characterization of a novel α-l-arabinofuranosidase from *Bifidobacterium longum* B667. *Applied and Environmental Microbiology*, *69*(9), 5096-5103.

Mewis, K., Lenfant, N., Lombard, V., & Henrissat, B. (2016). Dividing the large glycoside hydrolase family 43 into subfamilies: a motivation for detailed enzyme characterization. *Applied and Environmental Microbiology*, *82*(6), 1686-1692.

Nelson, N. (1944). A photometric adaptation of the Somogyi method for the determination of glucose. *Journal of Biological Chemistry*, *153*(2), 375-380.

Ordaz-Ortiz, J. J., & Saulnier, L. (2005). Structural variability of arabinoxylans from wheat flour. Comparison of water-extractable and xylanase-extractable arabinoxylans. *Journal of Cereal Science*, *42*(1), 119-125.

Orita, T., Sakka, M., Kimura, T., & Sakka, K. (2017). Characterization of *Ruminiclostridium josui* arabinoxylan arabinofuranohydrolase, RjAxh43B, and RjAxh43B-containing xylanolytic complex. *Enzyme and Microbial Technology*, *104*, 37-43.

Phuengmaung, P., Fujiwara, D., Sukhumsirichart, W., & Sakamoto, T. (2018). Identification and characterization of the first β-1, 3-d-xylosidase from a gram-positive bacterium, *Streptomyces* sp. SWU10. *Enzyme and Microbial Technology*, *112*, 72-78.

Raweesri, P., Riangrungrojana, P., & Pinphanichakarn, P. (2008). α-L-arabinofuranosidase from *Streptomyces* sp. PC22: Purification, characterization and its synergistic action with xylanolytic enzymes in the degradation of xylan and agricultural residues. *Bioresource Technology*, *99*(18), 8981-8986.

Saha, B. C. (2000). α-L-Arabinofuranosidases: biochemistry, molecular biology and application in biotechnology. *Biotechnology Advances*, *18*(5), 403-423.

Sarch, C., Suzuki, H., Master, E. R., & Wang, W. (2019). Kinetics and regioselectivity of three GH62 α-L-arabinofuranosidases from plant pathogenic fungi. *Biochimica et Biophysica Acta (BBA)-General Subjects*, *1863*(6), 1070-1078.

Sharma, K., Antunes, I. L., Rajulapati, V., & Goyal, A. (2018). Molecular characterization of a first endo-acting β-1, 4-xylanase of family 10 glycoside hydrolase (*Ps*GH10A) from *Pseudopedobacter saltans* comb. nov. *Process Biochemistry*, *70*, 79-89.

Shin, H. Y., Park, S. Y., Sung, J. H., & Kim, D. H. (2003). Purification and Characterization ofα-l-Arabinopyranosidase andα-l-Arabinofuranosidase from *Bifidobacterium breve* K-110, a Human Intestinal Anaerobic Bacterium Metabolizing Ginsenoside Rb2 and Rc. *Applied and Environmental Microbiology*, *69*(12), 7116-7123.

Somogyi, M. (1945). A new reagent for the determination of sugars. *Journal of Biological Chemistry*, *160*, 61-68.

Thakur, A., Sharma, K., & Goyal, A. (2019). α-l-Arabinofuranosidase: A potential enzyme for the food industry. In *Green Bio-processes*. Springer, Singapore. 229-244.

Viborg, A. H., Sørensen, K. I., Gilad, O., Steen-Jensen, D. B., Dilokpimol, A., Jacobsen, S., & Svensson, B. (2013). Biochemical and kinetic characterisation of a novel xylooligosaccharide-upregulated GH43 β-D-xylosidase/α-L-arabinofuranosidase (BXA43) from the probiotic *Bifidobacterium animalis* subsp. lactis BB-12. *AMB Express*, *3*(1), 1-8.

Wagschal, K., Franqui-Espiet, D., Lee, C. C., Kibblewhite-Accinelli, R. E., Robertson, G. H., & Wong, D. W. (2007). Genetic and biochemical characterization of an α-L-arabinofuranosidase isolated from a compost starter mixture. *Enzyme and Microbial Technology*, *40*(4), 747-753.

Wang, K., Pereira, G. V., Cavalcante, J. J., Zhang, M., Mackie, R., & Cann, I. (2016). *Bacteroides intestinalis* DSM 17393, a member of the human colonic microbiome, upregulates multiple endoxylanases during growth on xylan. *Scientific Reports*, *6*, 34360.

Wilkens, C., Andersen, S., Dumon, C., Berrin, J. G., & Svensson, B. (2017). GH62 arabinofuranosidases: structure, function and applications. *Biotechnology Advances*, *35*(6), 792-804.

Zhang, G., Li, S., Xue, Y., Mao, L., & Ma, Y. (2012). Effects of salts on activity of halophilic cellulase with glucomannanase activity isolated from alkaliphilic and halophilic *Bacillus* sp. BG-CS10. *Extremophiles*, *16*(1), 35-43.

Zhou, A., Hu, Y., Li, J., Wang, W., Zhang, M., & Guan, S. (2020). Characterization of a recombinant β-xylosidase of GH43 family from *Bacteroides ovatus* strain ATCC 8483. *Biocatalysis and Biotransformation*, *38*(1), 46-52.

Zhou, J., Bao, L., Chang, L., Zhou, Y., & Lu, H. (2012). Biochemical and kinetic characterization of GH43 β-D-xylosidase/α-L-arabinofuranosidase and GH30 α-L-arabinofuranosidase/β-D-xylosidase from rumen metagenome. *Journal of Industrial Microbiology & Biotechnology*, *39*(1), 143-152.

Chapter 4

Structure and dynamics analysis of α-L-arabinofuranosidase (*Ps*GH43_12) from *Pseudopedobacter saltans* by Computational modeling and Small angle X-ray scattering

4.1 Introduction

Plant cell wall is composed of complex polysaccharides, such as cellulose, hemicellulose and the lignin. Unlike cellulose, the hemicellulose is a heteropolysaccharide such as xylan, arabinan, glucan and mannan. Hemicellulose has more complex structure than cellulose owing to the existence of side chains. The common side-chain substitutions on the backbone are arabinose, acetic acid, glucuronic acid, ferulic acid, *p*-coumaric acid, or 4-*O*-methyl glucuronic acid (Thakur et al., 2019). These side chains interfere in the hemicellulose degradation by xylanolytic enzymes. Xylan is the most abundant hemicellulose and based on presence of side-chain it is further classified into arabinoxylan, glucuronoxylan and xyloglucan. Arabinose is a promising valuable sugar in the food industry as it is not easily absorbed and reduces glycemic response (Seri et al., 1996). α-L-Arabinofuranosidase catalyzes the removal of arabinose residues from arabinoxylan,

arabinan, arabinooligosacchrides and arabinoxylooligosacchrides. α-L-Arabinofuranosidase also displays synergistic action with other carbohydrate active enzymes and enhances the hydrolysis of lignocellulosic biomass (Alvira et al., 2011). In the CAZy database, α-L-arabinofuranosidases are placed in Glycoside hydrolase (GH) families 2, 3, 43, 51, 54 and 62 (Lombard et al., 2014) (http://www.cazy.org/). GH is one of the major classes of carbohydrate active enzymes, categorized into 166 families based on the amino acid sequence. Enzymes from families 2, 3, 51 and 54 show retaining type mechanism, whereas family 43 display inverting type mechanism of catalysis. The family 43 glycoside hydrolyses is further classified into 37 subfamilies. The subfamily 12 contains β-xylosidase, α-L-arabinofuranosidase, xylanase, α-1,2-L-arabinofuranosidase, exo-α-1,5-L-arabinofuranosidase, exo-α-1,5-L-arabinanase, β-1,3-xylosidase, exo-α-1,5-L-arabinanase, endo-α-1,5-L-arabinanase, exo-β-1,3-galactanase, β-D-galactofuranosidase. A total of 1115 genes are reported in subfamily12 of family 43 GH. Regardless of such a high number of genes reported in subfamily 12 only 13 proteins are characterized and out of which the structure of only 4 enzymes have been determined. *Ps*GH43_12 is the first arabinofuranosidase from *Pseudopedobacter saltans*. The enzyme shows sequence similarity of around 35% only with xylosidase from *G. thermoleovorans.* The only hemicellulase (*Ps*GH10) reported till date from *P. saltans* showed stability up to 45°C (Sharma et al., 2018). Whereas, *Ps*GH43_12 of this study is the first thermostable enzyme from *Pseudopedobacter saltans*. The modular behaviour, conformational dynamics, molecular arrangement and protein stability of this enzyme are still unknown. An α-L-arabinofuranosidase (EC 3.2.1.55) belonging to the subfamily 43_12 glycoside hydrolase (*Ps*GH43_12) (GeneBank: Acc No. ADY53124.1) from *Pseudopedobacter*

saltans containing 586 amino acid residues was cloned and expressed. In the present study, the three-dimensional structure of α-L-arabinofuranosidase (*Ps*GH43_12) was modeled. The modeled structure was used for molecular dynamics simulation and molecular docking study. The active site residues were identified by site-directed mutagenesis. Small-angle X-ray scattering of *Ps*GH43_12 was performed to study its structure in solution form.

4.2 Material and Methods

4.2.1 Chemical, reagents and substrates

The chemical salts *viz*. mono and dibasic sodium phosphate salts, sodium chloride, calcium chloride, EDTA, IPTG, Imidazole, Luria-Bertani medium and kanamycin were purchased from Himedia Laboratories India Pvt Ltd. Q5® Site-directed mutagenesis kit was procured from New England Biolabs (NEB), USA. The substrate, rye arabinoxylan was procured from Megazyme International, Ireland.

4.2.2 Amino acid sequence retrieval and analysis

The protein sequence of *Ps*GH43_12 from *P. saltans* (UniProt ID: F0S5G0) constituting 586 amino acid residues was retrieved from the UniProt Database (https://www.uniprot.org/uniprot/F0S5G0). BLASTp webserver was used to search the reported domains in *Ps*GH43_12 across the PDB database (Altschul et al., 1997). The physicochemical properties of *Ps*GH43_12 were predicted by the Protparam server (https://web.expasy.org/protparam/). Multiple sequence alignment of *Ps*GH43_12 with the homologous proteins whose structures are available was performed by the ClustalO tool of EMBL EBI services (http://www.ebi.ac.uk/Tools/msa/clustalo/) to identify the conserved of amino acid residues (Sievers et al., 2011). The alignment result was visualized and analyzed for the identification of conserved and semi-conserved amino acid residues by Esprit 3.0 webserver (Robert and Gouet 2014).

4.2.3 Comparative modeling, refinement and structure assessment of *Ps*GH43_12

The three-dimensional structure of *Ps*GH43_12 was modeled by the comparative modeling approach using Modeller v9.20 (Eswar et al., 2008). The homologous protein sequences and structures of Xyl (*PDB* ID: 5Z5D) from

Geobacillus thermoleovorans (Rohman et al., 2018), *Bo*XyGUL (*PDB ID: 5JOW*) from *Bacteroides ovatus* (Hemsworth et al., 2016) and *Bl*XynB *(PDB ID:* 6MS3) from *Bacillus licheniformis* (Zanphorlin et al., 2019) were selected as templates followed by multiple sequence alignment using 'salign( )' command. After that, the generated MSA was aligned with the query sequence (*Ps*GH43_12). The 'automodel' class command was used to generate a total of 50 independent models of *Ps*GH43_12. The Discrete Optimized Protein Energy (DOPE) scoring function was used to assess the resulted 50 models (Shen and Sali 2006). The top 5 models with least DOPE score were selected for energy minimization by using YASARA webserver. The energy minimized models were evaluated by using RAMPAGE (http://mordred.bioc.cam.ac.uk/~rapper/rampage.php), ProCheck (Laskowski et al., 1993), ERRAT (Colovos and Yeates 1993) and VERIFY3D (Eisenberg et al., 1997) tools compiled in SAVES server (https://services.mbi.ucla.edu/SAVES/). The ProSA web server (https://prosa.services.came.sbg.ac.at/prosa.php) was used to estimate the statistical Z-score deviation of the modeled structure from the high-resolution structures deposited in PDB. The best modeled *Ps*GH43_12 structure after energy minimization was used for further analysis. The topology diagram showing the secondary structures present in *Ps*GH43_12 was generated by using PDBSum (http://www.ebi.ac.uk/thornton-srv/databases/pdbsum/Generate.html).

4.2.4 Molecular dynamic simulation of the *Ps*GH13_12 structure

Molecular dynamic (MD) simulation of the modeled *Ps*GH43_12 structure was performed to determine the conformational stability and behavioral dynamics at the nanosecond level. GROMOS 96 43a1 force field compiled with GROMACS v5.1.4 software program installed in High-Performance Computing facility (Param-

Ishan) available at Indian Institute of Technology Guwahati, India was used. *Ps*GH43_12 was placed in a triclinic box with dimensions of 6.39x7.34x5.29 nm and volume 248.47 nm^3 and solvated with a single point charge (SPC) waters. The MD simulation system containing 4 Cl^- ions as counterions and 6,257 solvent (water) was energy minimized by using the Steepest descent method using cut-off up to 1000 kJ mol^{-1} and 20,000 iteration steps. The MD simulation system was equilibrated by performing NVT ensemble (constant number of particles, volume and temperature) followed by NPT ensemble (constant number of particles, pressure and temperature) for 500 ps each step. The equilibrated system was simulated for 100 ns to run the final MD simulation and the trajectories were recorded at 10 ps interval. The MD simulated system was analyzed for estimating the root-mean-square deviation (RMSD) by gmx rms command followed by room mean square function (RMSF) calculation by gmx rmsf. The intramolecular hydrogen bonds, the radius of gyration (Rg) and solvent accessible surface area (SASA) were determined by using gmx hbond, gmx gyrate and gmx sasa commands, respectively. The XMGRACE software (http://plasma-gate.weizmann.ac.il/Grace/) was used for data plotting and analysis.

4.2.5 Molecular docking analysis of *Ps*GH43_12

The amino acid residues involved in the formation of the active site and catalytically essential residues of *Ps*GH43_12 were identified by performing the molecular docking simulation analysis with its ligand. The ligands *viz.* Arabinose, arabinoxylobiose, arabinoxylotetraose, arabinoxylotriose, xylobiose, xylotriose and xylotetraose were retrieved from PubChem database (https://pubchem.ncbi.nlm.nih.gov/) and prepared in 3D format by OpenBabel 2.3.2a software. AutoDock v4.2.6 compiled with MGL Tools 1.5.6

(http://mgltools.scripps.edu/) was used for performing the molecular docking analysis. The protein and ligands were prepared and converted into PDBQT format by following the protocol reported earlier by Sharma et al., (Sharma et al., 2018). Grid box of 60x60x60 size in x, y and z-direction with default grid point spacing was arranged around the active site by using the grid centering option. The conformational search and docking simulation for different ligands were executed using the Lamarckian Genetic Algorithm (LGA). 100 different confirmation of ligands were generated by running a total of 100 GA cycles. These 100 conformations of ligands were ranked and clustered based on the energy of binding and the best conformation with the lowest binding energy was selected for protein-ligand interaction analysis. The protein-ligand complexes were further analyzed in PyMOL for the identification of hydrophobic contacts and polar interactions. 2D interaction of protein and ligand was generated by using Ligplot+ program (Laskowski and Swindells 2011).

4.2.6 Secondary structure and protein melting analysis of *Ps*GH43_12

The gene encoding *Ps*GH43_12 from *P. saltans* with a molecular mass of ~65 kDa protein was expressed and purified was used. *Ps*GH43_12 at a concentration of 15 µM dissolved in 50 mM HEPES buffer pH 6.5 was used for secondary structure determination by Circular Dichroism spectropolarimeter (JascoJ-815, Japan) coupled with Peltier temperature controller. The CD data were collected at 25°C by using a quartz cuvette of path length of 1 mm in a spectral range of 190-240 nm. Mean residue ellipticity was calculated and plotted against the wavelength. The secondary structure was determined by using K2D3 software (http://cbdm-01.zdv.uni-mainz.de/~andrade/k2d3/). The secondary structure of *Ps*GH43_12, was predicted by using Psipred (http://bioinf.cs.ucl.ac.uk/psipred/) software. PDBsum

(http://www.ebi.ac.uk/thornton-srv/databases/pdbsum/Generate.html) was used to create the topology plot.

The melting profile of *Ps*GH43_12 (50 µg/ml) in 50 mM HEPES buffer (pH 6.5) was determined by a CD spectrophotometer (JascoJ-815, Japan) at varying temperatures using a Peltier temperature controller. The change in absorbance at 216 nm (A_{216}) was recorded by attaining the equilibrium by *Ps*GH43_12 at a particular temperature for 3 min. The difference in the absorbance at 216 nm (A_{216}) with respect to the temperature was recorded. The melting studies experiments with *Ps*GH43_12 were also performed in the presence of 10 mM $MgCl_2$, and 10 mM EDTA to examine their effects. All experiments were conducted in triplicates. The absorbance was plotted against the temperature using a sigma plot.

4.2.7 Small Angle X-ray Scattering Analysis (SAXS) of *Ps*GH43_12

The detailed information about molecular shape and conformation behavior of *Ps*GH43_12 in solution was determined by performing small-angle X-ray scattering (SAXS) analysis. The SAXS pattern of *Ps*GH43_12 collection was performed by using small-angle X-ray scattering instrument (SAXSpace, Anton Paar GmbH, Graz, Austria) as described earlier (Sharma et al., 2018). The scattering profiles of *Ps*GH43_12 at a concentration of 5 mg/ml and 10 mg/ml and its matched buffer (50 mM Sodium phosphate pH 7.5) were collected at temperature 10°C. The SAXS profile of both protein and buffer was processed using SAXS analysis software. ATSAS v2.8.4 was used for SAXS data processing and analysis. The effect of radiation damage on SAXS data was evaluated by visual inspection and Guinier approximation analysis. The radius of gyration for globular shape (Rg) and road shape (Rc) was determined by using the PRIMUS program and the Rg was validated by

using the indirect Fourier transform method in GNOM software (Semenyuk and Syergun 1991). The maximum dimension of the molecule (D_{max}) was evaluated by distance distribution function P(R) by the GNOM program. The SAXSMow program was used to estimate the molecular mass of *Ps*GH43_12. Low-resolution dummy atom model (DAM) of *Ps*GH43_12 was constructed using the DAMMIF program (Franke and Syergun 2009). A total 20 independent *ab initio* low-resolution DAM were generated by the DAMMIN, followed by averaging by the DAMAVER program (Volkov and Syergun 2003). The resolution of the generated model was estimated by the SASRES program (Tuukkanen et al., 2016). SUPCOMB program was used to superpose the MD simulated *Ps*GH43_12 structure on DAM.

4.2.8 Mutation of active site residues by site-directed mutagenesis

The active site residues were determined by sequence analysis and molecular docking. To confirm the role of each residue point mutations into the gene encoding the catalytic module *Ps*GH43_12 of *Pseudopedobacter saltans,* were introduced by using a Q5® Site-Directed Mutagenesis Kit (New England Biolabs, NEB, USA). The recombinant plasmid containing pET-28a(+) vector and the *Ps*GH43_12 gene was used as template for the PCR. The three different sets of primers were used for the three individual mutations (Table 4.1). For PCR, the Q5 Hot Start High-Fidelity polymerase provided in the 2X master mix was used as per the manufacturer's protocol. In brief, 25 µl reaction was set up which contained 12.5 µl of the Q5 Hot Start High-Fidelity 2X master mix, 1 µl of the template DNA (1-25 ng/ µl), 1.25 µl each of forward and reverse primer (0.5 µM) and 9 µl of nuclease-free water. The polymerase used in the reaction amplifies both the strands with high fidelity and without displacing the mutated oligonucleotide primers. The thermal cycles used were

as follows: initial denaturation at 98°C for 30 s, followed by 25 cycles at 98°C for 10 s, 55°C for 1 min and 72°C for 5 min, with a final extension at 72°C for 10 min. The PCR product was given KLD (Kinase, Ligase and *Dpn*I) treatment for efficient phosphorylation by kinase enzyme, quick intramolecular ligation or circularization by ligase enzyme and template removal by *Dpn*I endonuclease enzyme which has activity against methylated and hemimethylated DNA, thus digesting the parental DNA template and maintaining the PCR amplified product in non-methylated form. For this, a 10 µl reaction mixture was prepared which contained 1 µl of the PCR product, 5 µl of 2X KLD buffer, 1 µl of KLD enzyme mix and 3 µl of nuclease-free water. All the components were carefully mixed and incubated at 25°C for 5 min. Further, 5 µl of this reaction mixture was transformed in 100 µl *E. coli* DH5α competent cells. After screening, the positive constructs were sequenced to verify the desired point mutations.

Table 4.1 Primers for site-directed mutagenesis of *Ps*GH43_12.

Name	Oligonucleotide (5'-3')
D71A-F	TTGTTATCCGGCTCCTGCAATCAC
D71A-R	CCCTGTAAGATACTTGTATAAAATTTATTG
D180A-F	TGATGGTATAGCCCCTTCTATGTTTTTC
D180A-R	AATTGAAGTTTTATGGGATCG
E247A-F	AATCTGGATTGCAGCGCCACACA
E247A-R	GGCTTTTTCGAAATATCAACGC

4.2.9 Purification of *Ps*GH43_12 mutants

The recombinant plasmid containing the mutated gene encoding *Ps*GH43_12 (D71A), *Ps*GH43_12 (D180A) and *Ps*GH43_12 (E247A) were transformed in *E. coli* BL-21 (DE3) cells. The *E. coli* BL-21(DE3) cells harboring the recombinant plasmids, expressing mutants (D71A, D180A or E247A) were grown in 100 ml LB

medium supplemented with kanamycin (50 µg/ml) and induced with an optimized concentration, 0.25 mM of IPTG and further incubated at 24°C for 12h for hyper-expression. The bacterial cells were harvested from the broth by centrifuging at 6,000g and 24°C for 15 min. The cell pellet was resuspended in 20 ml 50 mM sodium phosphate buffer, pH 7.5 and subjected to sonication for 10 min (10s on and 10s off 30 MHz). A single-step purification method, the immobilized metal ion affinity chromatography (IMAC), was employed for the purification of His_6-tag linked mutants (D71A, D180A and E247A). 1 ml HiTrap gravity column (GE Healthcare, USA) was activated with Ni^{2+} ions by using a 0.1M $NiSO_4$ solution. The cell-free extract obtained after sonication and centrifugation was loaded on to the 1 ml column. The column was washed with 40 ml of equilibration buffer (50 mM sodium phosphate and 300 mM NaCl buffer, pH 7.5) containing 60 mM imidazole. The column bound protein was eluted by elution buffer (50 mM sodium phosphate buffer, pH 7.5, 300 mM NaCl, 300 mM imidazole). The eluted protein was extensively dialyzed against 50 mM sodium phosphate buffer, pH 7.5 and the protein concentration was determined by the Bradford method using bovine serum albumin as the standard (Bradford 1976). The purified protein was run on 12% (w/v) SDS-PAGE after boiling for 5 min and stained with Coomassie brilliant blue for checking molecular mass and purity (Neuhoff et al., 1985).

4.2.10 Enzyme assay

Arabinofuranosidase activity of wild type (WT) *Ps*GH43_12 and its mutants was checked by using 1% (w/v) rye arabinoxylan dissolved in citrate phosphate buffer (50 mM, pH 6.5). The reaction volume, 100 µl contained 90 µl of the substrate and 10 µl of the enzyme WT *Ps*GH43_12 and its mutants D71A, D180A or E247A at 50

µg/ml. The reaction mixture was incubated at 50°C for 5 min. The method of Nelson (Nelson 1944) and Somogyi (Somogyi 1945) for estimating the reducing sugar concentration was followed by using the standard curve of L-arabinose. The specific activity of *Ps*GH43_12 was defined as the number of µmole of arabinose released from arabinoxylan per min per mg of the enzyme (µmol/min/mg) under the optimum conditions of the WT enzyme.

4.3 Results and Discussion

4.3.1 Sequence analysis of *Ps*GH43_12

The BLASTp analysis of α-L-arabinofuranosidase of family 43 glycoside hydrolase from *Pseudopedobacter saltans*, *Ps*GH43_12 displayed, that it belongs to GH43_62_32_68_117_130 superfamily and GH43_XynB like specific family (pfam04616). The sequence analysis of *Ps*GH43_12 revealed that it displays the amino acid sequence identity with previously characterized xylosidases *viz.* Xyl (35.6%) from *G. thermoleovorans*, BoXyGUL (35.4%) from *B. ovatus and Bl*XynB (31.6%) from *B. licheniformis* (Table 4.2). Molecular architecture analysis revealed that it comprises the signal peptide of 29 amino acid long at N-terminal and a catalytic module (557 amino acid residues) of family 43 glycoside hydrolase module (*Ps*GH43_12) at C-terminal. The physicochemical properties analysis of *Ps*GH43_12 by Protparam webserver displayed that it is composed of 586 amino acids with molecular mass 65.9 kDa and theoretical pI, 8.74. The sequences as mentioned above were retrieved from PDB and aligned and the catalytic amino acid residues (Asp71, Asp180 and Glu247) were identified (Fig. 4.1). The multiple sequence alignment shows, the conserved residues in red color background, and the semi-conserved residues highlighted red color. Multiple sequence alignment showed that 6 α helix and 39 β sheets.

Table 4.2 BLASTp analysis of *Ps*GH43_12 amino acid sequence.

Name	Enzyme name	Query Cover (%)	Identity (%)	E-value	Total Score	Resolution (A°)	PDB ID
G. thermoleovorans	Xyl	87	35.6	1e-85	277	1.7	5Z5D
B. ovatus	*Bo*XyGUL	87	35.4	1e-77	258	1.6	5JOW
B. licheniformis	*BI*XynB	97	31.6	2e-67	229	1.95	6MS3

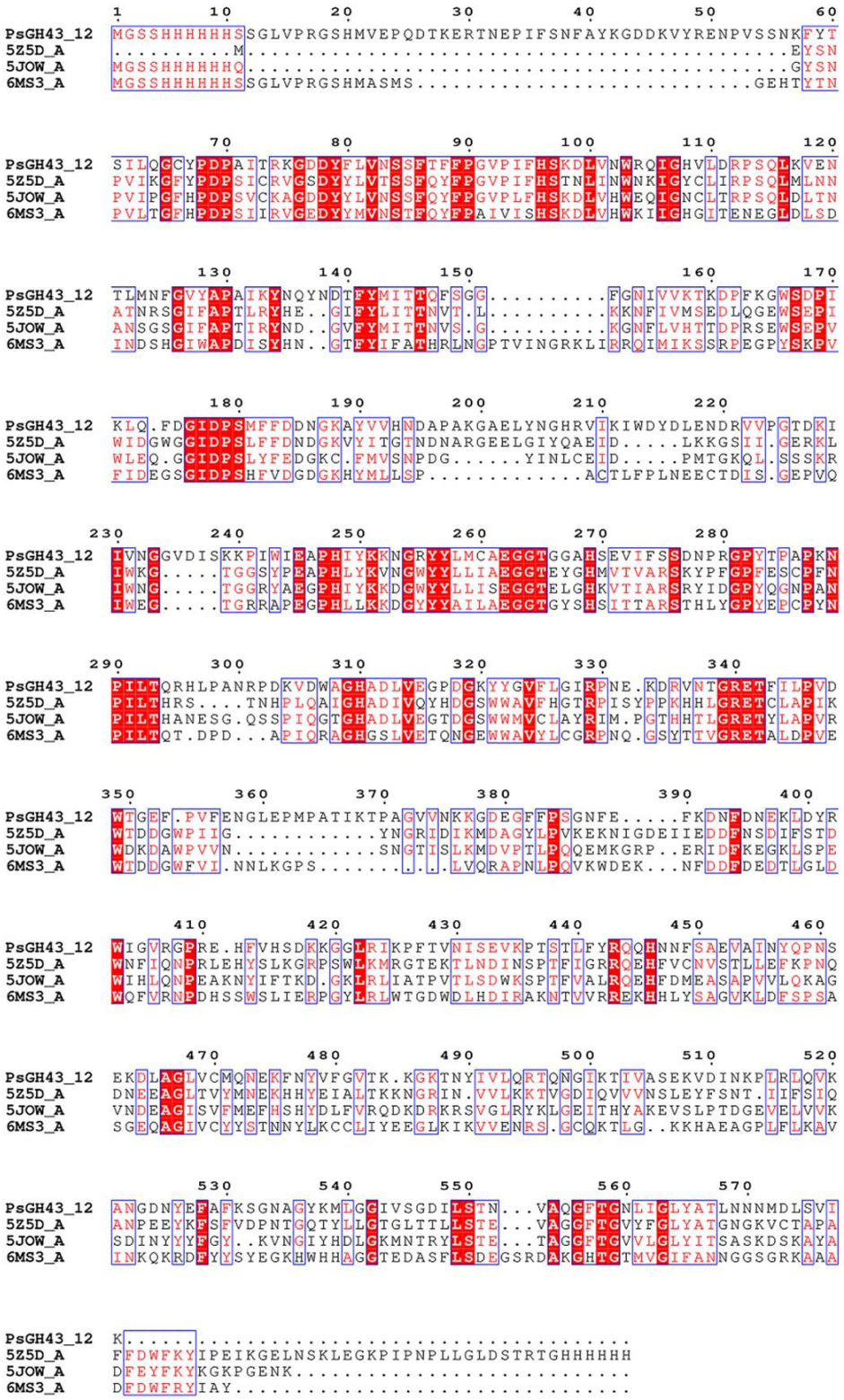

Fig. 4.1 Multiple Sequence Alignment of *Ps*GH43_12 with Xyl (PDB id: 5Z5D), BoXyGUL (PDB id: 5JOW) and *Bl*XynB (PDB id: 6MS3), as given in methods and Table 4.2. Conserved amino acid residues are displayed in red background and semi-conserved residues are highlighted in red color.

4.3.2 Structure modeling of *Ps*GH43_12 and validation

The homology modeled structure of *Ps*GH43_12 (Fig. 4.2A) displayed two independently folded domains *viz.* catalytic module at N-terminal spanning from Met1-Ile369 amino acid residues (including 22 residues of pET28a(+) vector and His6-tag), forming 5-bladed β-propeller fold and a β-sandwich fold from Trp441-Lys580 at the C-terminal (Fig. 4.2A). The catalytic and β-sandwich domain are connected by a 72 amino acid residue long linker peptide. A similar type of structure organization is also reported for several other GH43 enzymes *viz.* Xyl from *G. thermoleovorans* (Rohman et al., 2018), *Bo*XyGUL from *B. ovatus* (Hemsworth et al., 2016) *and Bl*XynB from *B. licheniformis* (Zanphorlin et al., 2019). The energy minimized modeled *Ps*GH43_12 structure was assessed by the tools available on the SAVES server for quality assessment. The Ramachandran plot analysis by RAMPAGE server displayed that 553 amino acid residues (95.7%) are in the favored region, 19 amino acid residues (3.3%) are in the allowed region and 6 amino acid residues Val94, Val225, Asn234, His298, Glu354 and Phe355 (1.0%) are in the disallowed region (Fig. 4.2B). The Ramachandra plot analysis revealed that the modeled structure follows the stereochemical property rule and follows all the possible dihedral, phi (ϕ) and psi (ψ) angle values. ProSA analysis of *Ps*GH43_12 displayed the Z score of -8.23, which displayed that the modeled structure lies in the X-ray zone (Fig. 4.2C). The quality factor analysis of *Ps*GH43_12 energy minimized structure by ERRAT plot was 87.83%, which further confirmed that the structure modeling is devoid of any errors (Fig. 4.2D). The VERIFY3D analysis of the *Ps*GH43_12 modeled structure displayed that 83.45% of amino acid residues have an overall average 3D-1D score ≥ 0.2 (Fig. 4.2E).

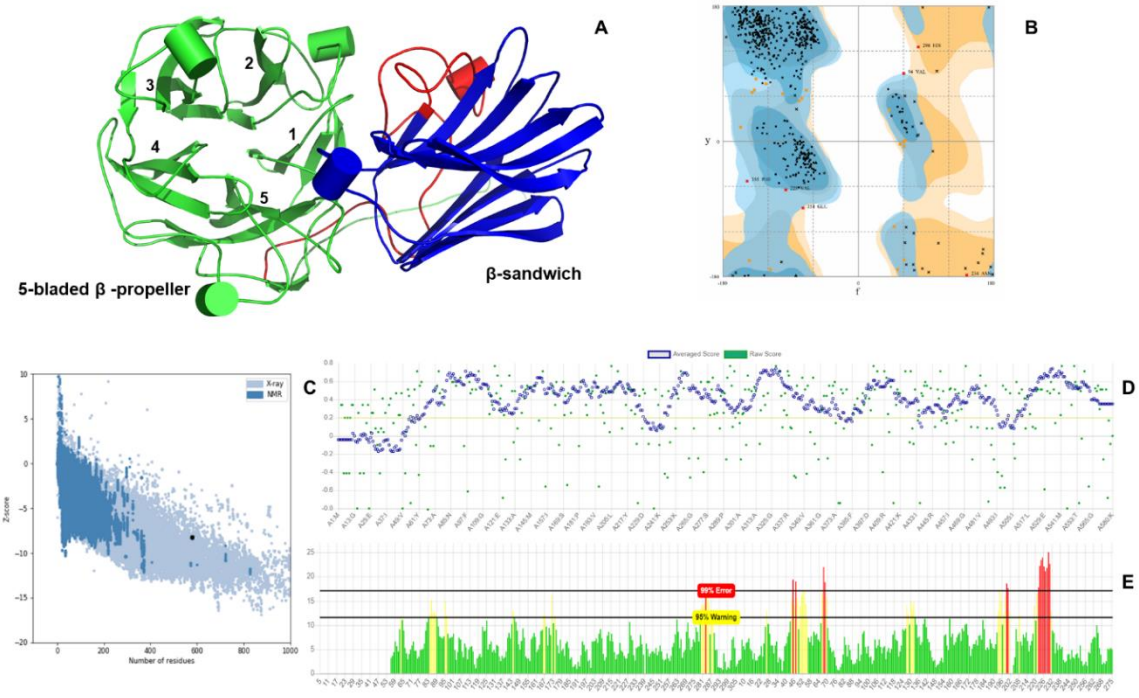

Fig. 4.2 Three-dimensional structure modeling of *Ps*GH43_12 and validation analysis. A) 3D structure B) Ramachandran Plot analysis by Rampage server showing the most favorable, additionally allowed and generously allowed regions of amino acid residues, C) ProSA plot showing Z-score, D) VERIFY 3D showing the threshold score more than 0.2, E) ERRAT Plot analysis showing the quality of the *Ps*GH43_12 modeled structure.

4.3.3 Molecular dynamics simulation analysis of *Ps*GH43_12

The global compactness and structure stability of *Ps*GH43_12 was analyzed by performing molecular dynamics (MD) simulation. The estimated root mean square deviation (RMSD) analysis of *Ps*GH43_12 for the entire trajectory from the initial structure, displayed 0.35 nm till 20 ns and after that the RMSD became stable at 0.40 nm up to 100 ns (Fig. 4.3A). The root means structure fluctuation (RMSF) analysis of *Ps*GH43_12 based on Cα atoms revealed that the structure changes occur in the loop forming region and displayed the high flexibility (Fig. 4.3B). The radius of gyration analysis of *Ps*GH43_12 for the estimation of global compactness displayed the fluctuation in Rg values (2.40 nm to 2.35 nm) for initial 15 ns indicating the

flexibility. Then the average Rg value was constant at 2.32 nm till 100 ns, showing that the protein attains its stable conformation resulting in the global compactness (Fig. 4.3C). *Ps*GH43_12 was subjected to intramolecular hydrogen bond analysis assisted the structure in achieving a stable state during the MD simulation. The MD simulation analysis revealed that it containing average of 368 intramolecular hydrogen bonds up to 100 ns (Fig. 4.3D). The estimated average solvent accessible surface area (SASA) for *Ps*GH43_12 up to 100 ns was 199 nm^2 that remained unchanged throughout the MD simulation (Fig. 4.3E). The structural changes in the secondary structure component of *Ps*GH43_12 were analyzed by DSSP software. The DSSP analysis throughout the MD simulation displayed no change in the secondary structure component and displayed the conservation in the structural component, as shown in Fig. 4.3F. The structure superimposition of the MD simulated *Ps*GH43_12 structure with initial *Ps*GH43_12 structure displayed that the unstructured region possesses the flexibility with the RMSD value of 0.0481 nm (all Cα atom aligned) (Fig. 4.3G). The final *Ps*GH43_12 structure obtained after MD simulation was compact and stable and can be used for molecular docking analysis.

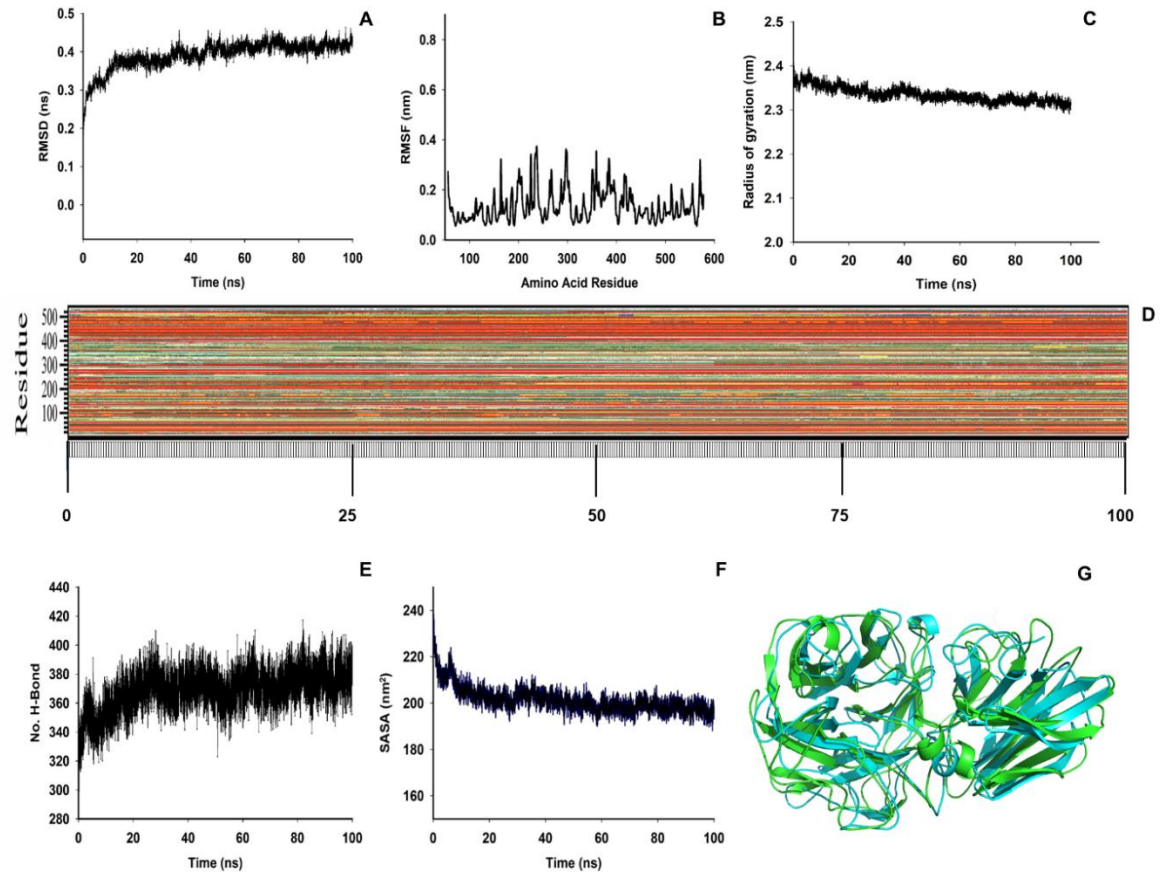

Fig. 4.3 Molecular dynamic simulation of *Ps*GH43_12 (A) RMSD Plot, (B) RMSF Plot, (C) The radius of gyration Plot, (D) Secondary structure analysis by DSSP, (E) Intramolecular hydrogen bond analysis, (F) SASA calculation and (G) Superposition of simulated *Ps*GH43_12 structure (Blue) with modeled *Ps*GH43_12 structure (Green).

4.3.4 Molecular docking analysis of *Ps*GH43_12

Molecular docking analysis of *Ps*GH43_12 with its probable ligands was performed to study their interactions. The *Ps*GH43_12-ligand interaction and free energy of binding for Arabinose, arabinoxylobiose, arabinoxylotetraose, arabinoxylotriose, xylobiose, xylotriose and xylotetraose are reported in Table 4.3. The maximum binding energy was found to be -8.98 kcal/mol for xylotetraose, followed by other xylooligosaccharides and arabinoxylooligosaccharides *viz.*

xylotriose, arabinoxylotriose, arabinoxylobiose, xylobiose, arabinoxylotetraose and arabinose.

Table 4.3 Active site residues of *Ps*GH_12 showing interaction with ligands.

Ligand	Binding Energy kcal mol^{-1}	Amino acid residues involved in hydrogen bonds formation	Amino acid residues involved in hydrophobic interactions
Xylotetraose	-8.98	Arg210, Gly 558	Phe127, Tyr130, Phe150, Ile179, Pro199, Trp245, Glu247, Gly265, Gly266, Thr267 Gly268, Gln557 and Phe559
Xylotriose	-8.77	Arg210, Thr267	Phe127, Tyr130, Phe150, Ile179, Trp245, Glu247, Gly266, Gly268 and Phe559
Arabinoxylotriose	-8.35	Arg210, Thr267	Phe127, Tyr130, Phe150, Ile179, Trp245, Gly266, Gly268, Trp309, Thr553, Gln557, Gly558 and Phe559
Arabinoxylobiose	-8.23	Arg210, Thr267	Asn126, Phe127, Tyr130, Phe150, Ile179, Trp245, Glu247, Gly266 and Phe559
Xylobiose	-7.51	Arg210, Thr267	Asn126, Phe127, Tyr130, Phe150, Ile179, Trp245, Glu247, Gly266 and Phe559
Arabinoxylotetraose	-5.96	Gly558	Asn126, Phe127, Tyr130, Phe150, Ile 179, Pro199, Arg210, Trp245, Gly 268 Trp309, Thr553, Gln557 and Phe559
Arabinose	-5.23	Arg210, Trp245	Gly208, His209 and Ile 244

The molecular docking analysis of *Ps*GH43_12 with Arabinose (Fig. 4.4A), Arabinoxylobiose (Fig. 4.4B), Arabinoxylotriose(Fig. 4.4C), arabinoxylotetraose (Fig. 4.4D), and xylobiose (Fig. 4.4E) displayed that the aromatic residues *viz.* Phe127,

Tyr130, Phe150, Trp245 and Phe559 and the catalytic residues Gly247 involved in the formation of catalytic pocket, whereas, Arg210 and Thr267 forms hydrogen bond with the ligand. The molecular docking analysis displayed that the *Ps*GH43_12 is more specific towards xylotriose and xylotetraose (Fig. 4.4F & G). The xylotriose interacts with Arg210 and Thr267 through H-bond formation and accommodated in the active site cleft and through hydrophobic interactions by Phe127, Tyr130, Phe150, Ile179, Trp245, Glu247, Gly266, Gly268 and Phe559 (Fig. 4.4F). In the *Ps*GH43_12-xylotetraose complex, xylotetraose is accommodated within the active site cleft with the help of hydrogen bond formation by Arg210 and Gly 558 and also hydrophobic interactions by Phe127, Tyr130, Phe150, Ile179, Pro199, Trp245, Glu247, Gly265, Gly266, Thr267 Gly268, Gln557 and Phe559 (Fig. 4.4G). The xylotetraose interacts with aromatic amino acid residues and these residues are involved in the formation of catalytic cleft, which further helps in orienting and accommodating the substrate for catalysis. The involvement of aromatic amino acid residues in the formation of active site pocket is also revealed by (Rohman et al., 2018; Hemsworth et al., 2016; Zanphorlin et al., 2019; Goyal et al., 2016).

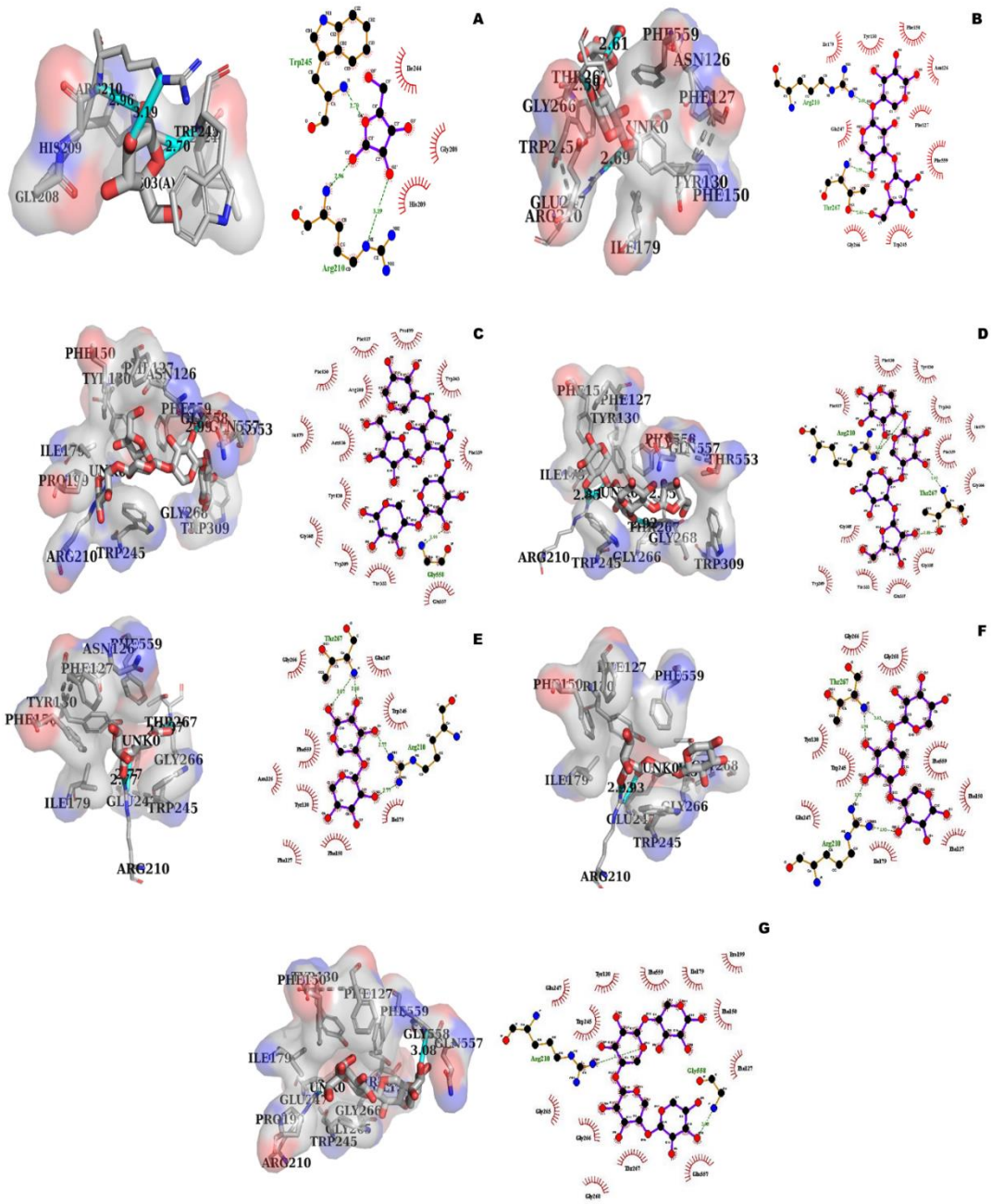

Fig. 4.4 Molecular docking analysis of *Ps*GH43_12 with its ligands. A) Arabinose, B) Arabinoxylobiose, C) Arabinoxylotetraose, D) Arabinoxylotriose, E) Xylobiose, F) Xylotriose and G) Xylotetraose.

4.3.5 Secondary structure and protein melting analysis of *Ps*GH43_12

The circular dichroism analysis of *Ps*GH43_12 displayed that it is composed of 2.7% α-helices, 30.33% of β-strands and the rest 66.97% forms random coils (Fig. 4.5A). The PsiPred prediction of *Ps*GH43_12 corroborated the CD results showing 0.3% of residues involved in the formation of α-helices and 33% residues involved in the β-strands formation. *Ps*GH43_12 was subjected to temperature dependent Circular Dichroism analysis for protein melting study. A curve of relative derivative absorption coefficient versus temperature was plotted to display the melting profile of *Ps*GH43_12 (Fig. 4.5B). The melting profile of native *Ps*GH43_12 suggested that the protein starts melting at 60°C and completely melts at 68°C (Fig. 4.5B). The addition of 10 mM Mg^{2+} or 10 mM EDTA or 10 mM of both Mg^{2+} and EDTA did not show any change in the melting curve (Fig. 4.5C, D & E). The optimal properties of *Ps*GH43_12 displayed that the enzyme did not show any activity or stability beyond 60°C. The biochemical parameter optimization results corroborate well with the protein melting analysis.

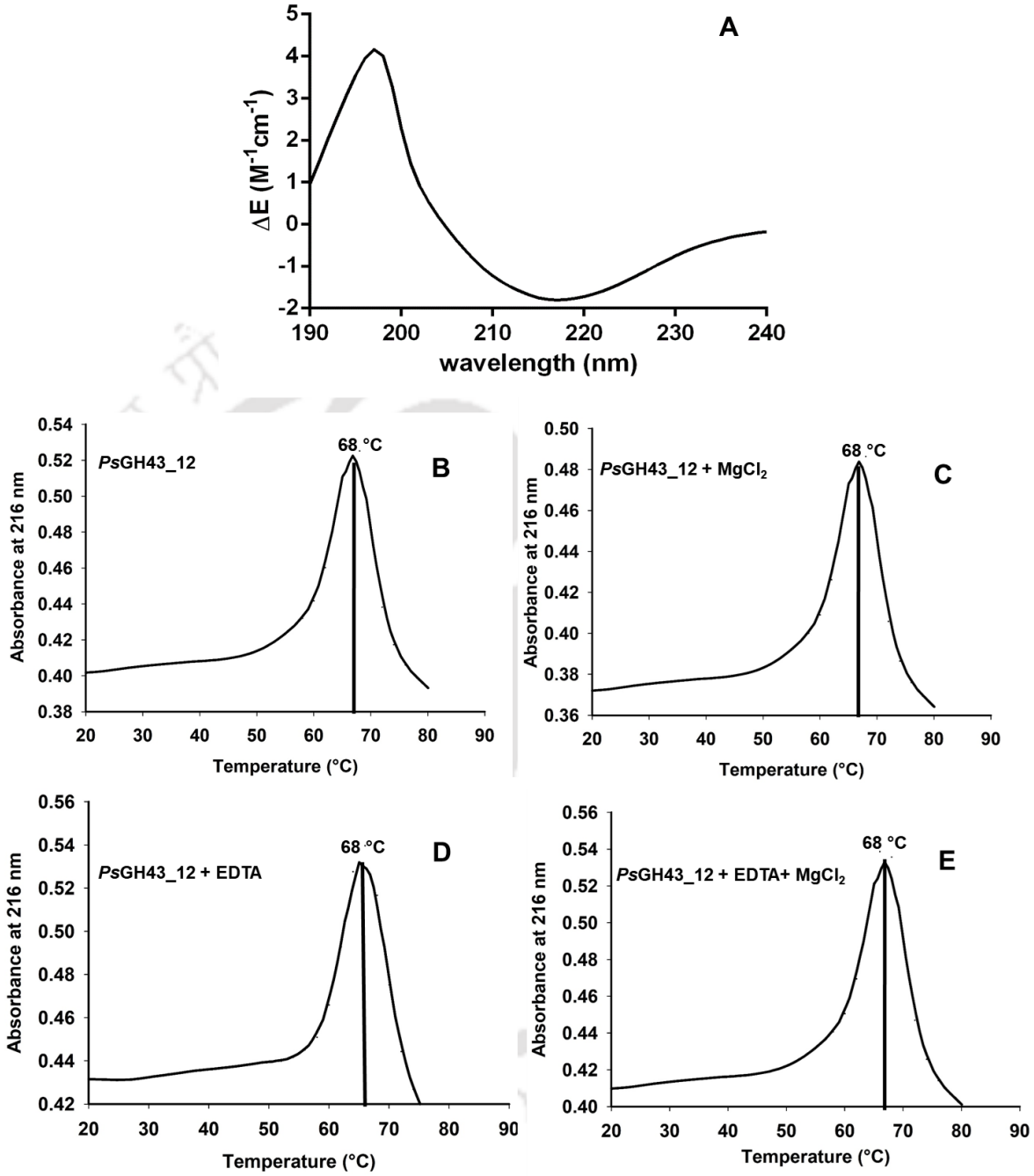

Fig. 4.5 A) Far-UV Circular Dichroism (CD) spectrum of *Ps*GH43_12. B) Protein melting curve analysis of *Ps*GH43_12, C) Melting curve analysis of *Ps*GH43_12 with 10 mM $MgCl_2$, D) Melting curve analysis of *Ps*GH43_12 with 10 mM EDTA and E) Melting curve analysis of *Ps*GH43_12 with 10 mM $MgCl_2$ & EDTA.

4.3.6 Low-resolution structure analysis of *Ps*GH43_12 by Small Angle X-ray Scattering

The scattering pattern of *Ps*GH43_12 collected at different concentrations is shown in Fig. 4.6A. The visual inspection analysis of the scattering curves displayed that the *Ps*GH43_12 is intact and monodispersed in nature. The SAXS data of *Ps*GH43_12 were processed and the results are reported in Table 4.4. The Guinier approximation analysis of *Ps*GH43_12 at both the concentrations (5 mg/ml and 10 mg/ml) displayed linear behavior, which indicates the monodispersity of the enzyme and the particles are free from aggregation effect or interparticle interaction (Fig. 4.6B). For further analysis, the SAXS data collected at 5 mg/mL were used. The Guinier approximation analysis displayed that the radius of gyration (Rg) for globular shape is 2.8±0.09 nm and for the rod-shaped (Rc) is 1.31±0.29 nm. The Rg and intensity [I(0)] analysis of *Ps*GH43_12 revealed that, as the concentration increases, the Rg values displayed the minimal change and the I(0) enhances from 68444 to 90266 au (Table 4.4). However, the increment in I(0), did not affect any other parameter, obtained from SAXS analysis. The SAXS analysis of *Ct*Araf43, a multi-modular protein comprising a catalytic module, *Ct*Abf43 and two carbohydrate binding modules, *i.e.* *Ct*CBM6A & *Ct*CBM6B revealed that, with the increase in the concentration of *Ct*Araf43, it under goes oligomerization followed by the aggregation (Sharma et al., 2019). The estimated persistence length of *Ps*GH43_12 was 8.60 nm. The pair wise distance distribution [P(R)] function analysis acquired by fourier transformation of *Ps*GH43_12 scattering profile displayed the maximum dimension (D_{max}) of 9.7 nm and the radius of gyration (Rg) of 2.81 nm (Fig. 4.6C). The asymmetric bell-shaped profile of P(R) plot particles displayed the shoulder between 6-8 nm confirming that it contains two spatially well

separated modules *i.e.* the catalytic module, *Ps*GH43_12 and the β-sandwich module connected through a very long linker peptide (Fig. 4.6C). The global compactness and flexibility analysis of *Ps*GH43_12 in solution was estimated by Kratky plot analysis (Fig. 4.6D). The Kratky plot analysis of *PS*GH43_12 displayed bell-shape peaks at the low Q region, confirming a compact and folded structure. The molecular mass of *Ps*GH43_12 obtained from the SAXSMow server using the SAXS scattering profile was 67 kDa, which is similar to the theoretically and experimentally calculated molecular mass (65 kDa).

The P(R) profile of *Ps*GH43_12 was further used to generate the 20 independent overall *ab initio* models by using DAMMIF and refined using DAMMIN program. The best fit envelope displaying the lowest $\chi 2$ value with respect to the experimental curve was used for further structure analysis and superposition. The averaged molecular envelope displayed the pendulum like structure containing a globular region and rod like structure (Fig. 4.6E). The structure superposition of the *Ps*GH43_12 modeled structure on the molecule envelope showed fitting with some minor deviations (Fig. 4.6F). The catalytic module and the associated β-sandwich module superpose well on the globular envelope region, while vector sequence containing the His_6 region superpose on the rod like molecule shape with some degree of deviation.

Table 4.4 SAXS data collection parameters and derived parameters of *Ps*GH43_12.

Data-collection parameters	***Ps*GH43_12**	
Instrument	SAXSPace 2.0	
Wavelength (Å)	1.54 Å	
Q range (nm^{-1})	0.14-6.0	
Exposure time (minutes)	60 (2x30 min)	
Temperature (°C)	10	
Protein Concentration mg/mL	5	10
Structural parameter		
Q range (nm^{-1}) used for Rg analysis	0.14-0.46	0.14-0.43
I(0) au from Guinier	68444.60±520.6	90266.1±714.6
Rg nm from Guinier	2.8±0.09	2.91±0.06
Rg nm from P(R)	2.81	2.91
I(0) au from P(R)	67600.00	88820.00
D_{max} (nm)	9.0	9.5
Porod volume estimate (nm^3)	93.24	100.50
Molecular Mass Determination		
Theoretical molecular mass (kDa)	65	65
Molecular Mass from SAXSMOW (kDa)	67	67.5
Modeling parameters		
NSD	0.511±0.016	0.518±0.010
Resolution (nm)	2.40±0.28	2.5±0.2
Q range (nm^{-1}) used from Crysol	0.14-0.59	0.145-0.63
χ^2 Value obtained from Crysol	0.30	0.35
Software employed		
Data processing	Primus	
P(R) function calculation	GNOM	
Ab initio modelling	DAMMIF	
Validation and averaging	DAMAVER	
Structure superposition	SUPCOMB	
3-D graphical representation	PyMOL	

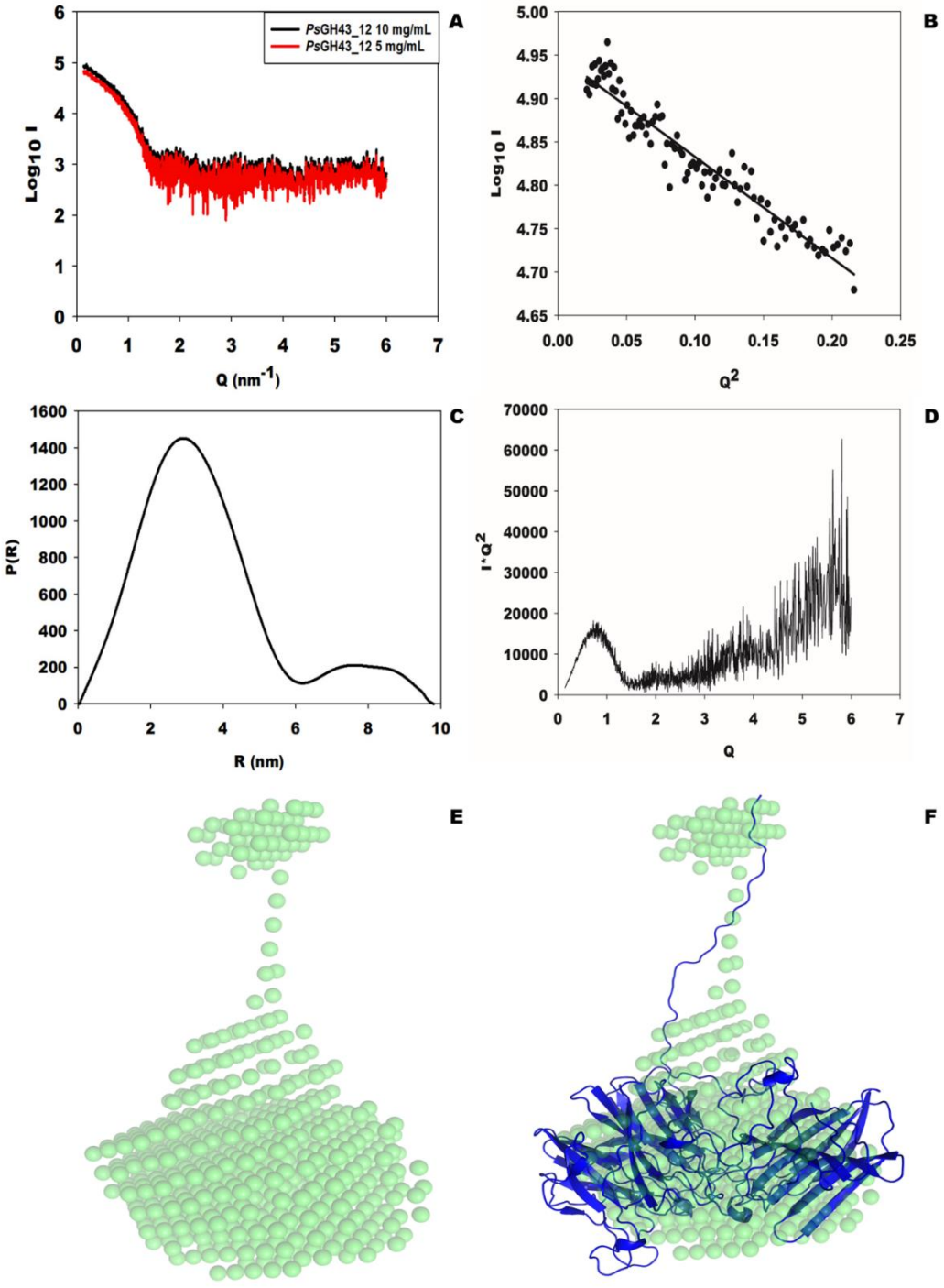

Fig. 4.6 SAXS analysis of *Ps*GH43_12. A) SAXS intensity profile of *Ps*GH43_12, (B) Guinier plot of SAXS intensities, C) Kratky plot analysis of *Ps*GH43_12, D) P(R) curve of *Ps*GH43_12 as a function of R, (E) *ab initio* shape of *Ps*GH43_12 and F) Superposition of *ab initio* model with homology modeled *Ps*GH43_12.

4.3.7 Active site mutation by site directed mutagenesis

All three active site residues of *Ps*GH43_12 were mutated and three mutants were constructed D71A, D180A and E225A, was confirmed by sequencing. The purified mutants on analysis by SDS-PAGE 12%, w/v gel displayed the single bands for all the three mutants with an approximate molecular mass of 65 kDa (Fig. 4.7). The specific activity was calculated for *Ps*GH43_12 and its three mutants. All the mutants were inactive against rye arabinoxylan, confirming that *Ps*GH43_12 contains Asp71, Asp180A and Glu225A as the catalytic residues.

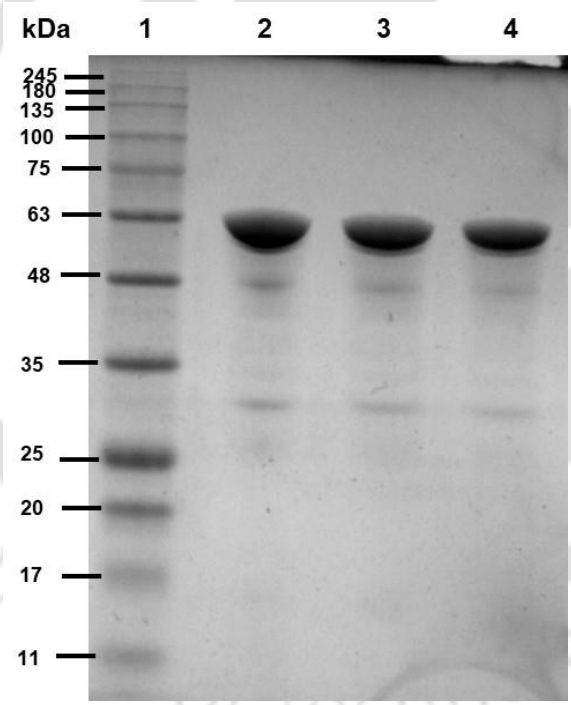

Fig. 4.7 SDS-PAGE (12%, w/v) gel showing purification of *Ps*GH43_12 mutants. Lanes: 1- protein marker, 2- Purified E247A, 3- D180A and 4- D71A each of approximately, 65 kDa.

4.4 Conclusions

The structure and molecular dynamics of α-L-arabinofuranosidase (*Ps*GH43_12) of family 43 glycoside hydrolase, subfamily 12 from *Pseudopedobacter saltans* were studied. *Ps*GH32_12 is the first α-L-arabinofuranosidase from *Pseudopedobacter saltans*. The 3D structure of α-L-arabinofuranosidase (*Ps*GH43_12) of a family 43, glycoside hydrolase from *Pseudopedobacter saltans* modeled by comparative modeling was compact and stable. Ramachandran plot showed 95.7% residues in favored and 3.3% in the generously allowed region and only 1% residues in the disallowed region. The modeled *Ps*GH43_12 structure displayed 5-bladed β-propeller fold at N-terminal and β–sandwich fold at C terminal. The secondary structure analysis of *Ps*GH43_12 by circular dichroism revealed 2.7% α-helices 30.33% β-strands and 66.97% random coils. The *Ps*GH43_12 modeled structure displayed 5-bladed β–propeller fold at N-terminal and β–sandwich fold at C terminal. The docking studies revealed that the active site of *Ps*GH43_12 can accommodate xylotetraose, followed by, xylotriose, arabinoxylotriose, arabinoxylobiose, arabinoxylotetraose, xylobiose and arabinose. Molecular docking analysis confirmed the involvement of active site residues Asp71, Asp180 and Glu247 in the catalysis, which was also confirmed by the site-directed mutagenesis of these residues. The protein melting study of *Ps*GH43_12 showed complete unfolding at 65°C and did not require any metal ion for its stability. SAXS analysis displayed that *Ps*GH43_12 is monomeric and a fully folded state in solution form. Guinier analysis gave the radius of gyration between (Rg) 2.8 ± 0.09 nm at 5 mg/ml protein concentration. The maximum dimension and Rg of *Ps*GH43_12 estimated from P(R) plot were 9.0 nm and 2.81 nm, respectively. Kratky plot analysis of *Ps*GH43_12 displayed a fully folded state in solution form. The *ab initio* derived

dummy model of *Ps*GH43_12 displayed a bell-like shape. The *ab initio* derived dummy model superposed well with its comparative modeled structure except the N-terminal His_6-tag region.

4.5 References

Altschul, S. F., Madden, T. L., Schäffer, A. A., Zhang, J., Zhang, Z., Miller, W., & Lipman, D. J. (1997). Gapped BLAST and PSI-BLAST: a new generation of protein database search programs. *Nucleic Acids Research, 25*(17), 3389-3402.

Alvira, P., Negro, M. J., & Ballesteros, M. (2011). Effect of endoxylanase and α-L-arabinofuranosidase supplementation on the enzymatic hydrolysis of steam exploded wheat straw. *Bioresource Technology, 102*(6), 4552-4558.

Bradford, M. M. (1976). A rapid and sensitive method for quantitation of microgram quantities of protein utilizing the principle of protein-dye binding. *Analytical Biochemistry, 72*, 248-254.

Colovos, C., & Yeates, T. O. (1993). Verification of protein structures: patterns of nonbonded atomic interactions. *Protein Science, 2*(9), 1511-1519.

Eisenberg, D., Lüthy, R., & Bowie, J. U. (1997). [20] VERIFY3D: assessment of protein models with three-dimensional profiles. In *Methods in Enzymology 277*, Academic Press, 396-404.

Eswar, N., Eramian, D., Webb, B., Shen, M. Y., & Sali, A. (2008). Protein structure modeling with MODELLER. In *Structural Proteomics* Humana Press, 145-159.

Franke, D., & Svergun, D. I. (2009). DAMMIF, a program for rapid ab-initio shape determination in small-angle scattering. *Journal of Applied Crystallography, 42*(2), 342-346.

Goyal, A., Ahmed, S., Sharma, K., Gupta, V., Bule, P., Alves, V. D., & Najmudin, S. (2016). Molecular determinants of substrate specificity revealed by the structure of *Clostridium thermocellum* arabinofuranosidase 43A from glycosyl hydrolase family 43 subfamily 16. *Acta Crystallographica Section D: Structural Biology, 72*(12), 1281-1289.

Hemsworth, G. R., Thompson, A. J., Stepper, J., Sobala, Ł. F., Coyle, T., Larsbrink, J., & Davies, G. J. (2016). Structural dissection of a complex *Bacteroides ovatus* gene locus conferring xyloglucan metabolism in the human gut. *Open Biology, 6*(7), 160142.

Laskowski, R. A., & Swindells, M. B. (2011). LigPlot+: multiple ligand–protein interaction diagrams for drug discovery. *Journal of Chemical Information and Modeling*, 2778-2786.

Laskowski, R. A., MacArthur, M. W., Moss, D. S., & Thornton, J. M. (1993). PROCHECK: a program to check the stereochemical quality of protein structures. *Journal of Applied Crystallography*, *26*(2), 283-291.

Lombard, V., Golaconda Ramulu, H., Drula, E., Coutinho, P. M., & Henrissat, B. (2014). The carbohydrate-active enzymes database (CAZy) in 2013. *Nucleic Acids Research*, *42*(D1), 490-495.

Nelson, N. (1944). A photometric adaptation of the Somogyi method for the determination of glucose. *Journal of Biological Chemistry*, *153*(2), 375-380.

Neuhoff, V., Stamm, R., & Eibl, H. (1985). Clear background and highly sensitive protein staining with Coomassie Blue dyes in polyacrylamide gels: a systematic analysis. *Electrophoresis*, *6*(9), 427-448.

Robert, X., & Gouet, P. (2014). Deciphering key features in protein structures with the new ENDscript server. *Nucleic Acids Research*, *42*(W1), 320-324.

Rohman, A., van Oosterwijk, N., Puspaningsih, N. N. T., & Dijkstra, B. W. (2018). Structural basis of product inhibition by arabinose and xylose of the thermostable GH43 β-1, 4-xylosidase from *Geobacillus thermoleovorans* IT-08. *PloSOne*, *13*(4). 10.1371/journal.pone.0196358

Semenyuk, A. V., & Svergun, D. I. (1991). GNOM–a program package for small-angle scattering data processing. *Journal of Applied Crystallography*, *24*(5), 537-540.

Seri, K., Sanai, K., Matsuo, N., Kawakubo, K., Xue, C., & Inoue, S. (1996). L-arabinose selectively inhibits intestinal sucrase in an uncompetitive manner and suppresses glycemic response after sucrose ingestion in animals. *Metabolism*, *45*(11), 1368-1374.

Sharma, K., Antunes, I. L., Rajulapati, V., & Goyal, A. (2018). Low-resolution SAXS and comparative modeling based structure analysis of endo-β-1, 4-xylanase a family 10 glycoside hydrolase from *Pseudopedobacter saltans* comb. nov. *International Journal of Biological Macromolecules*, *112*, 1104-1114.

Sharma, K., Fontes, C. M., Najmudin, S., & Goyal, A. (2019). Small angle X-ray scattering based structure, modeling and molecular dynamics analyses of family 43 glycoside hydrolase α-L-arabinofuranosidase from *Clostridium thermocellum*. *Journal of Biomolecular Structure and Dynamics*, 1-16.

Shen, M. Y., & Sali, A. (2006). Statistical potential for assessment and prediction of protein structures. *Protein Science*, *15*(11), 2507-2524.

Sievers, F., Wilm, A., Dineen, D., Gibson, T. J., Karplus, K., Li, W., & Thompson, J. D. (2011). Fast, scalable generation of high-quality protein multiple sequence alignments using Clustal Omega. *Molecular Systems Biology*, *7*(1). https://doi.org/10.1038/msb.2011.75

Somogyi, M. (1945). A new reagent for the determination of sugars. *Journal of Biological Chemistry*, *160*, 61-68.

Taylor, E. J., Smith, N. L., Turkenburg, J. P., D'souza, S., Gilbert, H. J., & Davies, G. J. (2006). Structural insight into the ligand specificity of a thermostable family 51 arabinofuranosidase, Ara f 51, from *Clostridium thermocellum*. Biochemical Journal, 395(1), 31-37.

Thakur, A., Sharma, K., & Goyal, A. (2019). α-l-Arabinofuranosidase: A Potential Enzyme for the Food Industry. In *Green Bio-processes* Springer, Singapore, 229-244.

Tuukkanen, A. T., Kleywegt, G. J., & Svergun, D. I. (2016). Resolution of ab initio shapes determined from small-angle scattering. *IUCrJ*, *3*(6), 440-447.

Volkov, V. V., & Svergun, D. I. (2003). Uniqueness of ab initio shape determination in small-angle scattering. *Journal of Applied Crystallography*, *36*(3), 860-864.

Zanphorlin, L. M., de Morais, M. A. B., Diogo, J. A., Domingues, M. N., de Souza, F. H. M., Ruller, R., & Murakami, M. T. (2019). Structure-guided design combined with evolutionary diversity led to the discovery of the xylose-releasing exo-xylanase activity in the glycoside hydrolase family 43. *Biotechnology and Bioengineering*, *116*(4), 734-744.

Chapter 5

Hemicellulose saccharification from Sugarcane bagasse by recombinant hemicellulases

5.1 Introduction

The demand for energy is increasing with increase in population. There is an extensive load on existing energy sources like coal and petroleum which will be depleted. The excessive consumption of these fossil fuels has led to drastic increase in the level of greenhouse gases (Hameed & Dignon, 1988). By the end of 2050, the demand of energy will increase from current demand of 13 billion to 45 billion tons of oil equivalent (Zhang & Konan, 2010). Therefore, there is an urgent need for alternate renewable sources of energy or fuels to cope with the climate change as well as the diminishing oil supply. To accomplish the energy requirement, renewable sources are focused like nuclear energy, wind energy, hydro energy, solar energy and bioenergy. Bioenergy contributes the highest share, 14% out of 18% of total renewable energy supply (Berndes et al., 2003). Bioenergy is harvested either from forest biomass or from agricultural residues. Utilization of renewable biomass sources like agricultural residues has emerged as a promising option for biofuel production, such as

bioethanol, biodiesel and biogas. Bioethanol and biodiesel are the two main alternative energy sources developing as transportation fuels. Keeping up the sustainable development, Government of India has made 5% bioethanol blending to gasoline, compulsory in India (Singh et al., 2016).

Indian economy largely depends on agriculture; major population of India relies on agriculture for their living. Wheat, rice, sugarcane, maize barley etc. are the major crops grown in India. Approximately, 200 billion tonnes of lignocellulosic biomass is produced from agriculture sector (Guo et al., 2010). Lignocellulosic biomass forms about 90% of total plant biomass (Lin & Tanaka, 2006). In 2018, worldwide production of sugarcane was 1.9 billion tonnes, where Brazil contributed 39% followed by India 20% to the world's total production. Sugarcane stem is used for the production of sugarcane juice, which is further used for sugar and bioethanol production. The left biomass, sugarcane bagasse (SB) and sugarcane trash (SCT) are burned for the energy production. The energy produced by burning causes emission of greenhouse gases which leads to environmental pollution. Instead of burning and causing the environmental pollution, both biomass SB and SCT can be used for the production of value added products like xylitol, furfural, lactic acid, biobutanol and bioethanol. SB contains 33-46% cellulose, 18-29% hemicellulose and 19-41% lignin (Canilha et al., 2012). Cellulose and hemicellulose can be converted to their respective mono sugars by treatment with cocktail of enzymes. Pretreatment of the biomass is an essential step before the enzymatic saccharification as it increases the surface area and decreases the degree of polymerization. Acid pretreatment (H_2SO_4, HCl, and HNO_3) causes loss of hemicellulosic sugars (Canilha et al., 2013). Generally, pretreatment with alkali (NaOH or KOH) and ammonia are preferred for

hemicellulosic polymer exposure. The composition and complexity of lignocellulosic biomass varies from species to species (Lempereur et al., 1997). Celluloses are homopolymers of glucose, but hemicellulose is complex because of the presence of side chain substitutions. Owing to the complexity and less abundance in comparison to cellulose, the saccharification of hemicellulosic part of lignocellulosic biomass is not much entertained. Therefore, this leads to lower Total Reducing Sugar (TRS) yield. The enzyme xylanase (endolytic) and xylosidase (exolytic) act on main chain of xylan polysaccharides (Jin et al., 2020; Sharma et al., 2018). The use of accessory enzymes like α-L-arabinofuranosidase, to hydrolyse side chains synergistically enhances the rate of hydrolysis and increases the production of mono sugars (Thakur et al., 2019). The aim of this study was to facilitate the hemicellulose saccharification by including additional enzyme α-L-arabinofuranosidase along with xylanase and xylosidase on sugarcane waste and achieve enhanced TRS yield, by optimizing the various conditions of the process. The pretreatment conditions were optimized and the saccharification of hemicellulose part was carried out by using recombinant hemicellulases. The optimized process conditions thus can be used for higher scale efficient hydrolysis.

5.2 Material and Methods

5.2.1 Chemical, reagents and substrates

Kanamycin, ampicillin and IPTG were purchased from Sigma-Aldrich Co. LLC., USA. The analytical grade reagents and chemicals *viz.*, sodium chloride, sodium acetate, glucose, yeast, extract, peptone, tryptone, di-potassium phosphate, monopotassium phosphate, glycerol, sodium carbonate, sodium bicarbonate, sodium potassium tartrate, sodium sulphate, copper sulphate, ammonium molybdate, trifluoroacetic acid (TFA), Coomassie Brilliant Blue G-250 and sodium arsenate were purchased from Himedia Pvt. Ltd. India. The substrate xylan from Carbosynth, UK and rye arabinoxylan from Megazyme, Ireland were purchased.

5.2.2 Biomass processing

SB was collected from local market, Kamrup district of Assam, India. SB biomass washed and dried in oven at 75°C for 16 h. The dried biomass was crushed and filtered by using 850 µm sieve.

5.2.3 Pretreatment of SB

5.2.3.1 Alkaline pretreatment

Three g of powdered SB and 50 ml of 0.6% (w/v) NaOH was added in a 100 ml of reagent bottle and incubated boiling water bath at 100°C for 1 h. After the pretreatment, biomass was filtered through a muslin cloth and washed with distilled water to remove residual NaOH. The filtered biomass was kept for drying in a hot air oven at 75°C for 12 h.

5.2.3.2 Microwave assisted inorganic salt (MAIS) pretreatment using NaCl and $FeCl_3$

Five g of SB biomass was mixed with 50 ml of 0.5 M or 1M NaCl separately, in 100 ml of reagent bottles, followed by heating the samples in microwave oven at 200 W for 5 min. The pretreated (ptd) biomass was then filtered by using muslin cloth, washed by distilled water and dried in an oven at 75°C for 12 h. Similarly, the biomass was also treated with 0.5 M and 1 M $FeCl_3$.

5.2.3.3 Soaking in aqueous ammonia (SAA) pretreatment

Three grams of SB was weighed and mixed with 30 ml of aqueous ammonia (15 wt%) in 100 ml of reagent bottle. The samples were kept at 60°C for 6 h. Then, the ptd biomass was filtered, washed by distilled water and dried at 75°C for 12 h.

5.2.4 Purification and activity assay of recombinant hemicellulases

The enzymes, endo-1,4-β-xylanase (*Ct*Xyn11A) from *Hungateiclostridium thermocellum*, α-L-arabinofuranosidase (*Ps*GH43_12) from *Pseudopedobacter saltans* and β-xylosidase (*Bo*GH43) from *Bacteroides ovatus* were used in the present study. The recombinant plasmids expressing *Ct*Xyn11A and *Bo*GH43 were gifted by Prof. Carlos Fontes of NZYTech Pvt. Ltd. Portugal. *Ps*GH43_12 was cloned and expressed in our laboratory, were purified by immobilized metal-ion affinity chromatography (IMAC) using Sepharose column (HiTrap Chelating, GE Healthcare, USA) (Jamaldheen et al., 2019). The concentration of reducing sugars was determined by following the method described earlier (Nelson, 1944) and (Somogyi, 1945). The xylanase (*Ct*Xyn11A) activity was measured by estimating the liberated reducing sugar (xylose) from xylan (Carbosynth). The reaction mixture contained 50 µl of 1% (w/v) xylan in sodium phosphate buffer (pH 7.5), 40 µl of sodium phosphate buffer (pH 7.5) and 10 µl of purified enzyme (5 µg/ml) solution. The reaction mixture was

incubated at 65°C for 1 min. The arabinofuranosidase (*Ps*GH43_12) activity was measured by estimating the liberated reducing sugar (arabinose) from rye arabinoxylan. The reaction mixture containing 90 µl of 1% (w/v) rye arabinoxylan dissolved in sodium phosphate buffer (pH 7.5) and 10 µl of enzyme solution (50 µg/ml) was incubated at 50°C for 5 min. The xylosidase (*Bo*GH43) activity was measured by estimating the liberated reducing sugar (xylose) from xylan (Carbosynth). The reaction mixture containing 90 µl of 1% (w/v) xylan dissolved in sodium phosphate buffer (pH 7.5) and 10 µl of enzyme solution (50 µg/ml) was incubated with xylan at 40°C for 5 min. The absorbance at 500 nm was taken using a spectrophotometer (Thermo Scientific Multiskan SKY, Singapore). One unit of enzyme activity was defined as the amount of enzyme required to release 1 µmole of product (xylooligosaccharides/xylose/arabinose) per min, under their respective optimum conditions.

5.2.5 Selection of best pretreatment method

The biomass obtained from each pretreatment was hydrolysed by endo-1,4-β-xylanase, *Ct*Xyn11A and the resulting TRS concentration was the basis for selection of the best pretreatment method. 10 mg (1%) of each pretreated biomass of SB was taken in a 2 ml microcentrifuge tube and 900 µl of 50 mM sodium phosphate buffer (pH 7.5) was added to it. This was followed by the addition of 100 µl of 10 U/ml xylanase to make it up 1 ml of total reaction volume. The total enzyme loading was 100 U/g of pretreated biomass. Then, the reactions were incubated in shaking water bath at 150 rpm, at 65°C for 3 h. After the incubation, TRS concentration was determined by the method of Nelson (Nelson, 1944) and Somoygi (Somogyi, 1945).

5.2.6 Optimization of SAA pretreatment

The parameters of the pretreatment process to be optimized were, percentage of aqueous ammonia used, temperature, time and solid-liquid ratio. After the optimized pretreatment, the hemicellulose content of pretreated SB was determined by TAPPI (1992), method by using 1 g of each of the biomass. The response factor chosen for analysis of the experimental run was TRS concentration. The TRS was estimated after the saccharification of pretreated biomass by treating with 100 U/g xylanase (*Ct*Xyn11A).

5.2.7 FTIR analysis of untreated and pretreated SB

The untreated and pretreated biomass SB sample by SAA (18.5 wt%, + heat treatment at 70°C for 14 h) were analysed by Fourier-transform infrared spectroscopy (FTIR). KBr (200 mg) was mixed with each dried biomass sample in a ratio of 100: 1 (KBr: Biomass) and grinded by using mortar and pestle and a pellet was made by using a hydraulic press. The pellets were scanned by using a FTIR spectroscope (Spectrum Two, Perkin-Elmer, Waltham, MA) within the wavenumber range, 4000-450 cm^{-1}.

5.2.8 Field emission scanning electron microscopic (FESEM) imaging of untreated and pretreated SB

SB biomass untreated and pretreated (by SAA, 18.5 wt%, combined with heat treatment at 70°C for 14 h) samples were placed on a carbon tape fixed to a stub. Each sample on the stub was gold coated and scanned by FESEM (Sigma, Zeiss, Germany).

5.2.9 Optimization of enzymatic saccharification

The optimization of enzymatic saccharification of the optimized SAA preteated SB was carried out in two steps. In the first step, the optimization was

performed by using Box-Behnken design. In the first step of saccharification, the biomass loading (1-5%, w/v) and enzyme loading of xylanase *Ct*Xyn11A (50-500 U/g) and α-L-arabinofuranosidase and *Ps*GH43_12 loading (20-200 U/g) were optimized. The reaction was carried out in 1 ml volume in 50 mM sodium phosphate buffer pH 7.0 in a 2 ml micro-centrifuge tube incubated at 40°C and 150 rpm for 24 h. The TRS containing XOS ($TRS_{(XOS)}$) obtained in the first step of enzyme saccharification was used for the second step of enzyme saccharification. The second step of enzyme saccharification was optimized by one variable at a time optimization strategy. After the first step $TRS_{(XOS)}$ concentration obtained was 3.2 mg/ml calculated and described in section 5.3.7. Therefore, the $TRS_{(XOS)}$ loading was varied from 0.5 mg/ml to 3 mg/ml for SB, keeping the constant enzyme loading at 100 U/g *Bo*GH43 and the constant reaction time at 4 h. The enzyme, *Bo*GH43 loading was varied from 4 U/g to 200 U/g using optimized $TRS_{(XOS)}$ loading and reaction time 4 h. The time period of enzyme saccharification was varied from 10 min to 4 h by using optimized $TRS_{(XOS)}$ concentration and optimized *Bo*GH43 loading. In the second step of enzyme saccharification, the reactions were carried out in 1.0 ml volume in 50 mM sodium phosphate buffer, pH 7.0 by incubating at 37°C and 150 rpm.

5.2.10 The TLC analysis

The hydrolysed products of the pretreated biomasses obtained from the enzymatic hydrolysis in the first step of saccharification by using *Ct*Xyn11A and *Ps*GH43_12 under the optimised conditions as mentioned in Section 5.2.9 and also the hydrolysed product obtained by *Bo*GH43 after the second step of saccharification were filtered through 0.4 µm filter membrane (PVDF), separately. The 0.5 µl of sample mixture of standards containing xylose, xylobiose, xylotriose, xylotetraose and

arabinose (2 mg/ml) procured from Sigma-Aldrich Co. LLC., USA were loaded on the TLC plate *(*4x11 cm, TLC Silica gel 60 F254, Merck, Germany) and dried at 70°C for 10 min. A mixture containing glacial acetic acid, chloroform and water in (6:7:1, v/v) ratio was used as the mobile phase. The TLC plate was kept inside the developing chamber and run for 90 min. After the run, the plate was dried and then immersed in the visualizing solution containing sulphuric acid: methanol (5:95, v/v) and 0.5%, w/v α-naphthol and then dried at 80°C to visualize the hydrolysed products.

5.2.11 Determination of released products after second step saccharification by HPLC

One gram of SB was treated with 1 ml of 2 M TFA in a 2 ml microcentrifuge tube (MCT) and kept in boiling water bath for 2 h. Both the tubes were centrifuged at 14000 g at 25°C for 15 min. The supernatants were filtered through the syringe filter by using 0.2 µm membrane and transferred to a fresh MCT and kept in a hot air oven at 75°C for 12 h. 1 ml of degassed milli-Q water was added to the tube and mixed well. The monosugars were estimated by HPLC. The total xylose and arabinose concentration in the TFA treated sample was taken as the total hemicellulose content available for the enzymes (*Ct*Xyn11A, *Ps*GH43_12 and *Bo*GH43) during the saccharification process under optimized conditions. The percentage of xylan to xylose conversion during saccharification was calculated by determining the xylose in the TFA treated sample (total xylan present) and the saccharified sample (hydrolysed xylose). The xylose concentration determination was carried out by HPLC method. The analysis was carried out by using HPLC system (LC-20AD, Shimadzu corporation, Japan) coupled with an autosampler (SIL-20AHT, Shimadzu corporation, Japan) and RI detector (RID-10A, Shimadzu corporation, Japan). Standard xylose and arabinose procured from Sigma-Aldrich Co. LLC., USA were used at concentrations,

0.2, 0.4, 0.6, 0.8 and 1.0 mg/ml. The HPLC column (Phenomenex Rezex ROA (H+) organic acid and monosaccharide column (300 x 7.8 mm) coupled with a guard column (50 x 7.8 mm) was used. A mobile phase of 0.005 N H_2SO_4 was run at a flow rate of 0.5 ml/min through the column. The concentration of each sugar in the sample was calculated with respect to the area of the corresponding peaks of the standard sugars.

5.3 Results and Discussion

5.3.1 Hemicellulose content determination

The hemicellulose content of raw SB was found to be 28.6%. After the treatment of raw SB with 0.6% (w/v) NaOH, the hemicellulose (%, w/w) and lignin (%, w/w) content was 20.1% and 12.7%, respectively (Table 5.1). The SAA pretreatment with 15 wt% aqueous ammonia followed by heat treatment at 60°C for 6 h gave 23.9% (w/w) hemicellulose and 14.2% (w/w) lignin (Table 5.1). The ammonia or alkali-based pre-treatments are known to selectively remove lignin and retain a relatively higher proportion of hemicellulose in the biomass with lesser inhibitor formation (Kim et al., 2016). The alkali pretreatment enhances the xylanase activity by exposing hemicelluloses was reported earlier (Barman et al., 2012). The MAIS pretreatment of SB with 1M NaCl and 1M $FeCl_3$ gave 16.1% and 13.8% (w/w) hemicellulose and 9.7% (w/w) and 6.9% (w/w) lignin, respectively (Table 5.1). Higher delignification was obtained with harsh pretreatment with $FeCl_3$ and NaCl, but both significantly lowered the hemicellulose content. The maximum of hemicellulose content was retained in SAA pretreated biomass as compared with NaOH or MAIS pretreatments.

Table 5.1 Hemicellulose and lignin content and TRS yield of untreated and pretreated SB.

Pretreatment	Hemicellulose (%, w/w)	Lignin (%, w/w)	*TRS yield (mg/g)
Untreated Biomass	28.6	21.1	0.7
0.06% (w/v) NaOH	20.1	12.7	6.8
Unoptimized SAA (15 wt%)	23.9	14.2	8.3
Optimized SAA (18.5 wt%)	22.4	13.2	15.3
1M NaCl	16.1	9.6	3.1
1M $FeCl_3$	13.8	6.9	3.8

**after hydrolysis by endo-1,4-β-xylanase*

5.3.2 Purification and activity assay of recombinant hemicellulases

The purified fractions after dialysis were analysed by SDS-PAGE using 12% (w/v) gel that displayed a single band of molecular mass approximately, 65 kDa for *Ps*GH43_12 (3.4 mg/ml), 40 kDa for *Bo*GH43 (1.8 mg/ml) and 25 kDa for *Ct*Xyn11A (2.1 mg/ml) (Fig. 5.1). The specific activities determined were 2716 U/mg for *Ct*Xyn11A against xylan (Carbosynth), 83.4 U/mg for *Ps*GH43_12 against rye arabinoxylan (Megazyme) and 78.7 U/mg for *Bo*GH43 against xylan (Carbosynth).

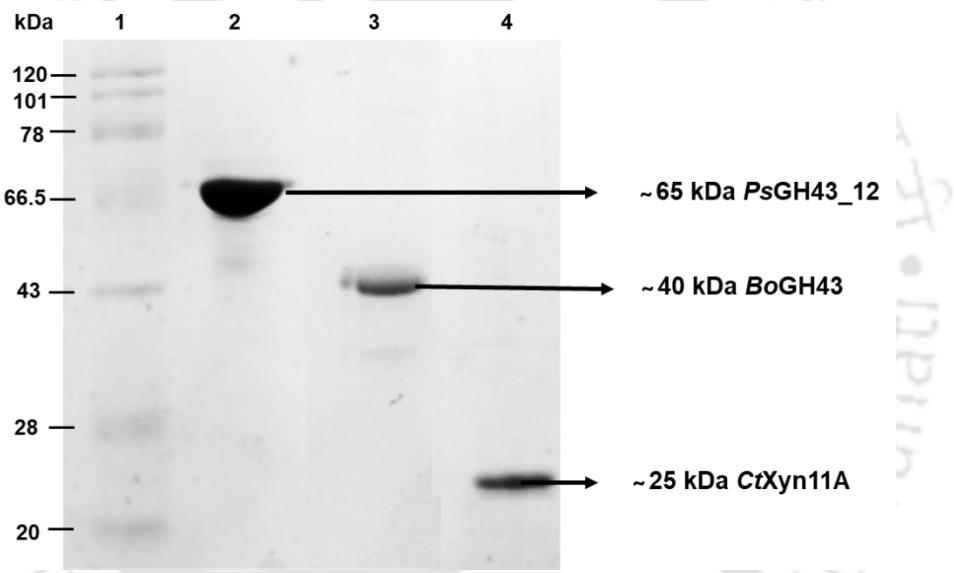

Fig. 5.1 SDS-PAGE (12%, w/v) gel showing hyper-expression and purification of hemicellulases. Lanes: 1- protein marker, 2- purified *Ps*GH43_12 (~65 kDa), 3- purified *Bo*GH43 (~40 kDa) and 4- purified *Ct*Xyn11A (~25 kDa).

5.3.3 Selection of best pretreatment based on saccharification by *Ct*Xyn11A

The enzyme saccharification of pretreated biomass by all methods was performed by using endo-1,4-β-xylanase, *Ct*Xyn11A (100 U/g) at 65°C, using 50 mM sodium-phosphate buffer, pH 7 for 3 h and the resulting TRS concentration was estimated. Among all the pretreatments, the unoptimized SAA gave the maximum TRS yield of 8.3 mg/g for SB, while the minimum TRS yield was observed with

harsh MAIS pretreatment (Table 5.1). There was over 10-fold increase in TRS yield from 0.7 mg/g to 8.3 mg/g for SB after the SAA, 15 wt% pretreatment. This could be due to the swelling and significant disruption of lignocellulosic biomass, leading to its enhanced accessibility to hydrolysing enzyme.

5.3.4 Optimization of soaking in aqueous ammonia (SAA) pretreatment

The optimized conditions for the SAA pretreatment process by using Box-Behnken design were aqueous ammonia concentration, 18.5 wt%, the temperature, 70°C, the solid-liquid ratio (S/L) ratio of 1:9 and the incubation time period, 14 h. After the optimized SAA pretreatment, from 100 g of raw SB, the remaining solid biomass residue was 78 g. The hemicellulose content of SB after optimized SAA pretreatment was 22.4% (17.5 g) (Tables 5.1 & 5.5). This after the saccharification by *Ct*Xyn11A gave TRS yield of 15.3 mg/g of pretreated SB. In an earlier report, the pretreatment of barley hull by 15 wt% aqueous ammonia at 75°C for 48 h at 1:12 S/L ratio, reduced the lignin from 19.3% to 7.5% and xylan content decreased by 10% to 20.5% (Kim et al., 2008). In another report, the pretreatment of SB with SAA (diluted) resulted in retaining 78% of hemicellulose content (Kim & Day, 2013).

5.3.5 FTIR spectroscopic analysis of untreated and pretreated SB

The relative change in the absorbance pattern was observed between the untreated and pretreated biomasses (Fig. 5.2). The peak at position 1732 cm^{-1} attributes to the ester-linked acetyl, feruloyl groups between hemicellulose and lignin and it started disappearing in pretreated SB. Thus, it showed the lignocellulose matrix disruption leading to the delignification. The diminished peak in pretreated SB at 1512 cm^{-1} also represented lignin removal as this peak occurred due to C=C stretching vibrations in phenol rings in lignin as also reported earlier (Jamaldheen et al., 2019).

The band at 1378 cm^{-1} displayed presence of hemicellulose in the pretreated SB, as also previously reported (Ren et al., 2016). The prominent peak obtained in pretreated SB at 897 cm^{-1} was assigned to the β-glycosidic linkage, which represented higher exposure of polysaccharide portion after the pretreatment as reported earlier (Kacurakova et al., 2000).

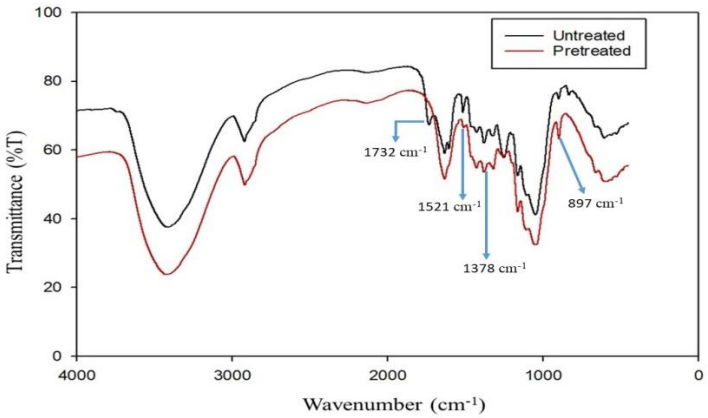

Fig. 5.2 FTIR plots of (A) untreated and optimized pretreated SB (18.5 wt%, Soaking in aqueous ammonia combined with heat treatment at 70°C for 14h.

5.3.6 FESEM analysis of untreated and pretreated SB

The FESEM images of raw biomass, SB displayed that their structure integrity was intact as the surface's evenness and insignificant surface porosity was observed (Fig. 5.3A). While, the SAA pretreated SB showed significant structure disruption, resulting in increased surface roughness and considerable pore formation (Fig. 5.3B). The high surface porosity and irregularities are required to enhance biomass accessibility to hydrolysing enzymes, which ultimately improves reducing sugar concentration. The similar results on barley hull pretreatment by SAA and structure disruption was observed by FESEM (Kim et al., 2008).

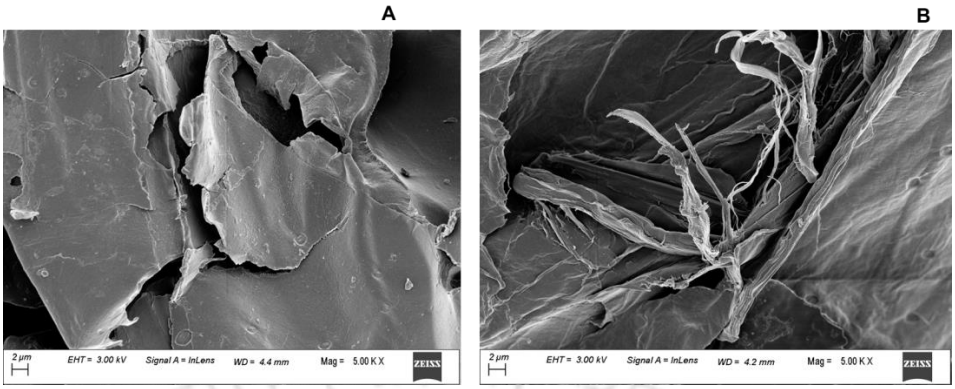

Fig. 5.3 FESEM images of (A) untreated SB and (B) optimized pretreated SB (Soaking in aqueous ammonia (SAA), 18.5 wt% + heat treatment at 70°C for 14 h).

5.3.7 Optimization of hemicellulose hydrolysis of pretreated SB in the first step by *Ct*Xyn11A and *Ps*GH43_12

The percent biomass loading, *Ct*Xyn11A and *Ps*GH43_12 loadings varied under defined levels as mentioned in Table 5.2, were optimized at 40°C and pH 7.0 for both the sugarcane biomasses. The optimum hydrolysis time was pre-determined as 24 h. The Box-Behnken design for the optimization of hydrolysis of hemicellulose from pretreated (SAA, 18.5 wt% + heat treatment at 70°C for 14 h) SB by endo-1,4-β-xylanase (*Ct*Xyn11A) and α-L-arabinofuranosidase (*Ps*GH43_12) and the response, TRS yield are shown in the Table 5.3.

Table 5.2 Process variables for optimization of hemicellulose hydrolysis from SAA pretreated SB by endo-1,4-β-xylanase (*Ct*Xyn11A) and α-L-arabinofuranosidase (*Ps*GH43_12).

Factor	Factor name	Level	
		Low (-1)	High (+1)
A	Biomass loading (%, w/v)	1	5
B	Xylanase loading (U/g ptd biomass)	50	500
C	Arabinofuranosidase loading (U/g ptd biomass)	20	110

The second-order quadratic equation for the hydrolysis process of pretreated SB was generated by Design-Expert 7.0 software and is as follows:

$$TRS\ yield\quad (mg/g\ ptd\ biomass) = 32.60236 + (14.826 \times Biomass\ loading) + (0.154 \times Xylanase\ loading) + (0.173 \times Arabinofuranosidase\ loading) - (0.0035 \times Biomass\ loading \times Xylanase\ loading) - (0.0109 \times Biomass\ loading \times Arabinofuranosidase\ loading) - (0.00015 \times Xylanase\ loading \times Arabinofuranosidase\ loading) - (2.56 \times Biomass\ loading^2) - (0.00014 \times Xylanase\ loading^2) - (0.00031 \times Arabinofuranosidase\ loading^2)$$

The suggested quadratic model fits well with the response data (Table 5.3).

Table 5.3 Box-Behnken design and responses for hemicellulose hydrolysis from pretreated SB by endo-1,4-β-xylanase (*Ct*Xyn11A) and α-L-arabinofuranosidase (*Ps*GH43_12).

Run order	Biomass loading (%, w/v) (A_1)	Xylanase loading (U/g ptd biomass) (B_1)	Arabinofuranosidase loading (U/g ptd biomass) (C_1)	TRS yield (mg/g ptd biomass)
1	3	275	110	89.74
2	5	275	20	72.2
3	5	500	110	76.5
4	1	275	20	79.1
5	3	275	110	90.08
6	3	500	20	90.9
7	3	275	110	88.03
8	1	500	110	90.6
9	3	275	110	90.4
10	3	500	200	91.9
11	3	275	110	90.9
12	3	50	20	62.2
13	5	275	200	71.1
14	1	50	110	65.3
15	1	275	200	85.9
16	3	50	200	75.9
17	5	50	110	57.6

The model F-value of 108.36 and p-value of <0.0001 from ANOVA showed that the model was significant. Among the three factors studied, the highest F-value of xylanase loading indicated that it is the most significant factor in sugarcane bagasse hydrolysis. The p-values of the model terms A_1, B_1, C_1, B_1C_1, A_1C_1, A_1^2, B_1^2 and C_1^2 were less than 0.05, which implied that all of these terms were significant. The

model's regression coefficient was found to be 0.9929, which showed high accuracy of the model (Table 5.4). The $TRS_{(XOS)}$ yield increased with increase in the xylanase and arabinofuranosidase loading (Fig. 5.4A, 4B and 4C). Initially, the $TRS_{(XOS)}$ yield also increased with increase in biomass loading up to 3.5%, and then it started to decrease (Fig. 5.4A, 4B). The predicted optimum biomass loading (A_1), xylanase loading (B_1) and arabinofuranosidase loading (C_1) for SB hydrolysis were 3.45% (w/v), 459 U/g ptd biomass and 111 U/g ptd biomass.

Table 5.4 ANOVA for quadratic model of hemicellulose hydrolysis from pretreated SB by endo-1,4-β-xylanase (*Ct*Xyn11A) and α-L-arabinofuranosidase (*Ps*GH43_12).

Source	SS	Df	Mean square	F-Value	p-value	
Quadratic model	2081.09	9	231.23	108.36	< 0.0001	Significant
A_1-Biomass loading	236.53	1	236.53	110.84	< 0.0001	
B_1-Xylanase loading	987.90	1	987.90	462.94	< 0.0001	
C_1-Arabinofuranosidase loading	52.02	1	52.02	24.38	0.0017	
A_1B_1	10.24	1	10.24	4.80	0.0646	
A_1C_1	15.60	1	15.60	7.31	0.0305	
B_1C_1	40.32	1	40.32	18.90	0.0034	
A_1^2	441.51	1	441.51	206.89	< 0.0001	
B_1^2	211.66	1	211.66	99.18	< 0.0001	
C_1^2	14.76	1	14.76	8.11	0.0096	
Residual	14.94	7	2.13			
Lack of Fit	10.16	3	3.39	2.83	0.1701	
Pure Error	4.78	4	1.20			
Model statistics						
S.D.	1.46		R^2	0.9929		
Mean	80.49		Adj-R^2	0.9837		
C.V. %	1.81		Pred-R^2	0.9189		

The predicted TRS yield at above mentioned conditions was 92.1 mg/g ptd biomass. It was validated by carrying out an experiment (triplicate) in 1 mL reaction volume at the predicted optimum conditions and the experimental TRS yield was 93.2 ± 3.2 mg/g ptd biomass. This after calculation gives the $TRS_{(XOS)}$ concentration of 3.2 mg/ml from optimized biomass loading of 3.45% (Table 5.5).

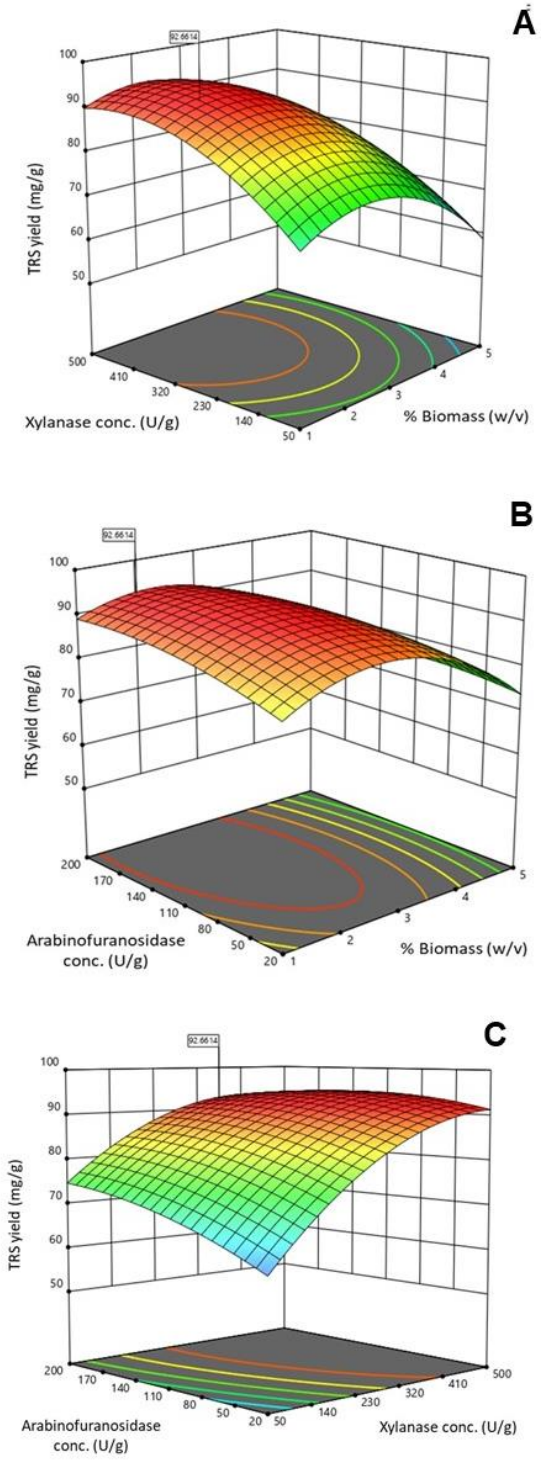

Fig. 5.4 3-D response surface plots for the interaction between the independent variables involved in the optimization of hemicellulose hydrolysis. (A) Pretreated SB loading (%, w/v) and xylanase loading (U/g biomass), (B) Pretreated SB loading (%, w/v) and arabinofuranosidase loading (U/g biomass), (C) xylanase loading (U/g biomass) and arabinofuranosidase loading (U/g biomass).

5.3.8 Optimization of hydrolysis of XOS produced in first step of saccharification from pretreated SB by *Bo*GH43 in the second step

In the second step saccharification, the $TRS_{(XOS)}$ produced in the first step, were hydrolysed to xylose by xylosidase, *Bo*GH43 at 37°C. The second step of saccharification was optimized by following one variable at a time optimization strategy. The maximum TRS yields of 1.77 mg/mg of $TRS_{(XOS)}$ was obtained at optimized concentrations of 3 mg/ml of $TRS_{(XOS)}$ by using 100 U/g *Bo*GH43 and reaction time of 4h (Fig. 5.5A). Optimum *Bo*GH43 loading was found to be 20 U/g by using optimum $TRS_{(XOS)}$ loading of 3.0 mg/ml, which gave TRS yield of 1.77 mg/mg $TRS_{(XOS)}$ after 4h of reaction (Fig. 5.5B). The optimized reaction time period was 1 h, where the maximum TRS yield of 1.77 mg/mg of $TRS_{(XOS)}$ from SB was achieved (Fig. 5.5C). In the first step of saccharification, TRS_{XOS} yield produced was 93.2 mg/g and from SB (Table 5.5). In the second step of saccharification, the TRS yield produced was 1.77 mg/mg of $TRS_{(XOS)}$ from SB (Fig. 5.5).

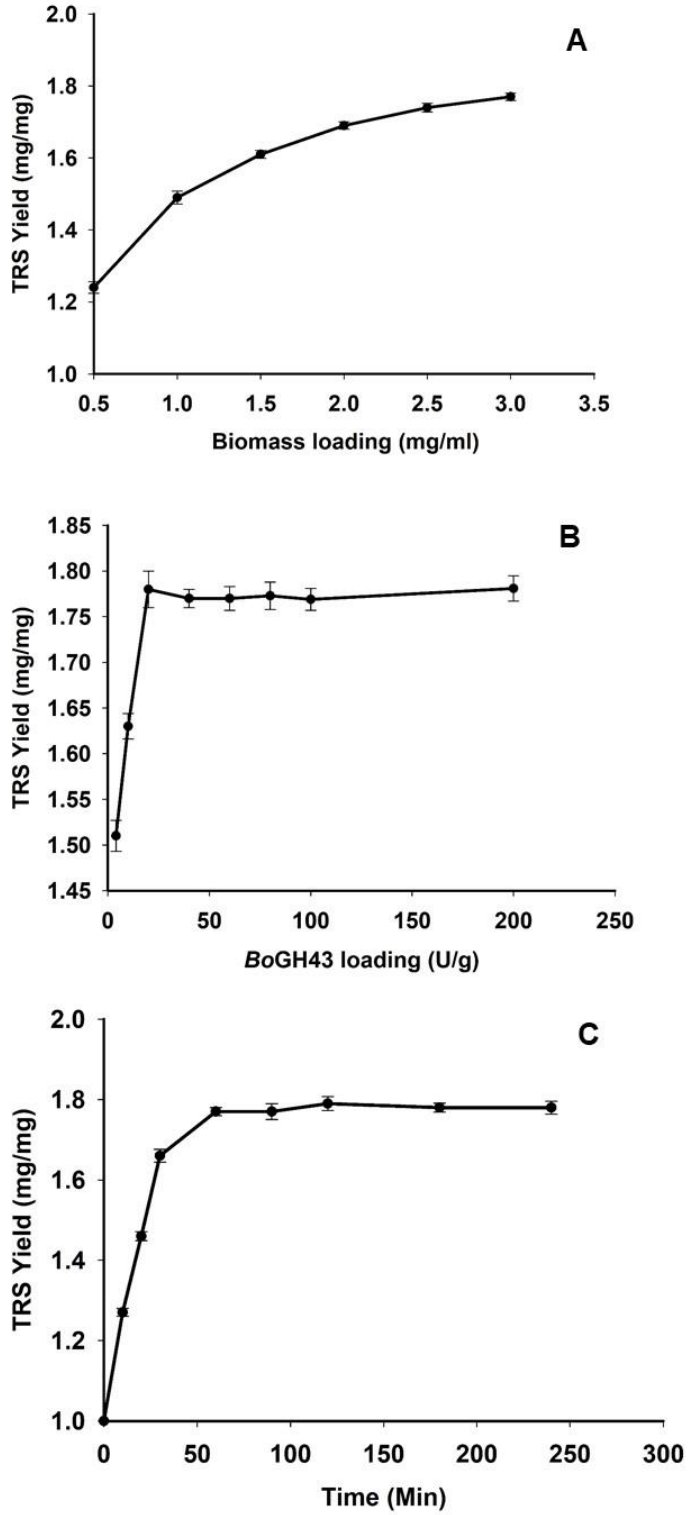

Fig. 5.5 Optimization of 2nd step hydrolysis of $TRS_{(XOS)}$ produced in 1st step saccharification by xylosidse, *Bo*GH43 (A) $TRS_{(XOS)}$ loading (B) *Bo*GH43 loading and (C) Time optimization of 2nd step saccharification.

Hence, after the 2nd step of saccharification, the final TRS yield from SB was 164.7 mg/g ptd SB (5.31 mg/ml) using the formula as follows.

$$Final\ TRS\ yield\left(\frac{mg}{g\ ptd\ biomass}\right) = TRS\ yield_{(1st\ step\ saccharification)} \times TRS\ yield_{(2nd\ step\ saccharification)}$$

The NaOH pretreated Finger millet stalk after saccharification by xylanase and xylosidase gave 70 mg/g ptd biomass (1.16 mg/ml) TRS yield (Jamaldheen et al., 2019). In another report, steam explosion and alkaline delignification was used for SB pretreatment and hydrolysis by cocktail of cellulase, glucosidase, arabinofuranosidase and pectinase resulted in TRS concentration of 3.3 mg/ml (da Silva Delabona et al., 2013).

5.3.9 Thin layer chromatography (TLC) analysis of hydrolysed products

The hydrolysed products obtained from the enzymatic hydrolysis of pretreated SB by *Ct*Xyn11A and *Ps*GH43_12 in the first step of saccharification and produced oligosaccharides by *Bo*GH43 in the second step of saccharification were visualized on the TLC plate (Fig. 5.6). The Fig. 5.6 displayed hydrolysis of SB, after first and second step of saccharification. The lane 1 showed the standards xylose, xylobiose, xylotriose and xylotetraose (Fig. 5.6). The spot in lane 2 represented the standard arabinose, while the lane 3 showed xylo-oligosaccharides and arabinose produced after first step of saccharification by endo-1,4-β-xylanase, *Ct*Xyn11A and α-L-arabinofuranosidase, *Ps*GH43_12 (Fig. 5.6). The xylo-oligosaccharides produced in first step of saccharification from SB on hydrolysis with *Bo*GH43 produced xylose, which could be seen as the major spot for xylose and arabinose along with the faint spot of XOS at bottom in the lane 4 (Fig. 5.6). The chromatogram also showed that SAA pretreated SB after the first step of saccharification by *Ct*Xyn11A and

*Ps*GH43_12 majorly produced xylobiose and xylotriose along with arabinose (Fig. 5.6, Lane 3). However, after the second step of hydrolysis, xylobiose and xylotriose disappeared and more prominently xylose and arabinose were formed (Fig. 5.6, lane 4). The TLC analysis confirmed the hydrolysis of hemicellulosic part of SB to xylose and arabinose.

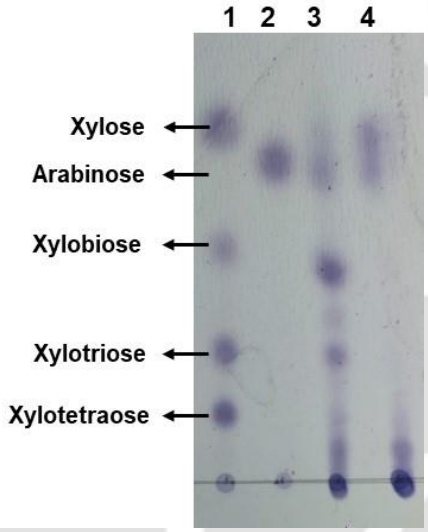

Fig. 5.6 Thin layer chromatogram (TLC) of the hydrolysed products from pretreated sugarcane bagasse by hemicellulases at optimised conditions. Lanes: 1- standards xylose, xylobiose, xylotriose and xylotetraose, 2- standard arabinose, 3- xylo-oligosaccharides and arabinose produced by endo-1,4-β-xylanase (*Ct*Xyn11A) and α-L-arabinofuranosidase (*Ps*GH43_12) from SB and 4- xylose production from SB xylo-oligosaccharides by the action of *Bo*GH43.

5.3.10 Monosugars analysis after second step of saccharification by HPLC

The TFA hydrolysis of optimized SAA pretreated SB yielded 173 mg/g of pretreated SB xylose and 21 mg arabinose/g of pretreated SB. The HPLC analysis of the hydrolysate after the second step of saccharification of SB gave 120.4 mg/g of pretreated SB xylose and 14 mg arabinose/g of pretreated SB. The HPLC results displayed conversion of 69.6% xylan to xylose with respect to the total xylose present in optimized SAA pretreated SB. The percentage of xylose conversion after second step hydrolysis was calculated by using the formula,

$$\%\ conversion = \frac{mg/g\ of\ xylose\ produced\ by\ sacchrification \times 100}{mg/g\ of\ xylose\ produced\ by\ TFA\ hydrolysis}$$

In an another report, for finger millet stalk, the xylan to xylose percent conversion obtained by using endo-1,4-β-xylanase and xylosidase was 24.7% (Jamaldheen et al., 2019). Alkali pretreated SB hydrolysed by xylanase along with accellerase from *Asperginllus nidulans* gave 19.6% xylan to xylose conversion (Maitan-Alfenas et al., 2016). From corn stover 59% xylan to xylose conversion was reported by using enzymes from *Caldicellulosiruptor owensensis*, with initial 2% xylan concentration (Peng et al., 2015). 44% xylan to xylose conversion was reported from ammonia pretreated brewers spent grain after hydrolysis with enzyme cocktail comprising xylanase, xylosidase, cellulase and cellobiase (Amore et al., 2015). Pretreatment of SB by ozonolysis followed by enzymatic hydrolysis by the enzyme produced by *Trichoderma reesei* converted 52.4% of xylan to xylose (Travaini et al., 2013). Higher percentage conversion of xylan to xylose in current study was because of synergistic behaviour of more efficient enzymes i.e. α-L-arabinofuranosidase (*Ps*GH43_12) with endo-1,4-β-xylanase (*Ct*Xyn11A).

5.3.11 Overall mass balance

The mass balance was carried out for optimized SAA pretreatment and two-step enzymatic hydrolysis. After, SAA pretreatment of raw biomass at optimized conditions, 78% of solid biomass was recovered for SB (Fig. 5.7). Out of 100 g of pretreated biomass, the remaining 78 g of solid residue of SB contained 17.5 g (22.4%) (Table 5.5). The pretreated SB upon two step enzymatic hydrolysis by *Ct*Xyn11A, *Ps*GH43_12 and *Bo*GH43 gave TRS yield of 164.7 mg/g ptd SB, which gave 12.86 g of TRS, from 17.5 g of hemicellulose from SB (Fig. 5.7). Hence, this

gave conversion of hemicellulose to TRS 73.5% (12.86 g/17.5 g) (Table 5.5). The whole process yielded 69.6% xylan to xylose conversion as analysed by HPLC (120.4 mg/ 173 mg) for ptd SB, as discussed in section 5.3.10 and listed in Table 5.5.

Table 5.5 Hemicellulose content and TRS yield after each step.

Steps followed	**SB**	**% of SB conversion**
Hemicellulose content in raw biomass	28.6 g/100 g	-
Hemicellulose content in optimized SAA ptd biomass	17.5 g/78 g	-
$TRS_{(XOS)}$ yield after first step saccharification	93.2 mg/g ptd SB (3.2 mg/ml)	-
TRS yield after second step saccharification	164.7 mg/g ptd SB (12.9 g TRS/17.5 g of hemicellulose)	73.5
TFA hydrolysis of ptd biomass (total xylose by HPLC)	173 mg/g ptd SB	-
TFA hydrolysis of ptd biomass (total arabinose by HPLC)	21 mg/g ptd SB	
Second step enzymatic hydrolysis (xylose by HPLC)	120.4 mg/g ptd SB	-
Second step enzymatic hydrolysis (arabinose by HPLC)	14 mg/g ptd SB	-
Xylan to xylose conversion	120.4 mg/ 173 mg	69.6

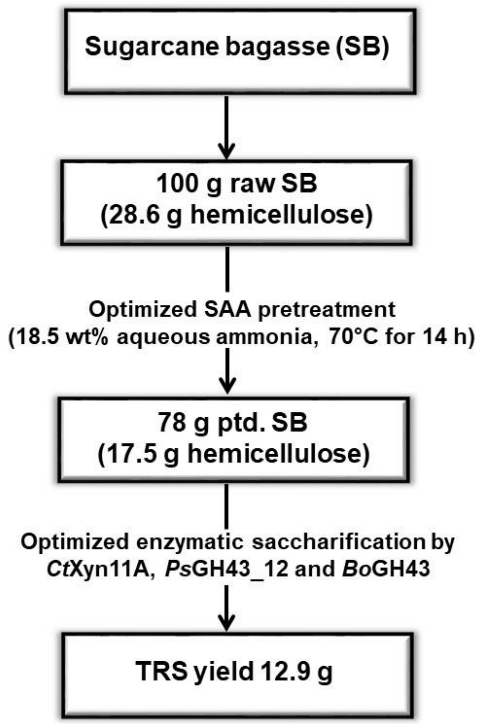

Fig. 5.7 The mass balance for SAA pretreated SB hemicellulose.

5.4 Conclusion

The biomasses, sugarcane bagasse (SB) was used for saccharification of its hemicellulose part. The SAA pretreatment gave the least hemicellulose loss than other pretreatments including alkali pretreatment. Moreover, SAA gave the maximum TRS yield of 8.3 mg/g of unoptimized SAA ptd SB after saccharification by endo-β-1,4-xylanase, *Ct*Xyn11A. The optimized conditions for SAA pretreatment process by Box-Behnken design were aqueous ammonia concentration, 18.5% wt%, temperature, 70°C solid to liquid (S/L) ratio of 1:9 and the incubation time period, 14 h. The TRS yield after *Ct*Xyn11A saccharification of optimised pretreated SAA was 15.3 mg/g of optimized SAA pretreated SB. Out of 100 g of pretreated biomass, the remaining 78 g of solid residue of SB contained 17.5 g (22.4%) hemicellulose. The FTIR and FESEM analyses of the SAA pretreated SB confirmed the structure disruption and delignification. The first step of saccharification of SB by *Ct*Xyn11A and *Ps*GH43_12 gave $TRS_{(XOS)}$ yield of 93.2 ± 3.2 mg/g ptd SB. The second step saccharification by xylosidase (*Bo*GH43) gave final TRS yield of 164.7 mg/g of ptd SB. The HPLC analysis of released products after second step saccharification displayed 69.6% xylan to xylose conversion. This study demonstrated the optimization of pretreatment method and enzymatic saccharification by recombinant hemicellulases, resulting in efficient saccharification of 73.5% from SB. The future prospective of the study can be the use of this hydrolysed product for xylitol and bioethanol fermentation. These pretreatment and saccharification conditions can be used for large scale hydrolysis of the biomass.

5.5 References

Amore, A., Parameswaran, B., Kumar, R., Birolo, L., Vinciguerra, R., Marcolongo, L., & Faraco, V. (2015). Application of a new xylanase activity from *Bacillus amyloliquefaciens* XR44A in brewer's spent grain saccharification. *Journal of Chemical Technology & Biotechnology*, *90*(3), 573-581.

Barman, D. N., Haque, M. A., Kang, T. H., Kim, M. K., Kim, J., Kim, H., & Yun, H. D. (2012). Alkali pretreatment of wheat straw (*Triticum aestivum*) at boiling temperature for producing a bioethanol precursor. *Bioscience, Biotechnology and Biochemistry*, 76(12), 2201-2207.

Berndes, G., Hoogwijk, M., & Van den Broek, R. (2003). The contribution of biomass in the future global energy supply: a review of 17 studies. *Biomass and Bioenergy*, *25*(1), 1-28.

Canilha, L., Chandel, A. K., Suzane dos Santos Milessi, T., Antunes, F. A. F., Luiz da Costa Freitas, W., das Graças Almeida Felipe, M., & da Silva, S. S. (2012). Bioconversion of sugarcane biomass into ethanol: an overview about composition, pretreatment methods, detoxification of hydrolysates, enzymatic saccharification, and ethanol fermentation. *BioMed Research International*, *2012*. doi:10.1155/2012/989572

Canilha, L., Rodrigues, R. C. L. B., Antunes, F. A. F., Chandel, A. K., Milessi, T. S. D. S., Felipe, M. D. G. A., & Silva, S. D. (2013). Bioconversion of hemicellulose from sugarcane biomass into sustainable products. *Sustainable Degradation of Lignocellulosic Biomass-Techniques, Applications and Commercialization*, 15-45. http://dx.doi.org/10.5772/53832

da Silva Delabona, P., Cota, J., Hoffmam, Z. B., Paixão, D. A. A., Farinas, C. S., Cairo, J. P. L. F., & da Cruz Pradella, J. G. (2013). Understanding the cellulolytic system of *Trichoderma harzianum* P49P11 and enhancing saccharification of pretreated sugarcane bagasse by supplementation with pectinase and α-l-arabinofuranosidase. *Bioresource Technology*, *131*, 500-507.

Guo, X. M., Trably, E., Latrille, E., Carrere, H., & Steyer, J. P. (2010). Hydrogen production from agricultural waste by dark fermentation: a review. *International Journal of Hydrogen Energy*, *35*(19), 10660-10673.

Hameed, S., & Dignon, J. (1988). Changes in the geographical distributions of global emissions of NOx and SOx from fossil-fuel combustion between 1966 and 1980. *Atmospheric Environment (1967)*, *22*(3), 441-449.

Jamaldheen, S. B., Thakur, A., Moholkar, V. S., & Goyal, A. (2019). Enzymatic hydrolysis of hemicellulose from pretreated Finger millet (*Eleusine coracana*) straw by recombinant endo-1, 4-β-xylanase and exo-1, 4-β-xylosidase. *International Journal of Biological Macromolecules*, *135*, 1098-1106.

Jin, X., Song, J., Ma, J., & Liu, G. Q. (2020). Thermostable β-xylosidase from *Aspergillus fumigatus*: Purification, characterization and potential application in lignocellulose bioethanol production. *Renewable Energy*, 155(2020), 1425-1431

Kacurakova, M., Capek, P., Sasinkova, V., Wellner, N., & Ebringerova, A. (2000). FT-IR study of plant cell wall model compounds: pectic polysaccharides and hemicelluloses. *Carbohydrate Polymers*, *43*(2), 195-203.

Kim, J. S., Lee, Y. Y., & Kim, T. H. (2016). A review on alkaline pretreatment technology for bioconversion of lignocellulosic biomass. *Bioresource Technology*, *199*, 42-48.

Kim, M., & Day, D. F. (2013). Enhancement of the enzymatic digestibility and ethanol production from sugarcane bagasse by moderate temperature-dilute ammonia treatment. *Applied Biochemistry and Biotechnology*, *171*(5), 1108-1117.

Kim, T. H., Taylor, F., & Hicks, K. B. (2008). Bioethanol production from barley hull using SAA (soaking in aqueous ammonia) pretreatment. *Bioresource Technology*, *99*(13), 5694-5702.

Lempereur, I., Rouau, X., & Abecassis, J. (1997). Genetic and agronomic variation in arabinoxylan and ferulic acid contents of durum wheat (*Triticum durumL.*) grain and its milling fractions. *Journal of Cereal Science*, *25*(2), 103-110.

Lin, Y., & Tanaka, S. (2006). Ethanol fermentation from biomass resources: current state and prospects. *Applied Microbiology and Biotechnology*, *69*(6), 627-642.

Maitan-Alfenas, G. P., Oliveira, M. B., Nagem, R. A., de Vries, R. P., & Guimarães, V. M. (2016). Characterization and biotechnological application of

recombinant xylanases from *Aspergillus nidulans*. *International Journal of Biological Macromolecules*, *91*, 60-67.

Nelson, N. (1944). A photometric adaptation of the Somogyi method for the determination of glucose. *Journal of Biological Chemistry*, *153*(2), 375-380.

Peng, X., Qiao, W., Mi, S., Jia, X., Su, H., & Han, Y. (2015). Characterization of hemicellulase and cellulase from the extremely thermophilic bacterium *Caldicellulosiruptor owensensis* and their potential application for bioconversion of lignocellulosic biomass without pretreatment. *Biotechnology for Biofuels*, *8*(1), 131.

Ren, H., Zong, M. H., Wu, H., & Li, N. (2016). Efficient pretreatment of wheat straw using novel renewable cholinium ionic liquids to improve enzymatic saccharification. *Industrial & Engineering Chemistry Research*, *55*(6), 1788-1795.

Sharma, K., Antunes, I. L., Rajulapati, V., & Goyal, A. (2018). Molecular characterization of a first endo-acting β-1, 4-xylanase of family 10 glycoside hydrolase (*Ps*GH10A) from *Pseudopedobacter saltans* comb. nov. *Process Biochemistry*, *70*, 79-89.

Singh, R., Srivastava, M., & Shukla, A. (2016). Environmental sustainability of bioethanol production from rice straw in India: a review. *Renewable and Sustainable Energy Reviews*, *54*, 202-216.

Somogyi, M. (1945). A new reagent for the determination of sugars. *Journal of Biological Chemistry*, *160*, 61-68.

TAPPI, (1992) Technical association of pulp and paper industry. Georgia, USA: Atlanta.

Thakur, A., Sharma, K., & Goyal, A. (2019). α-l-Arabinofuranosidase: A potential enzyme for the food industry. In *Green Bio-processes*. Springer, Singapore. 229-244.

Travaini, R., Otero, M. D. M., Coca, M., Da-Silva, R., & Bolado, S. (2013). Sugarcane bagasse ozonolysis pretreatment: effect on enzymatic digestibility and inhibitory compound formation. *Bioresource Technology*, *133*, 332-339.

Zhang, J., & Konan, D. E. (2010). The sleeping giant awakes: projecting global implications of China's energy consumption. *Review of Development Economics*, *14*(4), 750-767.

Published/accepted (*From Thesis*):

Book Chapter:

1. **Abhijeet Thakur**, Kedar Sharma and Arun Goyal (2018), α-L-arabinofuranosidase: A potential enzyme for the food industry "Green Bio-Processes: Industrial Enzymes for Food Applications" https://doi.org/10.1007/978-981-13-3263-0_12.

Submitted/to be submitted research articles:

1. **Abhijeet Thakur**, Kedar Sharma, Sumitha Banu Jamaldheen and Arun Goyal* (2020). Molecular characterization, regioselective and synergistic action of first recombinant type I α-L-arabinofuranosidase of family 43 glycoside hydrolase (*Ps*GH43_12) from *Pseudopedobacter saltans. Molecular Biotechnology*, (JIF 2).
2. **Abhijeet Thakur**, Kedar Sharma, Sumitha Banu Jamaldheen and Arun Goyal* (2020). Structure and dynamics analysis of a family 43 glycoside hydrolase α-L-arabinofuranosidase (*Ps*GH43_12) from *Pseudopedobacter saltans* by computational modeling and small-angle X-ray scattering. *International Journal of Biological Macromolecules*. (JIF 5.2).
3. **Abhijeet Thakur**[†], Aakash Sharma[†], Kaustubh Chandrakant Khaire, Vijayanand Suryakant, Moholkar[2,3] Puneet Pathak[4], Nishi Kant Bhardwaj[4] and Arun Goyal (2020) Efficient saccharification of sugarcane hemicellulose by recombinant hemicellulases. [†]*Equal contribution* (Submitted)

Other Publications:

1. Sumitha Banu J., **Abhijeet Thakur**, Vijayanand S. Moholkar and Arun Goyal (2019) Elucidating the impacts of various pretreatments on the structural composition of Finger millet (*Eleusine coracana*) straw and optimization of hemicellulose saccharification by recombinant hemicellulases. *International Journal of Biological Macromolecules.* (JIF 5.2).
2. Kedar Sharma, **Abhijeet Thakur**, Rajeev Kumar and Arun Goyal (2019). Structure and biochemical characterization of glucose tolerant β-1,4 glucosidase (*Ht*Bgl) of family 1 glycoside hydrolase from *Hungateiclostridium thermocellum*. *Carbohydrate Research* (JIF 1.9).
3. Dishant Goyal, Krishan Kumar, Maria SJ Centeno, **Abhijeet Thakur**, Virgínia MR Pires, Pedro Bule, Carlos MGA Fontes, and Arun Goyal. (2019). Molecular Cloning, Expression and Biochemical Characterization of a Family 5 Glycoside Hydrolase First Endo-Mannanase (*Rf*GH5_7) from *Ruminococcus flavefaciens* FD-1 v3. *Molecular Biotechnology*, (JIF 2).
4. Kedar Sharma, Kaustubh Chandrakant Khaire, **Abhijeet Thakur**, Vijayanand Suryakant Moholkar and Arun Goyal (2020). Acacia xylan as a substitute of commercially available xylan and its application in the production of xylooligosaccharides. *ACS Omega* (JIF 2.8)
5. Kedar Sharma, Sudhir Morla, Kaustubh Chandrakant Khaire, **Abhijeet Thakur**, Vijay Suryakant Moholkar, Sachin Kumar and Arun Goyal (2020). Extraction, characterization of xylan from neem sawdust and its application in xylanase

mediated production of anticancer xylooligosaccharides. *International Journal of Biological Macromolecules*. (JIF 5.2).

6. Kaustubh Chandrakant Khaire, Kedar Sharma, **Abhijeet Thakur**, Vijay Suryakant Moholkar, and Arun Goyal **(2020)**. Extraction, characterization of xylan from sugarcane leaf tops and its application. **(Submitted).**
7. Sunetra Mondal, **Abhijeet Thakur,** Carlos M.G.A. Fontes and Arun Goyal (2020) Cloning, expression and characterization of a novel lichenase (*Rf*GH16_21) of family 16 Glycoside Hydrolase from mesophilic bacterium *Ruminococcus flavefaciens* FD-1 v3 **(Submitted).**
8. Jebin Ahmed, **Abhijeet Thakur** and Arun Goyal (2020) Pectinolytic enzymes as biocatalysts for pectic substances and their applications **(Submitted).**

Other Book Chapters

1. **Abhijeet Thakur**, Kedar Sharma, Ruchi Mutreja and Arun Goyal (2019) Thermostable enzymes from *Clostridium thermocellum*. Ed. Sonali Mohapatra, Bioprospecting of Enzymes in Industry, Healthcare and Sustainable environment **(In Press).**
2. Ruchi Mutreja, **Abhijeet Thakur** and Arun Goyal (2018) Chapter 13. Chitin and chitosan: current status and future opportunities In "Hand book of chitin and chitosan" Editors: Sreerag Gopi, Sabu Thomas, Anitha Pius, Volume 3: Woodhead publishing, Elsevier. https://doi.org/10.1016/B978-0-12-817970-3.00013-4
3. **Abhijeet Thakur**, Kedar Sharma, Kaustubh Khaire, Vijay Suryakant Moholkar and Arun Goyal (2019) Enzymes: Key role in conversion of waste to biofuel. Ed Sonali Mohapatra, Microbial Fermentation and Enzyme Technology, CRC Press. https://doi.org/10.1201/9780429061257-16
4. Kedar Sharma, **Abhijeet Thakur** and Arun Goyal (2019), Xylanases for food applications "Green Bio-Processes: Industrial Enzymes for Food Applications" https://doi.org/10.1007/978-981-13-3263-0_7.

Conferences/Symposia/Meetings

1. Kedar Sharma, Kaustubh Chandrakant Khaire, **Abhijeet Thakur**, Vijayanand Suryakant Moholkar and Arun Goyal (2019). Isolation and characterization of glucuronoxylan from Babool as substitute of commercial xylan for xylanase activity evaluation. International Carbohydrate Conference on Emerging Frontiers in Carbohydrate Chemistry and Glycobiology, Dec. 5-7, 2019, University of Lucknow, UP, India.
2. Kedar Sharma, Sudhir Morla, Kaustubh Chandrakant Khaire, **Abhijeet Thakur**, Vijayanand Suryakant Moholkar, Sachin Kumar and Arun Goyal (2019) Extraction, characterization of xylan from neem sawdust and its application in xylanase mediated production of anticancer xylooligosaccharides. International Carbohydrate Conference on Emerging Frontiers in Carbohydrate Chemistry and Glycobiology, Dec. 5-7, 2019, University of Lucknow, UP, India.
3. Kedar Sharma, Kaustubh Chandrakant Khaire, **Abhijeet Thakur**, Vijayanand Suryakant Moholkar and Arun Goyal (2019) Acacia xylan as a potential commercial xylan and its application in production of xylooligosaccharides. International Conference on New Horizons in Biotechnology, November 20-24, 2019, Trivandrum, Kerala, India.
4. Kedar Sharma, Sudhir Morla, Kaustubh Chandrakant Khaire, **Abhijeet Thakur**, Vijayanand Suryakant Moholkar, Sachin Kumar and Arun Goyal (2019) Xylanase mediated production of xylooligosaccharides from neem sawdust xylan and its anticancer potential. International Conference on Nutraceuticals And Chronic Diseases (INCD 2019), September 23-25, 2019 Indian Institute of Technology Guwahati, Assam, India.
5. Sumitha Banu J., **Abhijeet Thakur**, Vijayanand S. Moholkar and Arun Goyal (2019) Hemicellulose saccharification from pretreated finger millet straw by recombinant hemicellulases for bioethanol production. 8th International Forum on Industrial Bioprocessing (IBA-IFIBiop 2019) "Bridging Sustainability and Industrial Revolution through Green Bioprocessing", 1-5 May, 2019, Imperial Hotel, Miri, Sarawak, Malaysia.
6. Dishant Goyal, Krishan Kumar, **Abhijeet Thakur** and Arun Goyal (2019) Expression, purification and biochemical characterization of family 5 glycoside hydrolase (RfGH5_7) from *Ruminococcus flavefaciens* FD-1 v3. Research Conclave, March, 14-17, 2019, IIT Guwahati, Assam.
7. **Abhijeet Thakur** and Arun Goyal (2019) Efficient saccharification of finger millet stalk by a new thermostable α-L-arabinofuranosidase (*Ps*GH43A) from *Pseudopedobacter saltans.* Research Conclave, March 14-17, 2019, IIT Guwahati, Assam. 3rd best poster prize.
8. Sumitha Banu J., **Abhijeet Thakur**, Vijayanand S. Moholkar and Arun Goyal (2019) Optimization of enzymatic hydrolysis of alkali-treated finger millet straw by recombinant β-1,4-endoxylanase. Research Conclave, March 14-17, 2019, IIT Guwahati, Assam.

9. Kedar Sharma, **Abhijeet Thakur**, Rajeev Kumar and Arun Goyal (2018). Structure and biochemical characterization of glucose tolerant β-1,4 glucosidase (*Ht*Bgl) of family 1 glycoside hydrolase from *Hungateiclostridium thermocellum*. Bioprocessing India 2018, Dec 16-18, 2018, IIT Delhi, India.
10. **Abhijeet Thakur** and Arun Goyal (2018) First α-L-arabinofuranosidase (*Ps*GH43) from *Pedobacter saltans* and efficient saccharification of finger millet stalk through synergism. Bioprocessing India 2018, December 16- 18, 2018, IIT Delhi.
11. Sumitha Banu J., **Abhijeet Thakur**, Vijayanand S. Moholkar and Arun Goyal (2018) Saccharification of hemicellulose from pretreated finger millet straw by β-1,4-endoxylanase for bioethanol production. 59th Annual Conference of AMI, Dec 9-12, 2018, University of Hyderabad, India.
12. Kedar Sharma, **Abhijeet Thakur**, Kaustubh Khaire and Arun Goyal (2018) Molecular characterization of halo and organic solvent stable xylanase from *Pseudopedobacter saltans* and its application in xylooligosaccharides production from Kans grass biomass. International Conference on Biotechnological Research and Innovation for Sustainable Development, 15th BRSI convention. CSIR-Indian Institute of Chemical Technology (CSIR-IICT), Nov. 22-25, 2018, Hyderabad, India.
13. Rajeev Kumar, Kedar Sharma, **Abhijeet Thakur** and Arun Goyal (2018) Molecular cloning and biochemical characterization of β-1,4 glucosidase (*Rt*Bgl) family 1 glycoside hydrolase (GH1) from *Ruminiclostridium thermocellum.* DBT National Workshop on Bioenergy, July 6-7 July 6-7, 2018, IIT Roorkee, Uttarakhand, India.
14. Sumitha Banu J., **Abhijeet Thakur**, Aruna Rani, Vijayanand S. Moholkar and Arun Goyal (2018) Pretreatment and clostridial enzymes hydrolysis of finger millet stalk for biofuel production. DBT National Workshop on Bioenergy, July 6-7, 2018, IIT Roorkee, Uttarakhand, India.
15. **Abhijeet Thakur**, Carlos M.G.A. Fontes and Arun Goyal (2018) Application of *Ps*GH43 in combination with other xylanolytic enzymes for conversion of lignocellulosic biomass into reducing sugars. Indo-Japan Bilateral Symposium on Future Perspective of Bioresource Utilization in North-Eastern Region. February 01-04, 2018, IIT Guwahati, India.
16. **Abhijeet Thakur** and Arun Goyal (2017) Sourdough fermentation using a novel α-L-arabinofuranosidase (*Ps*GH43) from *Pedobacter saltans.* Bioprocessing India, Recent Trends in Bioprocessing for Healthcare, Energy and Environment, Dec 9-11, 2017, IIT Guwahati, Assam India.
17. **Abhijeet Thakur** and Arun Goyal (2017) Cloning, expression, purification and biochemical characterization of first α-L-arabinofuranosidase (*Ps*GH43) from *Pedobacter saltans.* 86th Annual Meeting of Society for Biological Chemists, India, Nov. 16-19, Jawaharlal Nehru University, New Delhi, India.

18. Shweta Singh, **Abhijeet Thakur** and Arun Goyal (2016) Strain improvement of *Bacillus amyloliquefaciens* SS35 by UV mutagenesis for producing hyperactive mutants for improved carboxymethyl celluase activity. 57th International Annual Conference of The Association of Microbiologists of India (AMI-2016), Nov 24-27, 2016, Gauhati University and IASST, Guwahati, Assam India.
19. **Abhijeet Thakur** and Arun Goyal (2016) Molecular cloning, expression and purification of xylanase of family 11 Glycoside Hydrolase (GH11) from *Pedobacter saltans*. 57th International Annual Conference of The Association of Microbiologists of India (AMI-2016), Nov 24-27, 2016, Gauhati University and IASST, Guwahati, Assam India.
20. **Abhijeet Thakur**, Carlos M.G.A. Fontes and Arun Goyal (2016) Expression, purification and biochemical characterization of xylanase of family 11 Glycoside Hydrolase (*Ct*Xyn11A) from *Clostridium thermocellum* ATCC27405. CARBO-XXXI International Conference on "New Frontiers in Carbohydrate Chemistry and Biology" 14-16 November 2016, University of Delhi, India.
21. Shweta Singh, **Abhijeet Thakur** and Arun Goyal (2016) Enhancement of carboxymethyl cellulase activity of *Bacillus amyloliquefacians* SS35 by UV radiation induced mutagenesis. National Conference on Recent Advancement in Environmental Research, Center for the Environment, IIT Guwahati, 4-5 June, 2016.

Workshops/courses attended

1. Participated in workshop on SAXS data analysis organized by “Anton Paar India Limited, on **February 26, 2020.**
2. Participated in GIAN Course “**Latest Methods in X-ray Crystallography: Lecture Series and Practical Course** organized by School of Life Sciences, Jawaharlal Nehru University, New Delhi-110067, INDIA under MHRD scheme on Global Initiative for Academic Network on **November 14th to 25th, 2016.**

VITAE

The author was born on July 22, 1990 in the city of (Pusa) Samastipur, (Bihar). He passed Secondary Examination (10th Class) conducted by Central Board of Secondary Examination, New Delhi in 2005 and Higher Secondary Examination (12th Class) conducted by Central Board of Secondary Examination, New Delhi in 2007. He completed B.Sc. (Biotechnology) from University of Kota in July, 2011. He completed M.Sc. (Biotechnology) from Jiwaji University, Gwalior in July, 2014. Mr. Abhijeet Thakur joined the PhD program in July, 2015 at Department of Biosciences and Bioengineering, Indian Institute of Technology Guwahati, Guwahati 781 039, Assam, India. He successfully completed the coursework with 7.33/10 CPI. He delivered the open (PhD Synopsis) Seminar on May 11, 2020 and presented his thesis work before the Doctoral Committee and his performance was satisfactory. He submitted the PhD thesis in May 2020.